

Exploring the Physical Manifestation of Humanity's Subconscious Desires

A Practical Guide

Goro Akechi

Copyright © 2022 Goro Akechi

PUBLISHED BY PUBLISHER

BOOK-WEBSITE.COM

Licensed under the Creative Commons Attribution-NonCommercial 4.0 License (the “License”). You may not use this file except in compliance with the License. You may obtain a copy of the License at <https://creativecommons.org/licenses/by-nc-sa/4.0>. Unless required by applicable law or agreed to in writing, software distributed under the License is distributed on an “AS IS” BASIS, WITHOUT WARRANTIES OR CONDITIONS OF ANY KIND, either express or implied. See the License for the specific language governing permissions and limitations under the License.

First printing, March 2022



Contents

1	Introduction	13
1.1	Section Title	13
1.1.1	Subsection Title	13
I	Aging in threshold models	
2	Aging in binary state dynamics: The threshold model	17
2.1	Introduction	17
2.2	Aging and the Threshold model	18
2.3	Dynamics on Complex networks	19
2.3.1	Numerical results	20
2.3.2	General mathematical description	25
2.3.3	Analytical results	27
2.4	Dynamics on a Moore lattice	30
2.5	Conclusions	30
3	Aging effects in the Schelling segregation model	35
3.1	Introduction	35
3.2	Methods	37
3.2.1	Model	37
3.2.2	Metrics of segregation	37
3.3	Results	38
3.3.1	Phase diagram	38
3.3.2	Segregated phase: final state	39
3.3.3	Segregated phase: coarsening dynamics	40
3.3.4	Aging breaks the asymptotic time-translational invariance	43
3.4	Summary and discussion	44

4	Ordering dynamics and aging in the Symmetrical Threshold model	
	47	
4.1	Theorems	47
4.1.1	Several equations	47
4.1.2	Single Line	47
4.2	Definitions	47
4.3	Notations	47
4.4	Remarks	48
4.5	Corollaries	48
4.6	Propositions	48
4.6.1	Several equations	48
4.6.2	Single Line	48
4.7	Examples	48
4.7.1	Equation Example	48
4.7.2	Text Example	48
4.8	Exercises	48
4.9	Problems	49
4.10	Vocabulary	49

II

Real estate agency dynamics

5	Dynamics of the real state market	53
5.1	Theorems	53
5.1.1	Several equations	53
5.1.2	Single Line	53
5.2	Definitions	53
5.3	Notations	53
5.4	Remarks	54
5.5	Corollaries	54
5.6	Propositions	54
5.6.1	Several equations	54
5.6.2	Single Line	54
5.7	Examples	54
5.7.1	Equation Example	54
5.7.2	Text Example	54
5.8	Exercises	54
5.9	Problems	55
5.10	Vocabulary	55
6	Segmentation of the real state market	57
6.1	Table	57
6.2	Figure	57

Bibliography	59
Articles	59
Books	66
Index	67
Appendices	69
A Effect of a higher vacancy density ρ_v in the coarsening dynamics of the Schelling model	69
B ACTIVATION PROBABILITY EFFECT ON THE CASCADE CONDITION	71
C DERIVATION OF A GENERAL MASTER EQUATION FOR BINARY-STATE MODELS WITH AGING IN COMPLEX NETWORKS	73

List of Figures

2.1 Average density ρ of adopters for an Erdős-Rényi graph of mean degree z using a model with threshold T . Color-coded values of ρ are from Monte Carlo simulations of the model without aging in a graph with $N = 10,000$ agents. Black dashed and white dotted lines correspond to T_c value obtained numerically for the model with exogenous and endogenous aging, respectively. Monte Carlo simulations are averaged over $M = 5 \times 10^4$ realizations. The red solid line is the analytical approximation of the cascade boundary, from Eq. (2.17), which is the same with and without aging.	19
2.2 Cascade spreading for the original Threshold model (a), and the versions with endogenous (b) and exogenous (c) aging. Yellow nodes are adopters and purple nodes are non-adopters. Time increases from left to right. Monte Carlo simulations are performed in an Erdős-Rényi network with mean degree $z = 3$ and $T = 0.22$. System size is $N = 8,000$	21
2.3 Cascade dynamics and fall to the full-adopt state ($\rho \sim 1$) of the Threshold model without aging (a) and the versions with endogenous (b) and exogenous (c) aging effects. At (b-c), the evolution is plotted as a function of the logarithm of time $\log(t)$ in Monte Carlo steps, as in the insets. The underlying network is a 3-regular random graph and the threshold is $T = 0.2$. The exponent values are $\alpha \simeq 1.0$, $\beta \simeq 1.14$, $\gamma \simeq 0.38$ and $\delta \simeq 1.0$. Numerically integrated solutions of Eq. (2.4) (solid lines) describe accurately the numerical results. Monte Carlo simulations are averaged over $M = 5 \times 10^4$ realizations in a network of $N = 1.6 \times 10^5$ nodes.	22
2.4 Average time to reach the steady state ($\rho > 0.9$) τ as a function of the system size N for the original Threshold model and the versions with endogenous and exogenous aging. The underlying network is a 5-regular random graph and the threshold is $T = 0.12$. Monte Carlo simulations are averaged over $M = 5 \times 10^4$ realizations. Solid lines are the system size-dependent timescale: For the original model, $\tau_{\text{NOAG.}} = (1/\alpha) \log(N)$, for the endogenous ($\tau_{\text{ENDO}} = 2N^{1/\delta} - 2$) and for the exogenous aging ($\tau_{\text{EXO}} = 2(\log(N)/\beta)^{1/\gamma} - 2$), which follows from the dynamics from Eq. (2.1), (2.2) and (2.3). The exponents α , β , γ and δ are fitted exponents.	23
2.5 Cascade dynamics of the Threshold model with endogenous (a - c) and exogenous (d - f) aging. From the left column to the right: a random regular graph with degree $z = 5$ (a and d), an Erdős-Rényi graph with average degree $z = 5$ (b and e) and a Barabási-Albert graph with average degree $z = 8$ (c and f). Different colors indicate different values of T and markers correspond to different system sizes: $N = 2,500$ (plus), $10,000$ (circles), $40,000$ (triangles), $160,000$ (crosses) and $640,000$ (squares). Time is scaled according to the system size for each model: $\tau_{\text{EXO}} = 2(\log(N)/\beta)^{1/\gamma} - 2$, $\tau_{\text{ENDO}} = 2N^{1/\delta} - 2$, where β , γ and δ are the fitted exponents from the behavior according to Eq. (2.2) and (2.3). Solid lines are obtained from the solutions of Eq. (2.13). Monte Carlo simulations are averaged over $M = 5 \times 10^4$ realizations.	24

2.6 Exponent α for the original Threshold model (empty markers) and δ for the version with endogenous aging (filled markers) for different values of the average degree z (and $T = 0.1$) (left) and as a function of T for fixed z (right). Different markers indicate results from Monte Carlo simulations with different topologies: red triangles indicate an Erdős-Rényi (ER) graph, blue circles indicate a random regular (RR) graph and green squares indicate a Barabási-Albert (BA) graph. In the right panel, the average degree is fixed $z = 5$ for ER and RR, and $z = 8$ for the BA. Predicted values by Eq. (2.22) (solid lines) fit the results for each topology. System size is fixed at $N = 4 \times 10^6$ for the original model and $N = 3.2 \times 10^5$ for the version with aging.	28
2.7 Exponent γ for the Threshold model with exogenous aging for different values of the average degree z ($T = 0.1$) (left) and as a function of T for fixed z (right). Different markers indicate results from Monte Carlo simulations with different topology: red triangles indicate an Erdős-Rényi (ER) graph, blue circles indicate a random regular (RR) graph and green squares indicate a Barabási-Albert (BA) graph. In the right panel, the average degree is fixed $z = 5$ for ER and RR, and $z = 8$ for the BA. Predicted values by numerical integration of Eqs. (2.13) (solid lines) fit approximately the results for each topology. System size is fixed at $N = 3.2 \times 10^5$.	29
2.8 Cascade spreading of the original Threshold model (a) and the versions with exogenous (b) and endogenous (c) aging on a Moore neighborhood lattice with size $N = L \times L$, $L = 405$. Yellow and purple nodes are adopters and non-adopters, respectively. Time increases from left to right. Initial seeds are selected favoring cascades: one agent and all him/her neighbors are set as adopters at the center of the system.	31
2.9 Cascade dynamics of the Threshold model with exogenous (a) and endogenous (b) aging on a Moore neighborhood lattice. Different colors indicate different values of the threshold T . Different markers indicate the results of Monte Carlo simulations with different system size $N = L \times L$: $L = 50$ (crosses), 100 (triangles), 200 (circles) and 400 (squares). In (a), time is scaled according to size $\tau = L^{2/\zeta}$. Discontinuous solid lines indicate a power law behavior with exponent $\zeta = 4/3$ (blue), 1 (red) and $2/3$ (green). In (b), the system sizes are not scaled due to the slow dynamics. Discontinuous solid lines indicate a power-logarithmic behavior, $\rho(t)N \sim \log(t)^\nu$, with exponent $\nu = 7/3$ (blue), 2 (red) and $5/3$ (green).	32
3.1 Average interface density $\langle \rho_{st} \rangle$ (a) and segregation coefficient $\langle s \rangle$ (b) at the stationary regime as a function of the tolerance parameter T for two values of the vacancy density $\rho_v = 0.5\%$ and 15% . Results are shown for both the Schelling model and the variant with aging introduced in this paper. Simulations are performed on an 80×80 lattice and averaged over $5 \cdot 10^4$ realizations.	39
3.2 (a) Fraction of unsatisfied agents n_u at the stationary regime as a function of the tolerance parameter T . (b) Measure of the interface roughness between clusters of different kind of agents at the final stationary state P/\sqrt{S} as a function of the tolerance parameter T . Different markers indicate different system sizes: $L = 40$ (circles), 60 (squares), 80 (triangles) and 100 (crosses). Results are shown for both the Schelling model with and without aging. Numerical simulations are performed for $\rho_v = 0.5\%$ and averaged over $5 \cdot 10^4$ realizations. The frozen-segregated transition (dashed black line) and the segregated-mixed transition (gray dot-dashed line) are highlighted to differentiate the phases that the Schelling model exhibits. There are no values of P/\sqrt{S} for the Schelling model above $T = 3/4$ because the segregated-mixed transition occurs. (c) Final state interface zoom snapshot for $T = 0.57$ using the original model. (d) Final state interface zoom snapshot for $T = 0.57$ using the model with aging. (e) Same as c for $T = 0.86$.	40
3.3 Average interface density $\langle \rho(t) \rangle$ as a function of time steps for different values of the tolerance parameter T using the Schelling model (a) and the version with aging (b). Average performed over $5 \cdot 10^3$ realizations. Fitted power-law in a black dashed line highlighting the estimated exponent value. We set system size $L = 200$ and $\rho_v = 0.005$.	41
3.4 Coarsening towards the segregated state at two different values of T for both models. Snapshots are taken for 5, 500, 5000 and 50000 time steps ordered from left to right. We set system size $L = 200$ and $\rho_v = 0.005$.	42

3.5 Two-times autocorrelation $C(\tau, t_w)$ as a function of the time period passed since the waiting time t_w . First, the autocorrelation is shown for the Schelling model at $T = 0.71$ in **a**, and for the version with aging at $T = 0.71$ in **b** and $T = 0.86$ in **c**. The insets are the result of the collapse using $u(\tau, t_w) = \tau/t_w$ (**b**) and $u(\tau, t_w) = \log(\tau + t_w)/\log(t_w) - 1$ (**c**). The curves correspond to different values of the waiting time t_w . Calculations performed on a 100×100 lattice averaged over $5 \cdot 10^4$ realizations. 44

6.1 Figure caption.	57
6.2 Floating figure.	58

A.1 Average interface density $\langle \rho(t) \rangle$ as a function of time steps for different values of the tolerance parameter T fr the Schelling model (**a**) and the version with aging (**b**). The different plots show a the evolution at a different value of the vacancy density, increasing from left to right $\rho_v = 0.005, 0.15, 0.2, 0.3$ and 0.45 . Average performed over 10^3 realisations with system size 100×100 69

A.2 Snapshots of the system at the final segregated state (after 10^6 MC steps) for the Schelling model (**a**) and the version with (**b**). System size 200×200 with $\rho_v = 0.45$ and $T = 0.29$ 70

A.3 Cluster coefficient of vacancies as a function of the vacancy density ρ_v for the Schelling model (**a**) and the version with (**b**) for different values of the tolerance T 70

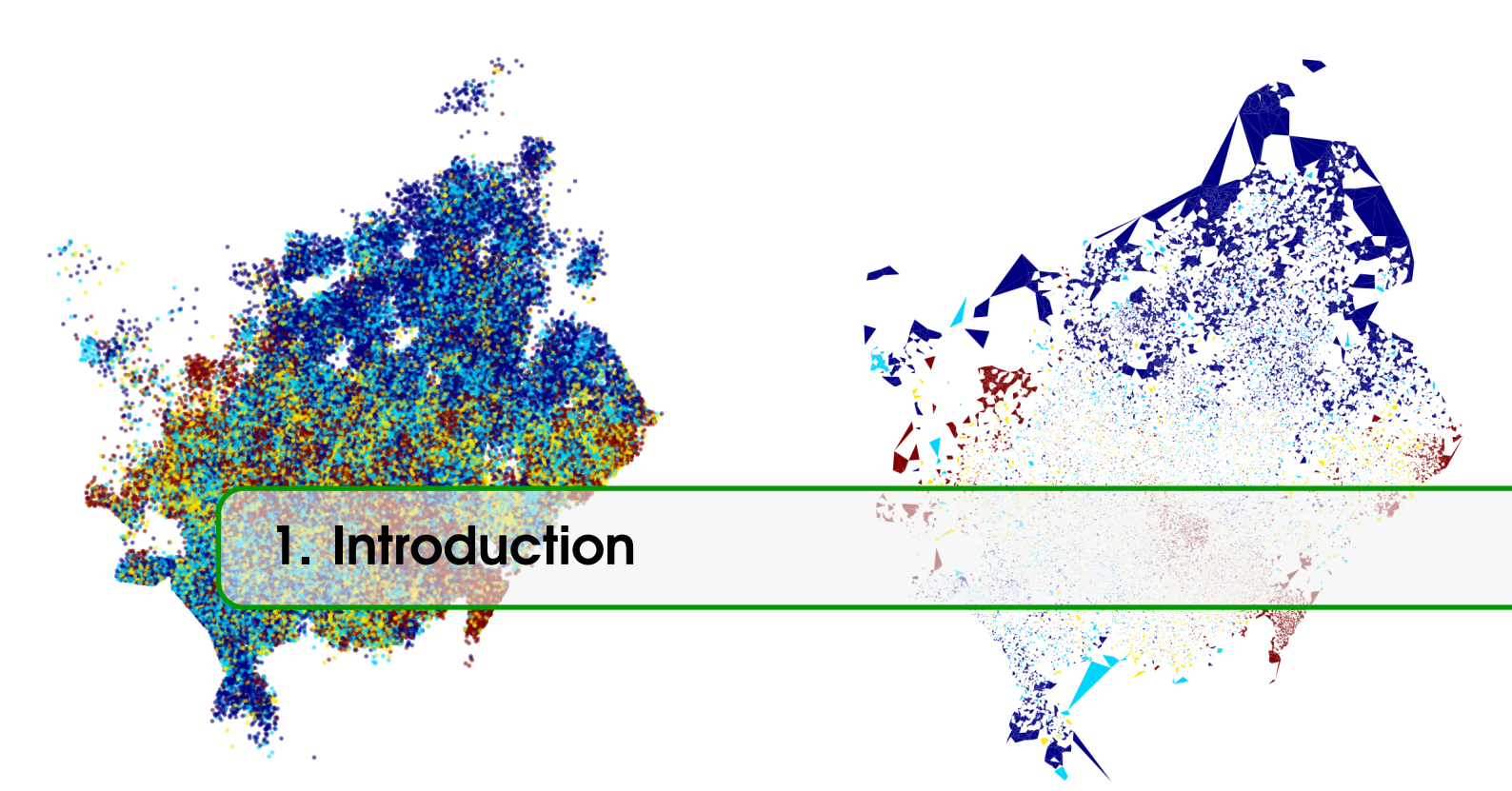
B.1 Average density ρ of adopters for an Erdős-Rényi graph of mean degree z using the Symmetrical threshold model with endogenous aging with threshold T . The activation probability is exponential $p_A(j) = \exp(-0.5 * (j + 1))$. Color-coded values of ρ are from Monte Carlo simulations of the model without aging in a graph with $N = 10,000$ agents. Monte Carlo simulations are averaged over $M = 5 \times 10^4$ realizations. 72

C.1 Schematic representation of the transitions to or from the set $s_{k,m,j}$ ($j > 0$). We show the central node with some neighbors for different values m and j . Purple nodes are susceptible or non-adopters or spin-down, and yellow are infected or adopters or spin-up. 74



List of Tables

6.1 Table caption.	57
6.2 Floating table.	58



1. Introduction

1.1 Section Title

Lorem ipsum dolor sit amet, consectetur adipiscing elit¹. Praesent porttitor arcu luctus, imperdiet urna iaculis, mattis eros. Pellentesque iaculis odio vel nisl ullamcorper, nec faucibus ipsum molestie. Sed dictum nisl non aliquet porttitor. Etiam vulputate arcu dignissim, finibus sem et, viverra nisl. Aenean luctus congue massa, ut laoreet metus ornare in. Nunc fermentum nisi imperdiet lectus tincidunt vestibulum at ac elit. Nulla mattis nisl eu malesuada suscipit.

Aliquam arcu turpis, ultrices sed luctus ac, vehicula id metus. Morbi eu feugiat velit, et tempus augue. Proin ac mattis tortor. Donec tincidunt, ante rhoncus luctus semper, arcu lorem lobortis justo, nec convallis ante quam quis lectus. Aenean tincidunt sodales massa, et hendrerit tellus mattis ac. Sed non pretium nibh. Donec cursus maximus luctus. Vivamus lobortis eros et massa porta porttitor.

1.1.1 Subsection Title

Fusce varius orci ac magna dapibus porttitor. In tempor leo a neque bibendum sollicitudin. Nulla pretium fermentum nisi, eget sodales magna facilisis eu. Praesent aliquet nulla ut bibendum lacinia. Donec vel mauris vulputate, commodo ligula ut, egestas orci. Suspendisse commodo odio sed hendrerit lobortis. Donec finibus eros erat, vel ornare enim mattis et. Donec finibus dolor quis dolor tempus consequat. Mauris fringilla dui id libero egestas, ut mattis neque ornare. Ut condimentum urna pharetra ipsum consequat, eu interdum elit cursus. Vivamus scelerisque tortor et nunc ultricies, id tincidunt libero pharetra. Aliquam eu imperdiet leo. Morbi a massa volutpat velit condimentum convallis et facilisis dolor.

In hac habitasse platea dictumst. Curabitur mattis elit sit amet justo luctus vestibulum. In hac habitasse platea dictumst. Pellentesque lobortis justo enim, a condimentum massa tempor eu. Ut quis nulla a quam pretium eleifend nec eu nisl. Nam cursus porttitor eros, sed luctus ligula convallis quis. Nam convallis, ligula in auctor euismod, ligula mauris fringilla tellus, et egestas mauris odio eget diam. Praesent sodales in ipsum eu dictum. Mauris interdum porttitor fringilla. Proin tincidunt sodales leo at ornare. Donec tempus magna non mauris gravida luctus. Cras vitae arcu vitae mauris eleifend scelerisque. Nam sem sapien, vulputate nec felis eu, blandit convallis risus. Pellentesque sollicitudin venenatis tincidunt. In et ipsum libero.

¹Footnote example text... Lorem ipsum dolor sit amet, consectetur adipiscing elit. Praesent porttitor arcu luctus, imperdiet urna iaculis, mattis eros. Pellentesque iaculis odio vel nisl ullamcorper, nec faucibus ipsum molestie.

1.1.1.1 Subsubsection Title

Maecenas consectetur metus at tellus finibus condimentum. Proin arcu lectus, ultrices non tincidunt et, tincidunt ut quam. Integer luctus posuere est, non maximus ante dignissim quis. Nunc a cursus erat. Curabitur suscipit nibh in tincidunt sagittis. Nam malesuada vestibulum quam id gravida. Proin ut dapibus velit. Vestibulum eget quam quis ipsum semper convallis. Duis consectetur nibh ac diam dignissim, id condimentum enim dictum. Nam aliquet ligula eu magna pellentesque, nec sagittis leo lobortis. Aenean tincidunt dignissim egestas. Morbi efficitur risus ante, id tincidunt odio pulvinar vitae.

Paragraph Title Nullam mollis tellus lorem, sed congue ipsum euismod a. Donec pulvinar neque sed ligula ornare sodales. Nulla sagittis vel lectus nec laoreet. Nulla volutpat malesuada turpis at ultricies. Ut luctus velit odio, sagittis volutpat erat aliquet vel. Donec ac neque eget neque volutpat mollis. Vestibulum viverra ligula et sapien bibendum, vel vulputate ex euismod. Curabitur nec velit velit. Aliquam vulputate lorem elit, id tempus nisl finibus sit amet. Curabitur ex turpis, consequat at lectus id, imperdiet molestie augue. Curabitur eu eros molestie purus commodo hendrerit. Quisque auctor ipsum nec mauris malesuada, non fringilla nibh viverra. Quisque gravida, metus quis semper pulvinar, dolor nisl suscipit leo, vestibulum volutpat ante justo ultrices diam. Sed id facilisis turpis, et aliquet eros.

In malesuada ullamcorper urna, sed dapibus diam sollicitudin non. Donec elit odio, accumsan ac nisl a, tempor imperdiet eros. Donec porta tortor eu risus consequat, a pharetra tortor tristique. Morbi sit amet laoreet erat. Morbi et luctus diam, quis porta ipsum. Quisque libero dolor, suscipit id facilisis eget, sodales volutpat dolor. Nullam vulputate interdum aliquam. Mauris id convallis erat, ut vehicula neque. Sed auctor nibh et elit fringilla, nec ultricies dui sollicitudin. Vestibulum vestibulum luctus metus venenatis facilisis. Suspendisse iaculis augue at vehicula ornare. Sed vel eros ut velit fermentum porttitor sed sed massa. Fusce venenatis, metus a rutrum sagittis, enim ex maximus velit, id semper nisi velit eu purus.

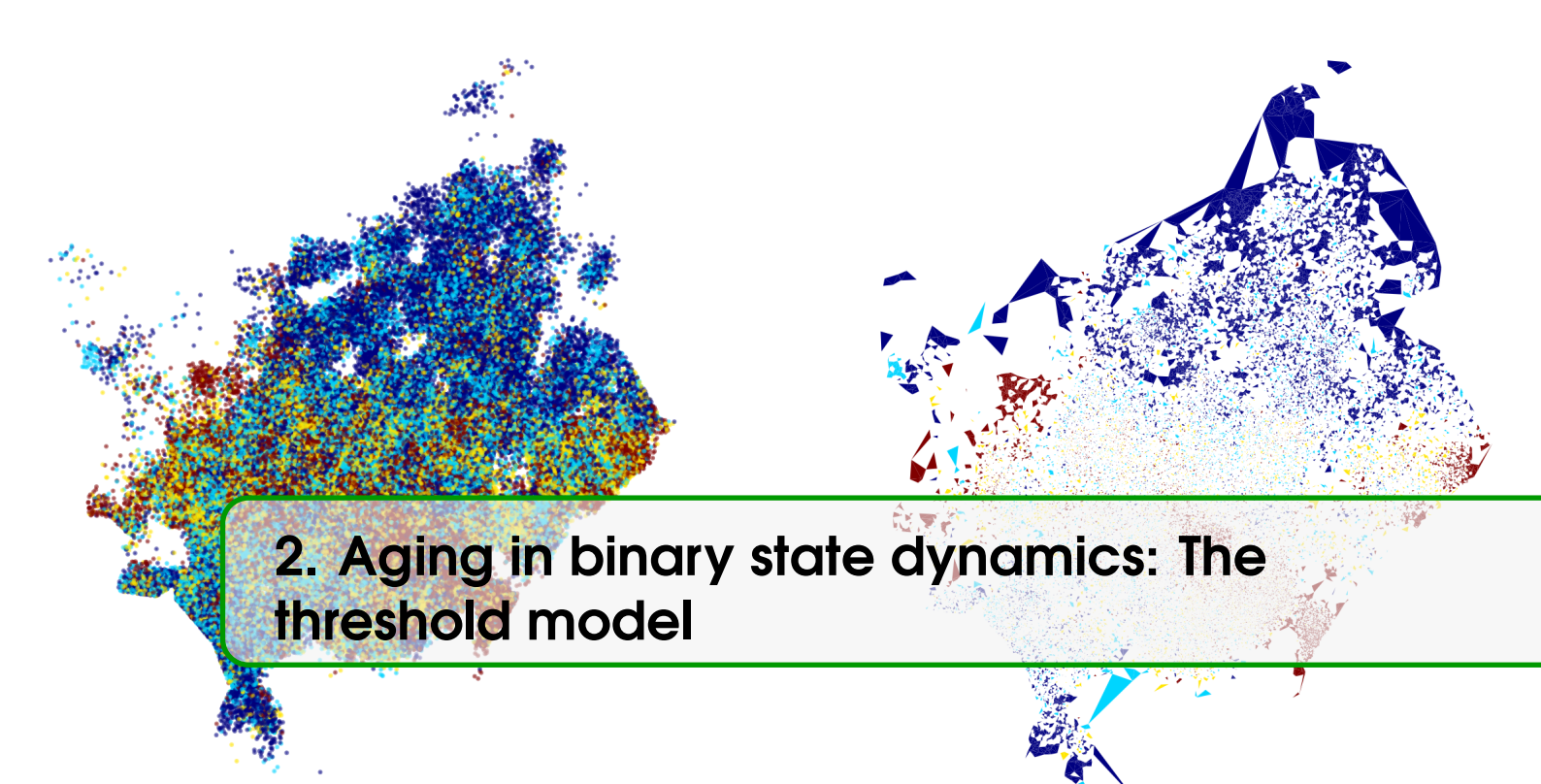
Unnumbered Section

Unnumbered Subsection

Unnumbered Subsubsection

Aging in threshold models

2	Aging in binary state dynamics: The threshold model	17
2.1	Introduction	17
2.2	Aging and the Threshold model	18
2.3	Dynamics on Complex networks	19
2.4	Dynamics on a Moore lattice	30
2.5	Conclusions	30
3	Aging effects in the Schelling segregation model	35
3.1	Introduction	35
3.2	Methods	37
3.3	Results	38
3.4	Summary and discussion	44
4	Ordering dynamics and aging in the Symmetrical Threshold model	47
4.1	Theorems	47
4.2	Definitions	47
4.3	Notations	47
4.4	Remarks	48
4.5	Corollaries	48
4.6	Propositions	48
4.7	Examples	48
4.8	Exercises	48
4.9	Problems	49
4.10	Vocabulary	49



2. Aging in binary state dynamics: The threshold model

We study the non-Markovian effects associated with aging for binary-state dynamics in complex networks. Aging is considered as the property of the agents to be less prone to change state the longer they have been in the current state, which gives rise to heterogeneous activity patterns. In particular, we analyze aging in the Threshold model, which has been proposed to explain the process of adoption of new technologies. Our analytical approximations give a good description of extensive Monte Carlo simulations in Erdős-Rényi, random-regular and Barabási-Albert networks. While aging does not modify the cascade condition, it slows down the cascade dynamics towards the full-adoption state: the exponential increase of adopters in time from the original model is replaced by a stretched exponential or power law, depending on the aging mechanism. Under several approximations, we give analytical expressions for the cascade condition and for the exponents of the adopters' density growth laws. Beyond random networks, we also describe by Monte Carlo simulations the effects of aging for the Threshold model in a two-dimensional lattice.

2.1 Introduction

Stochastic binary-state models are a versatile tool to describe a variety of natural and social phenomena in systems formed by many interacting agents. Each agent is considered to be in one of two possible states: susceptible/infected, adopters/non-adopters, democrat/republican, etc, depending on the context of the model. The interaction among agents is determined by the underlying network and the dynamical rules of the model. There are many examples of binary-state models, including processes of opinion formation [0, 0, 0, 0], disease or social contagion [0, 0], etc. Extended and modified versions of these models can lead to very different dynamical behaviors than in the original model. As examples, the use of multi-layer [0, 0, 0] or time-dependent networks [0], higher-order interactions [0, 0, 0], non-linear collective phenomena [0, 0], noise [0] and non-Markovian [0, 0, 0, 0] effects induce significant changes to the dynamics.

A well-known binary-state model is the Threshold model [0], introduced by M. Granovetter [0], for rumor propagation, adoption of new technologies, riots, stock market herds, political and environmental campaigns, etc. These are examples of *Complex Contagion* processes [0, 0] in which contagion, at variance with *Simple Contagion* (such as in the Voter and SIS models), requires simultaneous exposure to multiple adopter neighbors and a threshold fraction of neighboring agents that have already undergone contagion. Complex contagion implies a process of group or many-agent interactions built from a combination of pairwise interactions. The discontinuous phase transition and the cascade condition exhibited by the Threshold model were predicted with analytical tools in Ref. [0]. This model has been extensively studied in regular lattices and small-

world networks [0], random graphs [0], modular and community structure [0], clustered networks [0, 0], hypergraphs [0], homophilic networks [0], etc. Moreover, recent studies also include variants of the adoption rules including the impact of opinion leaders [0] and seed-size [0], on-off threshold [0] and the competition between simple and complex contagion [0, 0, 0]. Additionally, the Threshold model has been confronted with several sources of empirical data [Centola-2010, 0, 0, 0, 0, 0, 0, 0].

Theoretical and computational studies of stochastic binary-state models, including the Threshold model, usually rely on a Markovian assumption for its dynamics. However, there is strong empirical evidence against this assumption in human interactions. For example, bursty non-Markovian dynamics with heavy-tail inter-event time distributions, reflecting temporal activity patterns, have been reported in many studies [0, 0, 0, 0, 0, 0]. The understanding of these non-Markovian effects is in general a topic of current interest [0, 0, 0, 0]. In particular, for the Threshold model, memory effects have been included as past exposures' memory [0], message-passing algorithms [0], memory distributions for retweeting algorithms [0] and timers [0].

Aging is an important non-Markovian effect that we address in this paper for binary-state models. Aging accounts for the influence that the persistence time of an agent in a given state modifies the transition rate to a different state [0, 0, 0, 0, 0], so that, the longer an agent remains in a given state, the smaller is the probability to change it. Aging effects have been already shown to modify binary-state dynamics very significantly. For example, aging is able to produce coarsening towards a consensus state in the Voter model [0, 0], to induce continuous phase transitions in the noisy Voter model [0, 0] or to modify the phase diagram and non-equilibrium dynamics of Schelling segregation model [0].

In the specific context of innovation adoption, other mechanisms of inertia or resistance to adopt the technology have been already introduced. In fact, the original approach of Rogers [0] considers a fraction of "laggards" that will resist innovating until a large majority of the population has already adopted it. Similar articles highlight the importance of timing interactions [0] and the effect of "contrarians" (tendency to act against the majority), which has an important impact on the dynamics [0, 0]. In Ref. [0], it is discussed how different technologies may show different adoption cascades regarding the balance between advertisement and resistance to change.

In this paper, we provide a general theoretical framework to discuss aging effects building upon a general Markovian approach for binary-state models [0, 0]. We build a general master equation for any binary-state model with temporal activity patterns and we propose two different aging mechanisms giving rise to heterogeneous activity patterns, characterized by flat-tail inter-event time distributions. As an example, we apply this framework to the Threshold model for Complex Contagion. Theoretical predictions are matched with extensive Monte Carlo simulations in different networks. In addition, the role of both aging mechanisms is also studied in a two-dimensional Moore lattice.

The paper is organized as follows. In the next section, we describe the original Threshold model and introduce exogenous and endogenous aging in the model. In section 2.3, numerical results are reported and contrasted with theoretical predictions for different complex networks. For completeness, in section 2.4 the case of a 2D-lattice is analyzed. The final section contains a summary and a discussion of the results. The derivation of the Approximate Master Equation for general binary-state dynamics with aging effects is given in the Appendix.

2.2 Aging and the Threshold model

In the standard Threshold model [0, 0], one considers a network of N interacting agents. Each node of the network represents an agent i with a binary-state variable $\sigma_i = \{0, 1\}$ and a given threshold T ($0 < T < 1$). The state indicates if the agent has adopted a technology (or joined a riot, spread a meme or fake news, etc.) or not. We use the wording of a technology adoption process for the rest of the paper. If a node i (with k neighbors) has not adopted ($\sigma_i = 0$) the technology, becomes

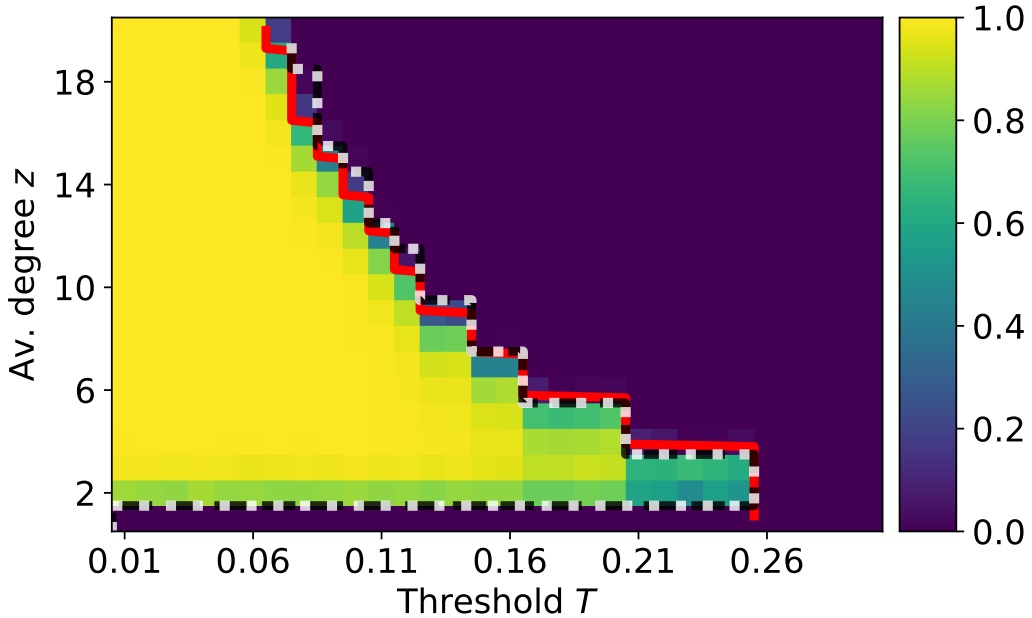


Figure 2.1: Average density ρ of adopters for an Erdős-Rényi graph of mean degree z using a model with threshold T . Color-coded values of ρ are from Monte Carlo simulations of the model without aging in a graph with $N = 10,000$ agents. Black dashed and white dotted lines correspond to T_c value obtained numerically for the model with exogenous and endogenous aging, respectively. Monte Carlo simulations are averaged over $M = 5 \times 10^4$ realizations. The red solid line is the analytical approximation of the cascade boundary, from Eq. (2.17), which is the same with and without aging.

adopter ($\sigma_i = 1$) if the fraction m/k of neighbors adopters exceeds the threshold T . Adopter nodes cannot go back to the non-adopter state.

In the Threshold model with aging, each agent has an internal time $j = 0, 1, 2, \dots$ (in Monte-Carlo units) as in Refs. [0, 0, 0, 0, 0, 0, 0, 0, 0]. As initial condition, we set $j = 0$ for all nodes. In Monte Carlo simulations, we follow a Random Asynchronous Update in which agents are activated in discrete time steps with probability $p_A(j) = 1/(j+2)$. When a non-adopter agent is activated, he/she changes state according to the threshold condition $m/k > T$. We will consider two different aging mechanisms, endogenous and exogenous aging [0], which account for the power law inter-event time distributions empirically observed in human interactions [0]. For endogenous aging, the internal time measures the time spent in the current state: If an agent in an updating attempt is not activated or does not adopt, the internal time increases by one unit. Therefore, the longer an agent has remained without adopting the technology, the more difficult it is for him/her to adopt it.

For exogenous aging, the internal time accounts for the time since the last attempt to change state: In each updating attempt in which the agent is activated, the internal clock resets to $j = 0$ even if there is no adoption. In this case, aging is understood as a resistance to adopt the technology the longer the agent has not been induced to consider adoption by some external influence.

2.3 Dynamics on Complex networks

In this section we discuss the Threshold model with endogenous and exogenous aging in three different complex networks: random-regular [0], Erdős-Rényi [0] and Barabási-Albert [0].

2.3.1 Numerical results

For the networks considered, the Threshold model undergoes a discontinuous phase transition at a certain critical value T_c , which is called cascade condition [0]. For $T < T_c$, a small initial seed of adopters triggers a global cascade where, on average, a significant proportion of agents in the system adopt the technology (change from $\sigma_i = 0$ to 1). In our analysis, the initial condition is set to favor cascades: one agent i with degree $k_i = z$ is selected randomly and all him/her neighbors are initially adopters, as in Ref. [0, 0]. For $T > T_c$, there are few cascade occurrences and none of them is global. The cascade condition dependence with the average degree z of the underlying network has been studied in Refs. [0, 0]. For the two aging mechanisms considered, Monte Carlo simulations in random graphs show that the T_c dependence on z is very similar to the one for the model without aging (see Fig. 2.1). Therefore, for large connected networks, tends to the same cascade condition derived for the original Threshold model (which for ER graphs is $T_c = 1/z$ [0]). This result is not obvious a priori because aging has been shown to modify the final state in several models [0, 0, 0, 0, 0, 0, 0, 0, 0]. This is discussed in detail in Appendix B.

Even though aging in the Threshold model does not modify the cascade condition, it has a large impact in the complex contagion cascade dynamics (Fig. 2.2). From Monte Carlo simulations in a random regular graph we find that, without aging, the average fraction of adopters follows an initial exponential increase with time (see Fig. 2.2a and 2.3a),

$$\rho(t) \sim \rho_0 e^{\alpha t}, \quad (2.1)$$

where ρ_0 is the initial fraction of adopters (seed). This behavior is universal for all values of the control parameters z and T below the cascade condition. In addition, we investigated the approach to the full-adopt state ($\rho = 1$) and we found that the number of non-adopters follows an exponential decay $1 - \rho(t) \sim e^{-t}$ for all values of the control parameters (see inset in Fig. 2.3a).

When aging is introduced, the cascade dynamics are much slower than an exponential law (see Fig. 2.2b). For endogenous aging, all agents non-adopters have the same activation probability $p_A(j)$, which decreases at each time step. This gives rise to cascade dynamics well-fitted by a power law increase (see Fig. 2.3b),

$$\rho(t) \sim \rho_0 \left(\frac{t+2}{2} \right)^\delta. \quad (2.2)$$

For exogenous aging, we observe a slow adoption spread at the beginning followed by a cascade where almost all agents adopt the technology (Fig. 2.2c). This behavior is well-fitted with a stretched exponential increase of the number of adopters (see Fig. 2.3c),

$$\rho(t) \sim \rho_0 e^{\beta((t+2)/2)^\gamma}. \quad (2.3)$$

For both aging mechanisms, in the last stages of evolution, a few “stubborn” non-adopters remain, although the environment favors the adoption. Due to the chosen activation probability, the number of non-adopters decay with a power law $1 - \rho(t) \sim 1/(t+2)$ in both cases (see insets at Fig. 2.3(b-c)).

Comparing the evolution of the original model with one of the versions with aging, we observe an important separation of time scales. While for the original model, the time to reach the steady state follows a logarithmic increase with the system size, the versions with endogenous and exogenous aging show a power law and a power-logarithmic dependence, respectively (see Fig. 2.4). Therefore, the time scale separation between the original model and the versions with aging increases as we increase the system size, and thus, the aging effects are more relevant for large systems.

The power law and the stretched exponential dynamics for endogenous and exogenous aging, respectively, are observed for all parameter values z and T below the cascade condition ($T < T_c$)

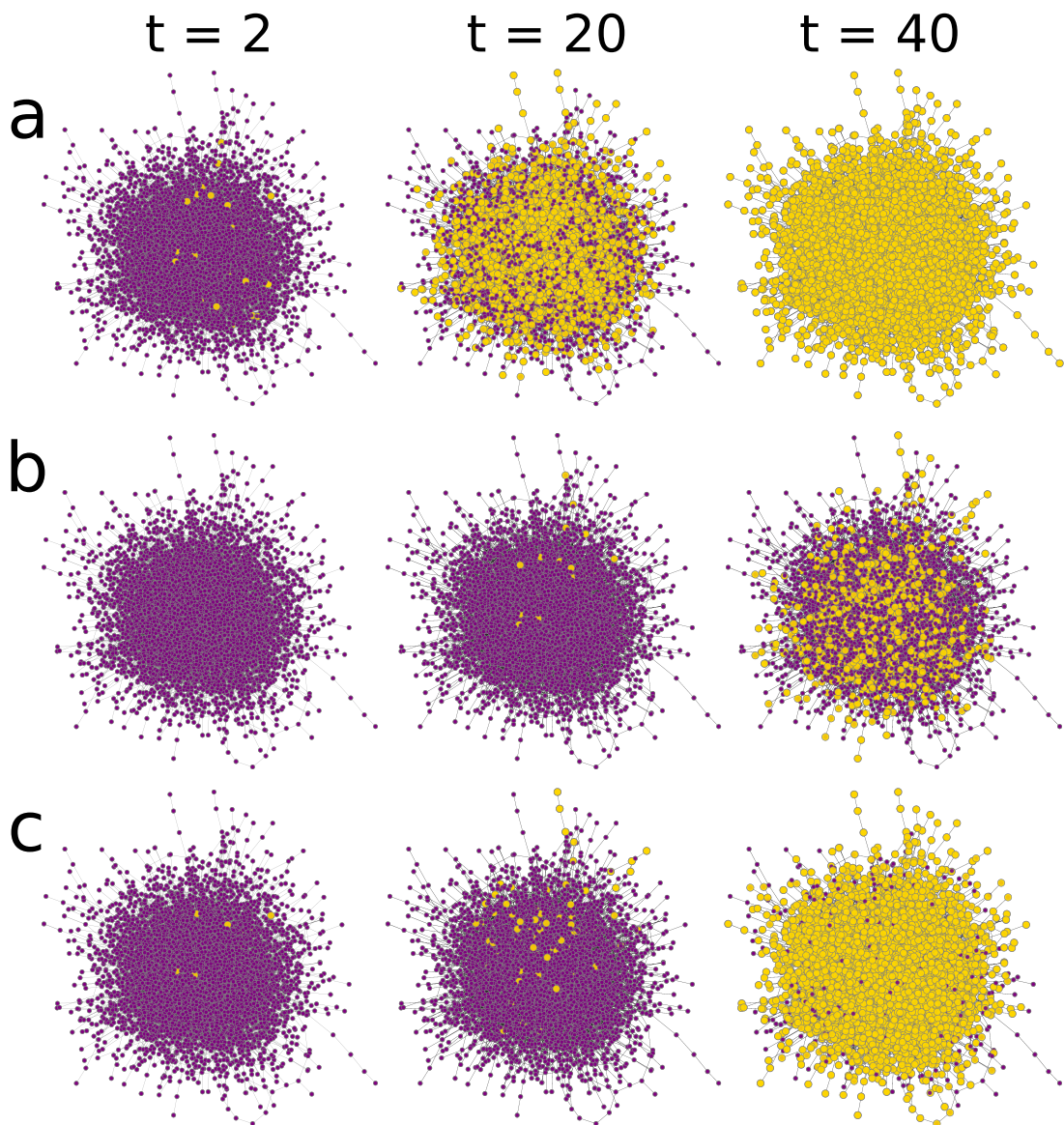


Figure 2.2: Cascade spreading for the original Threshold model (a), and the versions with endogenous (b) and exogenous (c) aging. Yellow nodes are adopters and purple nodes are non-adopters. Time increases from left to right. Monte Carlo simulations are performed in an Erdős-Rényi network with mean degree $z = 3$ and $T = 0.22$. System size is $N = 8,000$.

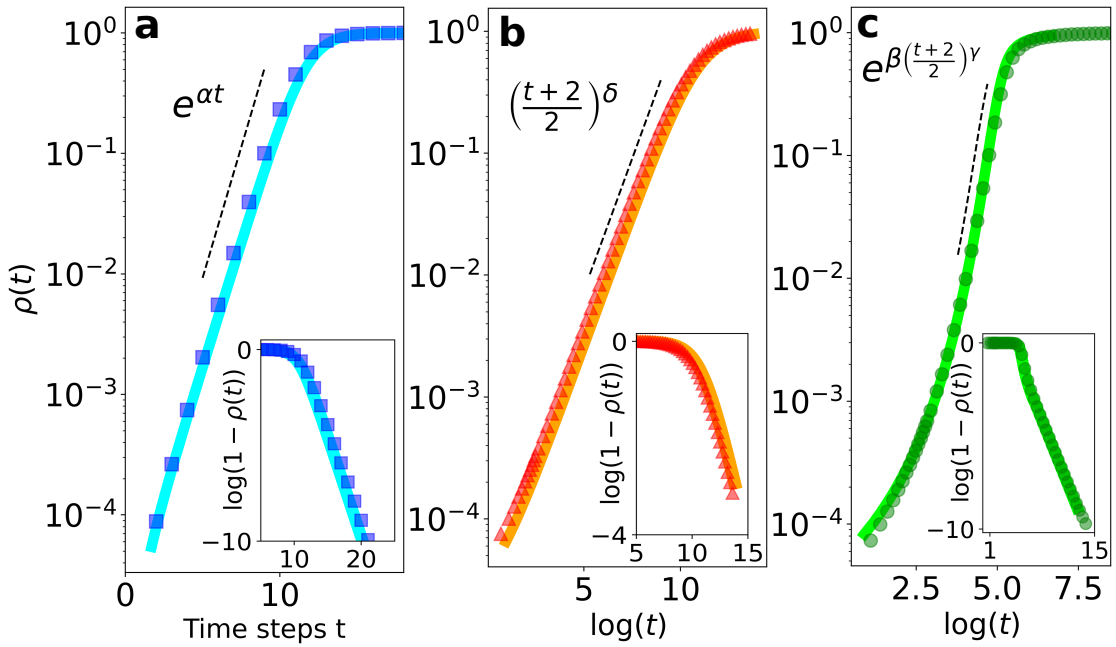


Figure 2.3: Cascade dynamics and fall to the full-adopt state ($\rho \sim 1$) of the Threshold model without aging (a) and the versions with endogenous (b) and exogenous (c) aging effects. At (b-c), the evolution is plotted as a function of the logarithm of time $\log(t)$ in Monte Carlo steps, as in the insets. The underlying network is a 3-regular random graph and the threshold is $T = 0.2$. The exponent values are $\alpha \simeq 1.0$, $\beta \simeq 1.14$, $\gamma \simeq 0.38$ and $\delta \simeq 1.0$. Numerically integrated solutions of Eq. (2.4) (solid lines) describe accurately the numerical results. Monte Carlo simulations are averaged over $M = 5 \times 10^4$ realizations in a network of $N = 1.6 \times 10^5$ nodes.

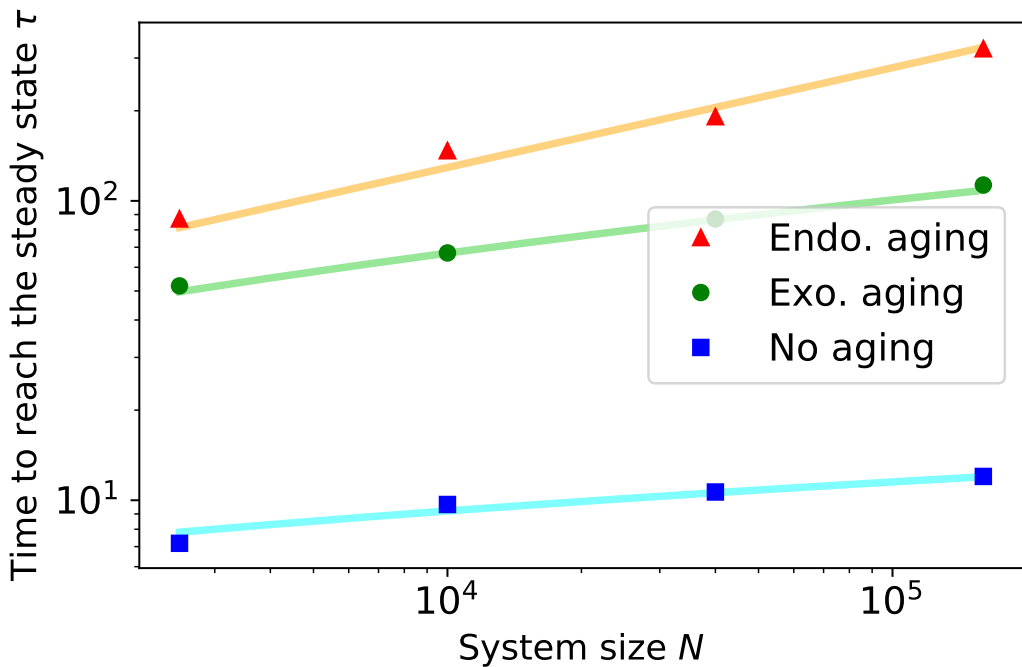


Figure 2.4: Average time to reach the steady state ($\rho > 0.9$) τ as a function of the system size N for the original Threshold model and the versions with endogenous and exogenous aging. The underlying network is a 5-regular random graph and the threshold is $T = 0.12$. Monte Carlo simulations are averaged over $M = 5 \times 10^4$ realizations. Solid lines are the system size-dependent timescale: For the original model, $\tau_{\text{NOAG}} = (1/\alpha) \log(N)$, for the endogenous ($\tau_{\text{ENDO}} = 2N^{1/\delta} - 2$) and for the exogenous aging ($\tau_{\text{EXO}} = 2(\log(N)/\beta)^{1/\gamma} - 2$), which follows from the dynamics from Eq. (2.1), (2.2) and (2.3). The exponents α , β , γ and δ are fitted exponents.

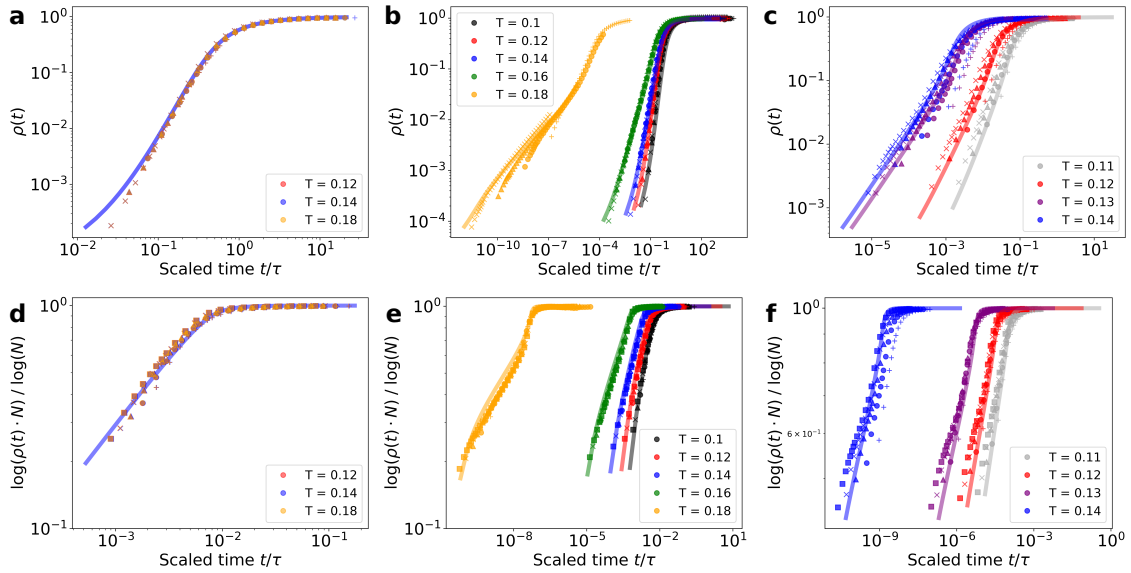


Figure 2.5: Cascade dynamics of the Threshold model with endogenous (a - c) and exogenous (d - f) aging. From the left column to the right: a random regular graph with degree $z = 5$ (a and d), an Erdős-Rényi graph with average degree $z = 5$ (b and e) and a Barabási-Albert graph with average degree $z = 8$ (c and f). Different colors indicate different values of T and markers correspond to different system sizes: $N = 2,500$ (plus), $10,000$ (circles), $40,000$ (triangles), $160,000$ (crosses) and $640,000$ (squares). Time is scaled according to the system size for each model: $\tau_{\text{EXO}} = 2(\log(N)/\beta)^{1/\gamma} - 2$, $\tau_{\text{ENDO}} = 2N^{1/\delta} - 2$, where β, γ and δ are the fitted exponents from the behavior according to Eq. (2.2) and (2.3). Solid lines are obtained from the solutions of Eq. (2.13). Monte Carlo simulations are averaged over $M = 5 \times 10^4$ realizations.

and for all system sizes. This is shown in Fig. 2.5 for a random regular, Erdős-Rényi and Barabási-Albert networks. In particular, we show that the time-dependent behavior for different system sizes collapses to a single curve when time is scaled with the system size-dependent timescale (previously analyzed in Fig. 2.4) that follows from either the power law dynamics ($\tau_{\text{ENDO}} = 2N^{1/\delta} - 2$) or the stretched exponential law ($\tau_{\text{EXO}} = 2(\log(N)/\beta)^{1/\gamma} - 2$). Notice that the scaling of the y-axis is necessary for Fig. 2.5(d-f) to show a linear dependence (for all system sizes) due to the stretched exponential increase.

A different question is the dependence of the exponents of the power law and stretched exponential with the parameters z and T . Numerical results from fitted Monte Carlo simulations for $\alpha(z, T)$, $\delta(z, T)$ and $\gamma(z, T)$ are shown in Figs. 2.6 and 2.7. For a random-regular graph, as apparent from Fig. 2.5, the exponents do not depend on the parameter T up to T_c (so the exponents are dependent only on z , $\alpha(z)$, $\gamma(z)$ and $\delta(z)$), while for Erdős-Rényi and Barabási-Albert networks the value of the exponents decrease with T when approaching T_c , indicating a slowing down of the dynamics. Also, for these two latter networks, the exponents present a maximum value at a certain value of z . This maximum value at a certain z for a fixed T can be understood as being between the two critical lines of Fig. 2.1.

2.3.2 General mathematical description

To account for the non-Markovian dynamics introduced by the aging mechanism, we need to go beyond the standard mathematical descriptions of the Threshold model [0, 0, 0]. We do so using a Markovian description by enlarging the number of variables [0, 0]. Namely, we classify the agents with degree k , number of adopter neighbors m and age j as different sets in a compartmental model in a general framework for binary-state dynamics in complex networks [0, 0, 0]. Assuming a local tree-like network structure, as the one generated using the configuration model for a generic degree distribution p_k [0, 0] or Erdős-Rényi model, we derive a general master equation¹ for binary-state dynamics with temporal activity patterns in complex networks considering the following possible transitions (see Appendix C for details):

- A susceptible (infected) node changes state and resets internal age with probability $F(k, m, j)$ ($R(k, m, j)$);
- A susceptible (infected) node remains in the same state and resets internal age to zero ($j \rightarrow 0$) with probability $F_R(k, m, j)$ ($R_R(k, m, j)$);
- A susceptible (infected) node remains in the same state and ages ($j \rightarrow j + 1$) with probability $F_A(k, m, j)$ ($R_A(k, m, j)$).

See a schematic representation in Fig. C.1. Note that we introduce here epidemics notation of susceptible/infected nodes [0, 0], but it is immediately translated to the non-adopter/adopter situation of our model. For the specific case of the Threshold model, dynamics are monotonic and $R(k, m, j) = 0$ (no adopter becomes a non-adopter). Moreover, when an agent becomes an adopter, there are neither resetting nor aging events $R_R(k, m, j) = R_A(k, m, j) = 0$. This means as well that equations for the non-adopters $s_{k,m,j}$ and adopters $i_{k,m,j}$ nodes are independent. Thus, we can write the following rate equations for the evolution of the fraction $s_{k,m,j}(t)$ of k -degree non-adopters

¹We use here the term “master equation” for consistency with Refs. [0, 0], but the word “master” has a different meaning than the one used to describe an equation for the probability distribution [0]

nodes with m infected neighbors and age j :

$$\begin{aligned} \frac{ds_{k,m,j}}{dt} &= -s_{k,m,j} - (k-m)\beta^s s_{k,m,j} \\ &\quad + (k-m+1)\beta^s s_{k,m-1,j-1} \\ &\quad + F_A(k, m, j-1) s_{k,m,j-1}, \\ \frac{ds_{k,m,0}}{dt} &= -s_{k,m,0} - (k-m)\beta^s s_{k,m,0} \\ &\quad + \sum_{l=0} F_R(k, m, l) s_{k,m,l}, \end{aligned} \tag{2.4}$$

where β^s is a non-linear function of $s_{k',m',j'}$ for all values of k',m' and j' (see Eq. (C.4)). The remaining step is to define explicitly the transition probabilities for our aging mechanisms. For both exogenous and endogenous aging, the adoption probability is the probability that an agent is activated and has a fraction of adopters that exceeds the threshold T , which means that

$$F(k, m, j) = p_A(j) \theta(m/k - T), \tag{2.5}$$

where $\theta(\cdot)$ is the Heaviside step function.

The reset and aging probabilities for endogenous and exogenous aging mechanisms are different. The simplest case is endogenous aging where there is no reset $F_R(k, m, j) = 0$ and agents increase by one the age with probability

$$\begin{aligned} F_A(k, m, j) &= 1 - F(k, m, j) \\ &= 1 - p_A(j) \theta(m/k - T). \end{aligned} \tag{2.6}$$

When aging is exogenous, the reset probability is the probability to activate and not adopt

$$F_R(k, m, j) = p_A(j) (1 - \theta(m/k - T)). \tag{2.7}$$

Thus, agents that age are just the ones that do not activate, $F_A(k, m, j) = 1 - p_A(j)$.

Using these definitions, we have integrated numerically Eq. (2.4) for the Threshold model with both endogenous and exogenous aging. Numerical solutions give good agreement with Monte Carlo simulations (see Fig. 2.3). However, in a general network, considering a cutoff for the degree $k = 0, \dots, k_{\max}$ and age $j = 0, \dots, j_{\max}$, the number of differential equations to solve is $(k_{\max} + 1)(k_{\max} + 1)(j_{\max} + 1)$ according to the three subindexes of the variable $s_{k,m,j}$. This number grows with the largest degree square and largest age considered and thus, some further approximations are needed to obtain a convenient reduced system of differential equations.

As an ansatz, we assume that timing interactions can be effectively decoupled from the adoption process so the solution of Eq. (2.4) can be written as

$$s_{k,m,j}(t) = s_{k,m}(t) G_j(t), \tag{2.8}$$

where $s_{k,m}$ is the fraction of non-adopters with degree k and m infected neighbors $s_{k,m} = \sum_j s_{k,m,j}$ and there is an age distribution $G_j(t)$, independent of the adoption process.

If we sum over the variable age j in Eq. (2.4), we can rewrite the following rate equations for the variables $s_{k,m}$

$$\begin{aligned} \frac{ds_{k,m}}{dt} &= -\langle p_A \rangle \theta(m - kT) s_{k,m} \\ &\quad - (k-m)\beta^s s_{k,m} + (k-m+1)\beta^s s_{k,m-1}, \end{aligned} \tag{2.9}$$

where aging effects are just included in $\langle p_A \rangle(t)$:

$$\langle p_A \rangle(t) = \sum_{j=0}^{\infty} p_A(j) G_j(t). \tag{2.10}$$

Using the definition of the fraction of k-degree agents adopters $\rho_k(t)$,

$$\rho_k(t) = 1 - \sum_{j=0}^{\infty} \sum_{m=0}^k s_{k,m,j}, \quad (2.11)$$

and along lines of Ref. [0], we use the exact solution

$$s_{k,m} = (1 - \rho_k(0)) B_{k,m}[\phi], \quad (2.12)$$

where $B_{k,m}[\phi]$ is the binomial distribution with k attempts, m successes and with success probability ϕ . From this point, we derive from Eq. (2.9) a reduced system of two coupled differential equations for the fraction of adopters $\rho(t) = \sum_k p_k \rho_k(t)$ and an auxiliary variable $\phi(t)$ (see details in Ref. [0]):

$$\frac{d\rho}{dt} = \langle p_A \rangle [h(\phi) - \rho], \quad (2.13)$$

$$\frac{d\phi}{dt} = \langle p_A \rangle [g(\phi) - \phi],$$

where $\phi(t)$ can be understood as the probability that a randomly chosen neighbor of a non-adopter node is an adopter at time t . The functions $h(\phi)$ and $g(\phi)$ are nonlinear functions of this variable ϕ

$$h(\phi) = \sum_{k=0}^{\infty} p_k \left(\rho_k(0) + (1 - \rho_k(0)) \sum_{m=kT}^k B_{k,m}[\phi] \right), \quad (2.14)$$

$$g(\phi) = \sum_{k=0}^{\infty} \frac{k}{z} p_k \left(\rho_k(0) + (1 - \rho_k(0)) \sum_{m=kT}^k B_{k-1,m}[\phi] \right).$$

When $\langle p_A \rangle$ is replaced by a constant, Eqs. (2.13) reduce to previous results for the original model [0].

Determining the distribution $G_j(t)$ is not easy. For endogenous aging, all non-adopters have the same age at each time step and $G_j(t) = \delta(j-t)$ (where $\delta(\cdot)$ is the Dirac delta function). Therefore, $\langle p_A \rangle = 1/(t+2)$. The numerical solution of Eq. (2.13) gives a good agreement with Monte Carlo simulations (see Fig. 2.5(a-c)). For the case of exogenous aging, the reset of the internal clock makes more difficult a choice for $G_j(t)$. Inspired on the stretched exponential behavior of $\rho(t)$ observed from Monte Carlo simulations, we propose $\langle p_A \rangle = 1/(t+2)^\mu$. For $\mu = 0.75$, the numerical solutions of Eq. (2.13) gives a very good agreement with our Monte Carlo simulations (see Fig. 2.5 (d-f)).

2.3.3 Analytical results

To obtain an analytical result for the cascade condition and for the exponents of the predicted exponential, stretched-exponential and power law cascade dynamics that we fitted from Monte Carlo simulations, we need to go a step beyond the numerical solution of our approximated differential equations (Eqs. (2.4) and (2.13)).

For a global cascade to occur, it is needed that the variable $\phi(t)$ grows with time. If we assume a small initial seed ($\rho_k(0) \rightarrow 0$), Eq. (2.13) can be rewritten as in Ref. [0]

$$\frac{d\phi}{dt} = \langle p_A \rangle \left(-\phi + \sum_{k=1}^{\infty} \frac{k}{z} p_k \sum_{m=kT}^k B_{k-1,m}[\phi] \right). \quad (2.15)$$

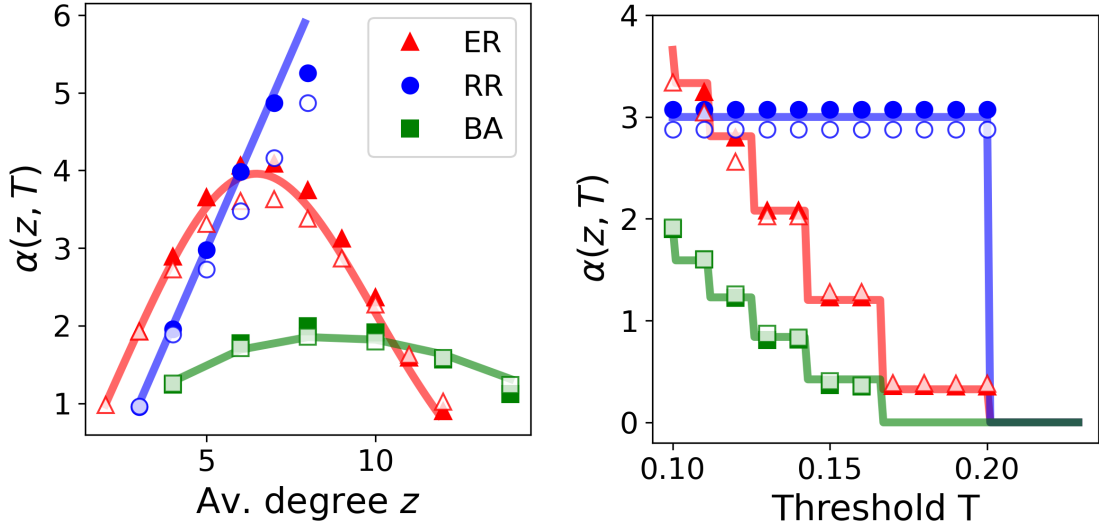


Figure 2.6: Exponent α for the original Threshold model (empty markers) and δ for the version with endogenous aging (filled markers) for different values of the average degree z (and $T = 0.1$) (left) and as a function of T for fixed z (right). Different markers indicate results from Monte Carlo simulations with different topologies: red triangles indicate an Erdős-Rényi (ER) graph, blue circles indicate a random regular (RR) graph and green squares indicate a Barabási-Albert (BA) graph. In the right panel, the average degree is fixed $z = 5$ for ER and RR, and $z = 8$ for the BA. Predicted values by Eq. (2.22) (solid lines) fit the results for each topology. System size is fixed at $N = 4 \times 10^6$ for the original model and $N = 3.2 \times 10^5$ for the version with aging.

Rewriting the sum term as $\sum_{l=0}^{\infty} C_l \phi^l$, with coefficients

$$C_l = \sum_{k=l}^{\infty} \sum_{m=0}^l \binom{k-1}{l} \binom{l}{m} (-1)^{l+m} \frac{k}{z} p_k \theta(m/k - T), \quad (2.16)$$

we linearize Eq. (2.15) around $\phi = 0$:

$$\frac{d\phi}{dt} \approx \langle p_A \rangle (C_1 - 1) \phi. \quad (2.17)$$

The solution for Eq. (2.17) is then

$$\phi(t) = \rho_0 e^{(C_1 - 1) \int_0^t \langle p_A \rangle(s) ds}, \quad (2.18)$$

given that $\phi(0) = \rho_0$.

Since $\langle p_A \rangle(t)$ is always positive, global cascades occur when $(C_1 - 1) > 0$. This cascade condition does not depend on the aging term $\langle p_A \rangle(t)$ and thus, it is the same as for the Threshold model without aging. In Fig. 2.1, the red solid line is the result of this analytical calculation, and it is in good agreement with the numerical results.

Linearization is also useful to determine the time dependence of the cascade process. Assuming a small initial seed and rewriting the term $h(\phi)$ as $\sum_{l=0}^{\infty} K_l \phi^l$, the linearized equation for the fraction of adopters $\rho(t)$ becomes

$$\frac{d\rho}{dt} \approx \langle p_A \rangle (K_1 - 1) \phi, \quad (2.19)$$

where the coefficients K_l are

$$K_l = \sum_{k=l}^{\infty} \sum_{m=0}^l \binom{k}{l} \binom{l}{m} (-1)^{l+m} p_k \theta(m/k - T). \quad (2.20)$$

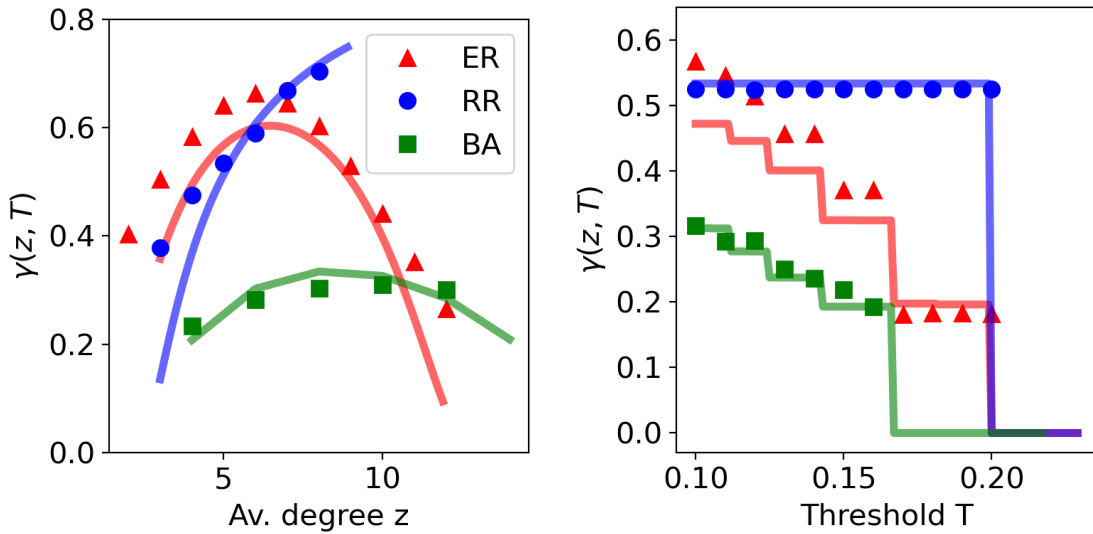


Figure 2.7: Exponent γ for the Threshold model with exogenous aging for different values of the average degree z ($T = 0.1$) (left) and as a function of T for fixed z (right). Different markers indicate results from Monte Carlo simulations with different topology: red triangles indicate an Erdős-Rényi (ER) graph, blue circles indicate a random regular (RR) graph and green squares indicate a Barabási-Albert (BA) graph. In the right panel, the average degree is fixed $z = 5$ for ER and RR, and $z = 8$ for the BA. Predicted values by numerical integration of Eqs. (2.13) (solid lines) fit approximately the results for each topology. System size is fixed at $N = 3.2 \times 10^5$.

A solution for the fraction of adopters $\rho(t)$ can be obtained from Eqs. (2.18) and (2.19). For the case of the Threshold model without aging, setting $\langle p_A \rangle = 1$, the solution is an exponential cascade dynamics

$$\rho(t) = \rho_0 e^{(C_1 - 1)t}. \quad (2.21)$$

Therefore, the number of adopters $\rho(t)$ follows an exponential increase with exponent $\alpha(z, T)$:

$$\alpha(z, T) = C_1 - 1 = \sum_{k=0}^{\lfloor 1/T \rfloor} \frac{k(k-1)}{z} p_k - 1, \quad (2.22)$$

where C_1 is computed from Eq. (2.16).

For endogenous aging, the same derivation is valid to determine the exponents $\delta(z, T)$. Using $\langle p_A \rangle = 1/(t+2)$, the fraction of adopters follows a power law dependence,

$$\rho(t) = \rho_0 \left(\frac{t+2}{2} \right)^{(C_1 - 1)}. \quad (2.23)$$

The exponent reported for the power law cascade dynamics $\delta(z, T)$ turns out to be, therefore, the same exponent as the one for the exponential behavior where there is no aging: $\delta(z, T) = \alpha(z, T) = C_1 - 1$. Fig. 2.6 compares the prediction of Eq. (2.22) with the results computed from Monte Carlo simulations. There is a good agreement for both Barabási-Albert and Erdős-Rényi networks for all values of T and z . For a random-regular graph, the predicted dependence, $\alpha(z) = z - 2$, is not a good approximation for large z . This is because the presence of small cycles increases importantly in a random-regular graph as the average degree z grows [0] and the locally-tree assumption made for the derivation of the rate equations (Eq. (2.4)) is not valid anymore. A different approach is necessary for clustered networks (as in Ref.[0] for the Threshold model).

For exogenous aging, an analytical expression for the exponent $\gamma(z, T)$ is not obtained following this methodology. Still, we can fit the exponent from the numerical solutions in Fig. 2.5 (d-f). Fig.2.7 shows a good comparison between the exponent calculated from the numerical solutions (from the AME) and the one calculated from Monte Carlo simulations. The dependence of $\gamma(z, T)$ with the parameters z and T is qualitatively similar to the dependence of $\alpha(z, T)$.

2.4 Dynamics on a Moore lattice

The Threshold model in a two-dimensional regular lattice with a Moore neighborhood (nearest and next nearest neighbors) is known to have a critical threshold (cascade condition) $T_c = 3/8$ [0]. Below this value, cascade dynamics follows a power law increase in the density of adopters $\rho(t) \sim t^2$, which does not depend on the threshold value T . In Fig. 2.8a, we show a typical realization of this model: From an initial seed, the adoption radius increases linearly with time until all agents adopt the technology.

When aging is considered, cascade dynamics become much slower and a dependence on T appears. When the aging mechanism is exogenous, Monte Carlo simulations indicate cascade dynamics following a power law $\rho(t) \approx t^{\zeta(T)}$. Qualitatively, we observe that while in the case without aging there was a soft interface between adopter and non-adopters, aging causes a strong roughening in the interface and the presence of non-adopters inside the bulk (see Fig. 2.8b). In addition, the exponent values fitted from Monte Carlo simulations allow us to collapse curves for different system sizes (see Fig. 2.9a). Due to finite size effects, the interface between adopters and non-adopters eventually reaches the borders of the system and the remaining non-adopters, in the bulk, will slowly adopt with the density of adopters following the functional shape $\rho(t) = 1 - 1/(t+2)$.

Fig.2.8c shows the dynamics towards global adoption for endogenous aging. In comparison with the case of exogenous aging, we do not observe strong interface roughening between adopters and non-adopters, because non-adopters are not present in the bulk. Monte Carlo simulations indicate a very slow increase of the density of adopters ρ , similar to a power-logarithmic growth $\rho(t) \approx (\log(t))^\nu$, with a threshold dependent exponent $\nu(T)$ (Fig. 2.9b). Unfortunately, we were not able to find an analytical framework for the Threshold model in a Moore lattice. Our general approximation used for complex networks assumes a tree-like network, and it is not appropriate for this case.

2.5 Conclusions

We have addressed in this work the role of aging in general models with binary-state agents interacting in a complex network. Temporal activity patterns are incorporated by means of a variable that represents the internal time of each agent. We have developed an approximate Master Equation for this general situation. In this framework, we have explicitly studied the effect of aging in the Threshold model as a paradigmatic example of Complex Contagion processes. Aging implies a lower probability to change state when the internal time increases. We considered two aging mechanisms: endogenous aging, in which the internal time measures the persistence time in the current state, and exogenous aging, in which the internal time measures the time since the last update attempt.

Our theoretical framework with some approximations to attain analytical results provide a good description of the results from Monte Carlo simulations for Erdős-Rényi, random-regular and Barabási-Albert networks. For these three types of complex networks, we found that the cascade condition T_c (critical value of the threshold parameter T as a function of mean degree z of the network) for the full spreading from an initial seed is not changed by the aging mechanisms. However, aging modifies in non-trivial ways cascade dynamics of the process. The exponential growth with exponent $\alpha(z, T)$ of the density of adopters in the absence of aging becomes a power

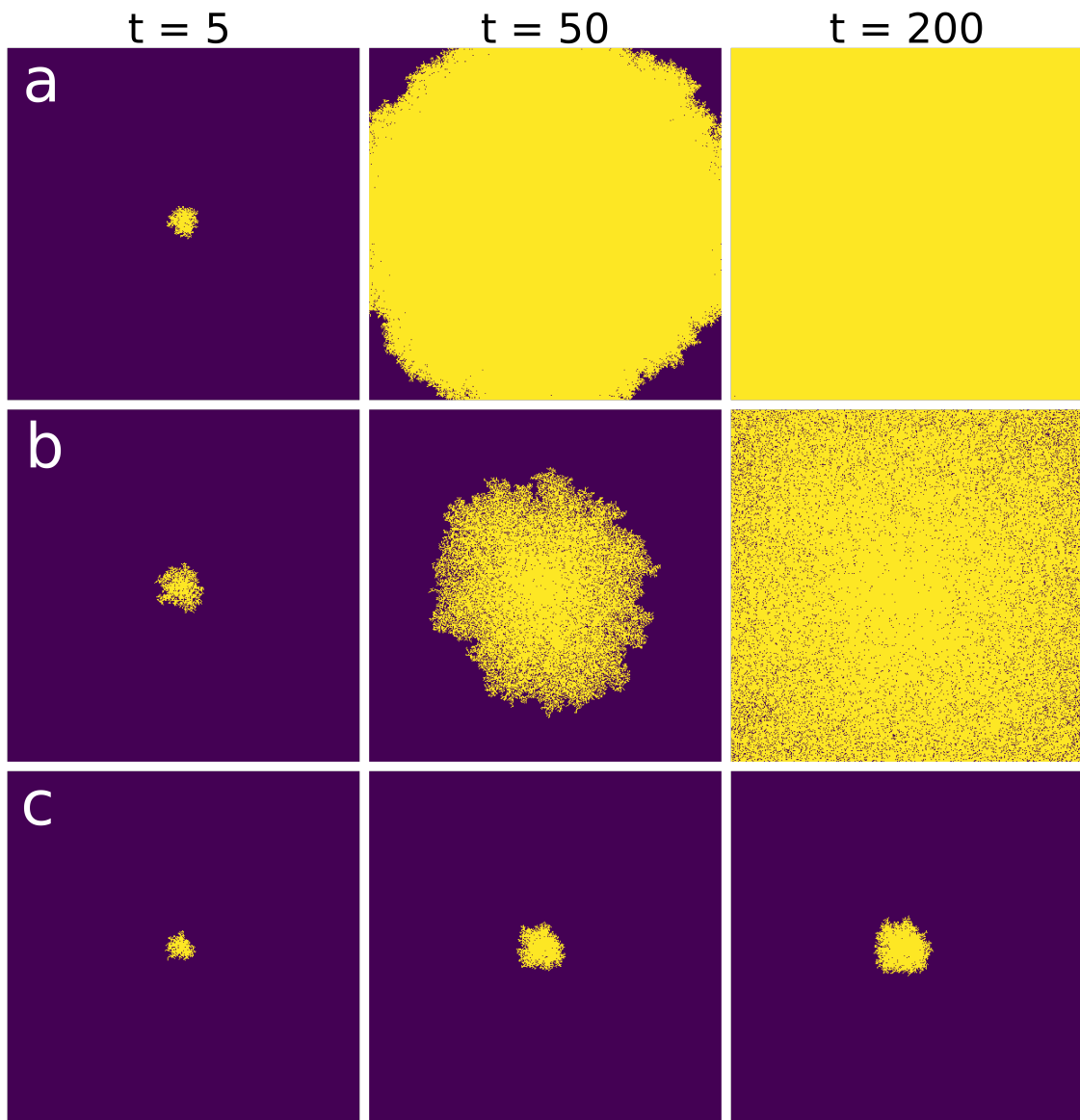


Figure 2.8: Cascade spreading of the original Threshold model (a) and the versions with exogenous (b) and endogenous (c) aging on a Moore neighborhood lattice with size $N = L \times L$, $L = 405$. Yellow and purple nodes are adopters and non-adopters, respectively. Time increases from left to right. Initial seeds are selected favoring cascades: one agent and all him/her neighbors are set as adopters at the center of the system.

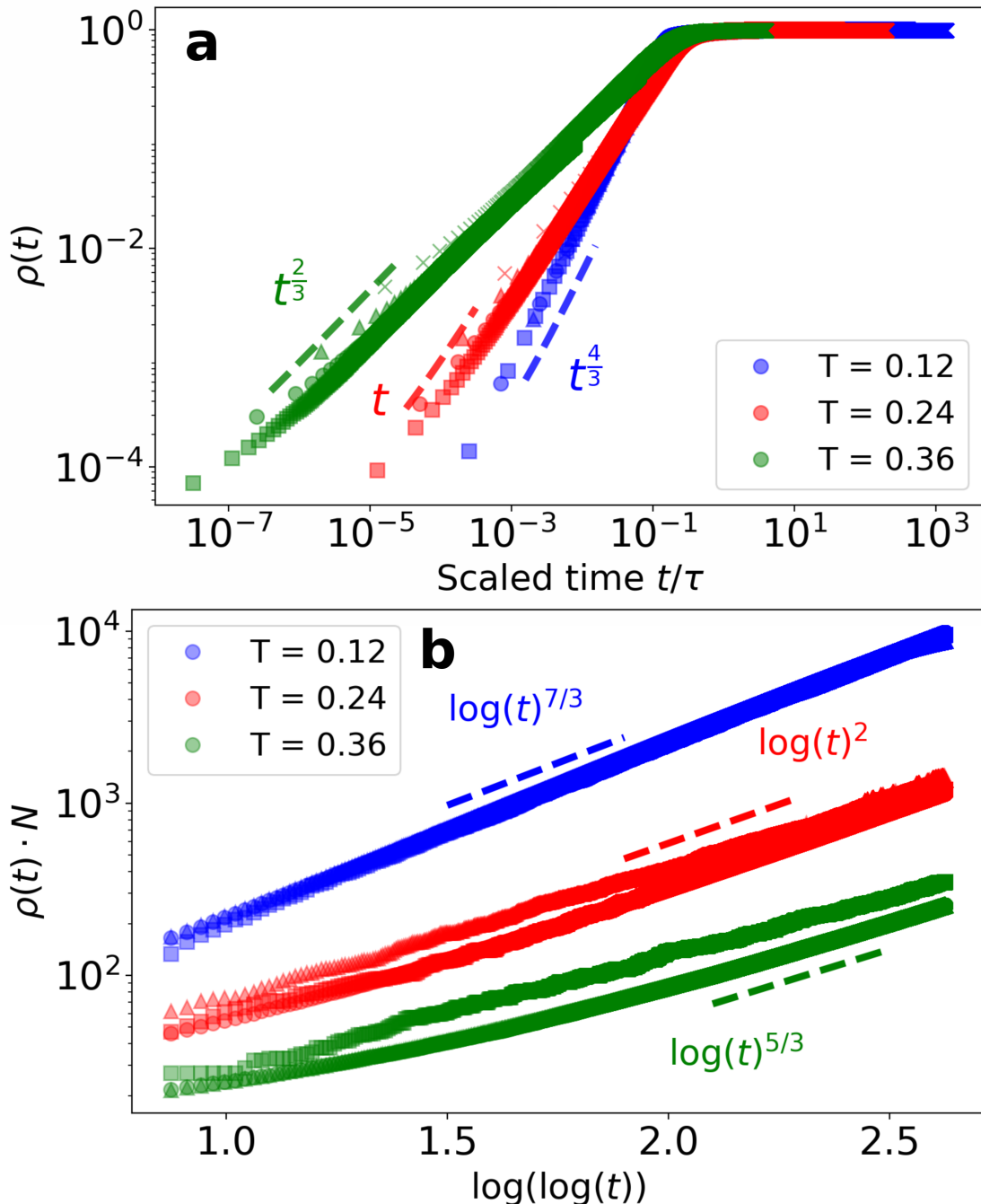
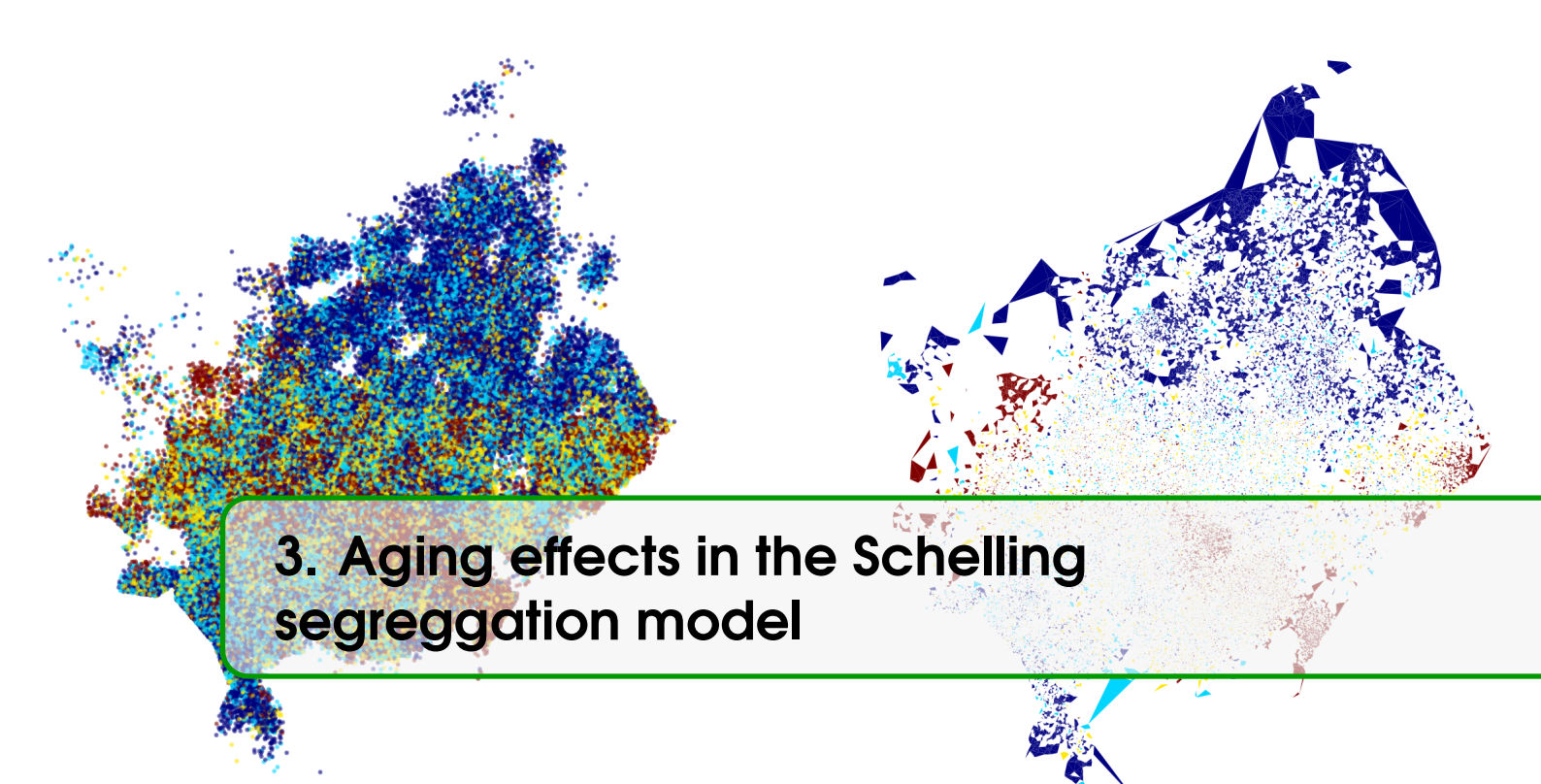


Figure 2.9: Cascade dynamics of the Threshold model with exogenous (a) and endogenous (b) aging on a Moore neighborhood lattice. Different colors indicate different values of the threshold T . Different markers indicate the results of Monte Carlo simulations with different system size $N = L \times L$: $L = 50$ (crosses), 100 (triangles), 200 (circles) and 400 (squares). In (a), time is scaled according to size $\tau = L^{2/\zeta}$. Discontinuous solid lines indicate a power law behavior with exponent $\zeta = 4/3$ (blue), 1 (red) and $2/3$ (green). In (b), the system sizes are not scaled due to the slow dynamics. Discontinuous solid lines indicate a power-logarithmic behavior, $\rho(t)N \sim \log(t)^v$, with exponent $v = 7/3$ (blue), 2 (red) and $5/3$ (green).

law with exponent $\delta(z, T)$ for endogenous aging, and a stretched exponential characterized by an exponent $\gamma(z, T)$ for exogenous aging. We have analyzed the exponents' dependence with the order parameters $\alpha(z, T)$, $\delta(z, T)$, $\gamma(z, T)$ and shown that $\delta(z, T) = \alpha(z, T)$.

Our general theoretical framework, based on the assumption of a tree-like network, is not appropriate for a regular lattice. In this case, we have been only able to run Monte Carlo simulations. Our results indicate that exogenous aging gives rise to adoption dynamics characterized by an increase in the interface roughness, by the presence of non-adopters in the bulk, and by a power law growth of the density of adopters with exponent $\zeta(T)$, while in the absence of aging $\zeta = 2$ independently of T . Endogenous aging, on the other hand, produces very slow (logarithmic-like) dynamics, with a threshold-dependent exponent $v(T)$.

This work highlights the importance of non-Markovian dynamics in general binary-state dynamics and, specifically, in the Threshold model. For the problem of innovation adoption that this model addresses, we show how persistence times have an important impact on the adoption cascade. In fact, in the lattice, for $T = 2/8$ and exogenous aging we recover a linear evolution for the number of adopters as in Ref. [0] for a mean-field model. Further work in this direction would be to categorize technologies according to the adoption curve, to show if the system has important resistance to the previous technology (endogenous aging) or a balance between memory and external influence or advertisement (exogenous aging). Furthermore, the theoretical framework presented here gives a basis for further investigations of the memory effects and non-Markovian dynamics in networks, and in particular for binary-state models with aging. Still, a number of theoretical developments remain open for future work, such as the consideration of stochastic finite size effects [0]. Also, proper approximations need to be developed to account for some of our numerical results for random-regular networks with high degree, as well as for high clustering, degree-degree correlations networks and for regular lattices, including continuous field equations for this latter case.



3. Aging effects in the Schelling segregation model

The Schelling model has become a paradigm in social sciences to explain the emergence of residential spatial segregation, even in the presence of high tolerance to mixed neighborhoods by the side of citizens. In particular, we consider a noisy constrained version of the Schelling model, in which agents maximize its satisfaction, related to the composition of the local neighborhood, by infinite-range movements towards satisfying vacancies. We add to it an aging effect by making the probability of agents to move inversely proportional to the time they have been satisfied in their present location. This mechanism simulates the development of an emotional attachment to a location where an agent has been satisfied for a while. The introduction of aging has several major impacts on the model statics and dynamics: the phase transition between a segregated and a mixed phase of the original model disappears, and we observe segregated states with a high level of agent satisfaction even for high values of tolerance. In addition, the new segregated phase is dynamically characterized by a slow power-law coarsening process similar to a glassy-like dynamics.

3.1 Introduction

Thomas Schelling introduced a simple segregation model [0, 0, 0, 0] in which agents of two colors are distributed randomly on a chess-board, leaving some locations free. Agents are unsatisfied if more than a half of the eight nearest neighbors have different color. Randomly, the unsatisfied agents will move to available satisfying locations of the neighborhood. This model has had a very significant impact for several reasons: The “hand-made” simulations performed by T. Schelling by moving pawns on a chessboard are an early precedent of the use of agent-based simulations in Social Sciences. It is also one of the first social models to show emergent behavior as a result of simple interactions among agents, a characteristic of complex systems. A robust result of the model is that segregation occurs even when individuals have a very mild preference for neighbors of their own type, so collective behavior is not to be understood in terms of individual intentions. In addition, the model introduced the concept of behavioral threshold that inspired a number of other models of collective social behavior [0]. But still currently, Schelling’s model is at the basis of fundamental studies of the micro-macro paradigm in Social Sciences [0], while it continues to have important implications for social and economic policies addressing the urban segregation problem [0, 0, 0, 0]. A main limitation of the Schelling model is that it has no history or memory by which, for example, residents might prefer to maintain their present location [0]. In this paper we address this limitation on the effects of memory.

As a result of the notable implications of this model and the robustness of the emerging

segregation, there exists a vast literature around Schelling's results. Many variants of the original Schelling model have been reported modifying the rules that govern the dynamics, the satisfaction condition, or including other mechanisms, network effects, or specific applications [0, 0, 0, 0, 0, 0, 0, 0, 0, 0, 0, 0, 0, 0, 0, 0, 0, 0, 0, 0]. In particular, the Schelling model has been studied from a Statistical Physics point of view due to its close relation to different forms of Kinetic Ising-like models [0, 0], and also addressing general questions of clustering and domain growth phenomena, as well as for the existence of phase transitions from segregated to non-segregated phases. For example, the relation with phase separation in binary mixtures has been considered [0, 0], as well as the connection with the phase diagram of spin-1 Hamiltonians [0, 0, 0, 0]. In this context a useful classification of models is to distinguish between two possible types of dynamics [0]: "constrained", where agents just move to satisfying vacancies (if possible), and "unconstrained", where agents' motion does not prevent them to remain unsatisfied. In addition, the motion can be short-range (only to neighboring sites, as in the original model) or long-range. Constrained motion has been named "solid-like" because it generally leads to frozen small clusters, while unconstrained motion has been considered "liquid-like" because it allows for large growing clusters [0]. Including the motion of satisfied agents leads to a noisy effect playing the role of temperature in a statistical physics approach.

It is known that human interactions do not occur at a constant rate. They rather show a bursty character with a non-Poissonian inter-event time distribution that reflects a memory from past interactions. [0, 0, 0, 0, 0, 0] However, most social simulations, including simulations of variants of the Schelling model, implicitly assume a constant rate of interactions or state updating. "Aging" is one form of memory effect on which the rate of interactions depends on the persistence time of an agent in a state, modifying the transition to a different state [0, 0, 0]. This concept of aging, or "social inertia" [0], constrains the transitions in a way that the longer an agent remains in a given state, the smaller the probability to change it. Aging has been already shown to modify social dynamics very significantly. For example, in opinion dynamics, aging is able to produce coarsening towards a consensus state in the voter model [0, 0] or to induce a continuous phase transition in the noisy voter model [0]. With the motivation of established relevant effects of aging in opinion dynamics, our goal is to characterize how "aging" modifies the segregation dynamics of the Schelling model. In this context, aging must be understood as an emotional/economic attachment to a certain location linked to the persistence time in this location. This attachment balances the memory-less and purely rational considerations of the original model [0]. The aging-induced inertia, which results in resistance to movement, is minimalist modeling of behavior with many different possible causes. Besides the moving out cost due to the housing market fluctuations, aging accounts for the links established with the neighborhood's public goods, venues, schools, etc, which are known to be highly relevant in this context [0, 0, 0]. These urban elements are also a major consideration when households locate [0, 0, 0] and aging also accounts for the memory of this decision.

In this paper, aging is introduced in the Schelling model by considering that agents are less prone to change their location as they get older in a satisfying place. In other words, aging is introduced giving a smaller probability for satisfied agents to "move-out" the longer they have remained in a satisfying neighborhood. We implement this aging mechanism in the long-range noisy constrained version of the Schelling Model [0], for which a detailed phase diagram was reported. We study how this phase diagram is modified by the aging mechanism, finding that aging inhibits a segregated-mixed phase transition. This implies that aging favors segregation, a counter-intuitive result. We also describe the coarsening dynamics in the segregated phase showing that aging gives rise to a slower coarsening that breaks the time-translational invariance.

3.2 Methods

3.2.1 Model

The model considered in this work is a variant of the noisy constrained Schelling model [0] in which we explicitly include aging effects. For simplicity, we refer to this variant as the Schelling model during the rest of the paper to compare with the model presented here: the Schelling model with aging. For both, the system is established on a $L \times L$ Moore lattice with 8 neighbors per site and periodic boundary conditions, where agents of two kinds (representing, for instance, wealth levels, race, language, etc) occupy the sites. There are also empty sites (vacancies), where agents can move to, depending on their state and on the vacancy neighborhood. The condition of each site i of the lattice will be described with a variable σ_i that takes three possible values: $\sigma_i = \pm 1$ for the two kinds of agents and $\sigma_i = 0$ for vacancies. In addition, depending on the local environment, agents can be in two states: satisfied or unsatisfied. In our case, agents are satisfied if their neighborhood is constituted by a fraction of unlike agents lower than a fixed homogeneous parameter T . Otherwise, they are unsatisfied. Therefore, this control parameter T is a measure of how tolerant the population of the system is. We also need a non-zero vacancy density, $\rho_v > 0$, for agents to change their location. This ρ_v is understood as an extra parameter of the model. The initial configuration is built by randomly distributing the agents ($N_{\text{agents}} = L^2(1 - \rho_v)$). We always consider one half of agents of each kind.

In the Schelling model considered, an agent chosen by chance moves to a random satisfying vacancy (if any exists) independently of his/her initial state and of the distance. This process is repeated until the system reaches a stationary state. The movement of unsatisfied agents behaves as a driver for the system dynamics, while the motion of satisfied agents plays the role of noise. When tolerance T becomes larger, more satisfying vacancies are present in the system and the noise consequently increases.

The aging mechanism in our model is introduced by considering an activation probability of the agents inversely proportional to the time spent at a satisfied location, motivated by the definition for opinion dynamics [0]. This methodology was proposed to mimic the power-law like inter-event time distributions observed in real-world social systems [0, 0]. If an agent j is initially satisfied in her neighborhood, the internal time is set $\tau_j = 0$. Then, in every time step, a randomly chosen agent j follows different rules depending on whether she is originally satisfied or not. If unsatisfied, j moves to any random satisfying vacancy of the system. Otherwise, she moves to another satisfying vacancy with an activation probability $p_j = 1/(\tau_j + 2)$. In both cases, if no vacancy has a satisfying neighborhood, the agent j remains in the initial site. As before, these rules are iterated until the system reaches a stationary state (if possible). The time is counted in Monte-Carlo steps; after each Monte-Carlo step, that is after N_{agents} iterations, the internal time increases for all satisfied agents in one unit, $\tau_j \rightarrow \tau_j + 1$. Notice that, when an unsatisfied agent becomes satisfied due to the neighbor's motion, an internal time $\tau_j = 0$ is set for that agent. As for the Schelling model, there is a noise effect associated with the motion of satisfied agents. In this case, the intensity of this noise is related not only to the tolerance parameter T , but to the presence of aging as well. In fact, aging introduces more constraints to the movements and contributes to decreasing the noise.

Given the number of neighbors available in the Moore lattice, numerical simulations are only performed for a finite set of meaningful tolerance values: $\{1/8, 1/7, 1/6, \dots, 6/7, 7/8\}$. During all our analysis, we focus on the low vacancy density region of the phase diagram. In this region, there is an even smaller number of meaningful T values $\{1/8, 2/8, \dots, 7/8\}$, because the majority of agents do not see vacancies in their surroundings.

3.2.2 Metrics of segregation

Many metrics have been introduced in the literature to discern if the final state is segregated or not [0, 0, 0, 0]. The number of clusters is known to be directly related to the segregation because a high

presence of small clusters indicates a mixing between agents. As for the Schelling model[0], we compute the following metric related to the second moment of the cluster size distribution:

$$s = \frac{2}{(L^2(1-\rho_v))^2} \sum_{\{c\}} n_c^2, \quad (3.1)$$

where the index of the sum c runs over all the clusters $\{c\}$ and n_c is the number of agents in the cluster c . The average of s over realizations after reaching a stationary state is defined as the segregation coefficient $\langle s \rangle$. This metric is bounded between 0 and 1: $\langle s \rangle \rightarrow 1$ if there are only 2 equally-sized clusters, and $\langle s \rangle \rightarrow 0$ if the number of clusters tends to the number of agents. The cluster detection is performed using the Hoshen-Kopelman algorithm [0].

Another metric of segregation is the interface density [0], defined as the fraction of links connecting agents of different kinds. The calculation is done in two steps: estimating the interface density for each agent j , ρ_j , and then the average over all the agents ρ :

$$\rho_j = \frac{1}{2} \left(1 - \frac{\sigma_j \sum_{k \in \Omega_j} \sigma_k}{\sum_{k \in \Omega_j} \sigma_k^2} \right) \quad \text{and} \quad \rho = \frac{1}{N_{\text{agents}}} \sum_{j=1}^{N_{\text{agents}}} \rho_j, \quad (3.2)$$

where the indices k run over the neighborhood of agent j , Ω_j . If an agent j is surrounded only by vacant sites, we define by convention $\rho_j = 0$. Performing a realization average of ρ , we obtain the average interface density $\langle \rho \rangle$ in the stationary state is denoted as $\langle \rho_{\text{st}} \rangle$. The evolution of this metric allows us to study the coarsening process.

3.3 Results

3.3.1 Phase diagram

To discuss the phase diagram of our model, we focus on the region of parameters with a vacancy density $\rho_v < 50\%$ to avoid diluted states with a majority of vacancies. For this region, the Schelling model presents 3 different phases [0]: frozen, segregated and mixed. For low tolerance values, the system freezes in a disordered state, given that there are no satisfying vacancies for any kind of agent. With increasing tolerance, the system undergoes a transition toward a segregated state, which is characterized by a 2-clusters dynamical final state. Finally, for high values of T , after another transition, we find a dynamical disordered (mixed) state, in which a vast majority of vacancies are satisfying for both kinds of agents, and small clusters are continuously created and annihilated.

These three phases are characterized by measuring the segregation coefficient $\langle s \rangle$ and the average interface density $\langle \rho_{\text{st}} \rangle$ at the final state. The results for the original model are depicted as a function of the tolerance T in Fig. A.1a for the interface density and in Fig. A.1b for the segregation coefficient. At low values of T , both indicators show a disordered state that falls in the frozen phase. We also observe a dependence of the transition point with the vacancy density. On the other hand, for high T values, the transition point between segregated and mixed states has no dependence on the parameter ρ_v . Notice that mixed and frozen states present a very similar value of $\langle s \rangle$ but can be differentiated by the stationary value of the average interface density $\langle \rho_{\text{st}} \rangle$. These results are in agreement with the results reported for the Schelling model[0], with the extra information provided by the average interface density.

The first quite dramatic effect of including aging in the system is the disappearance of the mixed state from the phase diagram. In both metrics, the difference between the models with and without aging is clearly manifested. For low T values, the frozen-segregated transition behaves similarly to the original model since aging has no implications as the system gets quickly frozen. Nevertheless, for high values of the tolerance $T > 0.5$, the segregated-mixed transition disappears, and the segregated phase is always present. This is not an intuitive effect and one would think

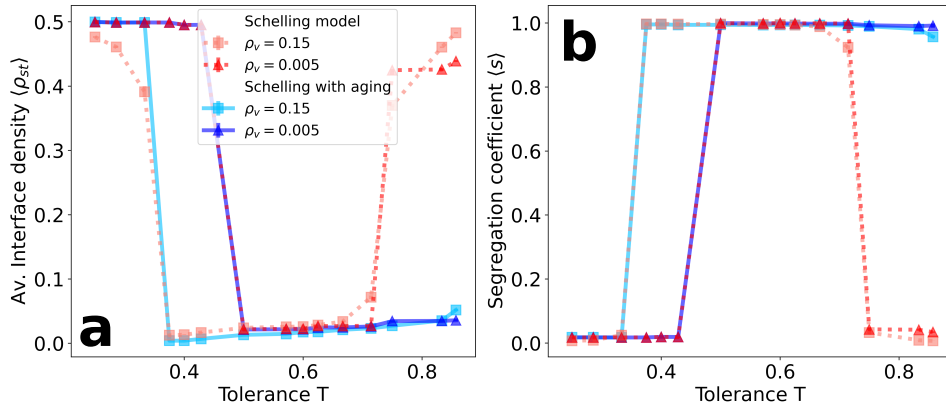


Figure 3.1: Average interface density $\langle \rho_{st} \rangle$ (a) and segregation coefficient $\langle s \rangle$ (b) at the stationary regime as a function of the tolerance parameter T for two values of the vacancy density $\rho_v = 0.5\%$ and 15% . Results are shown for both the Schelling model and the variant with aging introduced in this paper. Simulations are performed on an 80×80 lattice and averaged over $5 \cdot 10^4$ realizations.

that aging, contributing to difficult agent's mobility, should prevent the system from forming fully developed segregated clusters. However, it is just the opposite, and it favors cluster emergence.

3.3.2 Segregated phase: final state

To gain further insights into the differences in the system dynamics that lead to the extended segregated phase, we compute the fraction of unsatisfied agents at the stationary regime n_u (see Fig. A.2a). This metric plays a role as a marker for the frozen-segregated transition, as shown for the 1D Schelling model [0]. The frozen phase presents a big majority of unsatisfied agents for both models. After the transition, this parameter decays to very low values in the segregated phase, where a majority of agents are satisfied. In this phase, we observe a step-like increasing behavior of the unsatisfied agents with T . As the tolerance grows, the number of satisfying vacancies increases and the noisy movement of satisfied agents drives the system evolution, creating eventual unsatisfied agents in the sites that they abandon or target. However, in the Schelling model, the transition to a mixed state at $T = 0.75$ inhibits the creation of clear fronts between agents of different kinds, and it is also associated to a sharp increase of $n_u \simeq 0.05$ (red squares in Fig. A.2a). The Schelling model with aging, on the other hand, shows a lower fraction of unsatisfied agents during all values of the tolerance above the frozen-segregated transition (blue triangles in Fig. A.2a). So much so, that many realizations reach $n_u = 0$ and this causes the large error bars in Fig. A.2a after the transition. In a counterintuitive way, the introduction of aging causes a higher global satisfaction when compared with the original model in both the segregated and the mixed phases.

The creation of new unsatisfied agents at the final stationary state occurs at the interface between the segregated agent kinds. This is why we study the interface roughness (perimeter) P as a function of the tolerance parameter. To compute this measure, we compute the number of agents of one kind in contact with different kind agents. To perform this calculation, we smooth the interface by considering vacancies surrounded by a majority of agents of a certain kind as members of that kind. In our system of $L \times L$ with periodic boundary, the minimum interface size (perimeter) P between clusters of agents of different kind is $P = 2L$. To avoid the L dependency, we calculate an adimensional magnitude P/\sqrt{S} , where S is the number of agents of each kind $S = N_{\text{agents}}/2 = L^2(1 - \rho_v)/2$ (surface). This metric P/\sqrt{S} is computed starting from a flat interface as an initial condition and evolving it for $t_{\max} = 10^4$ MC steps to reach well within the stationary state. With the metric P/\sqrt{S} , we are able to estimate how close is the final state interface of our system to the flat interface ($P/\sqrt{S} = 2\sqrt{2}$). The results show an increasing dependence of

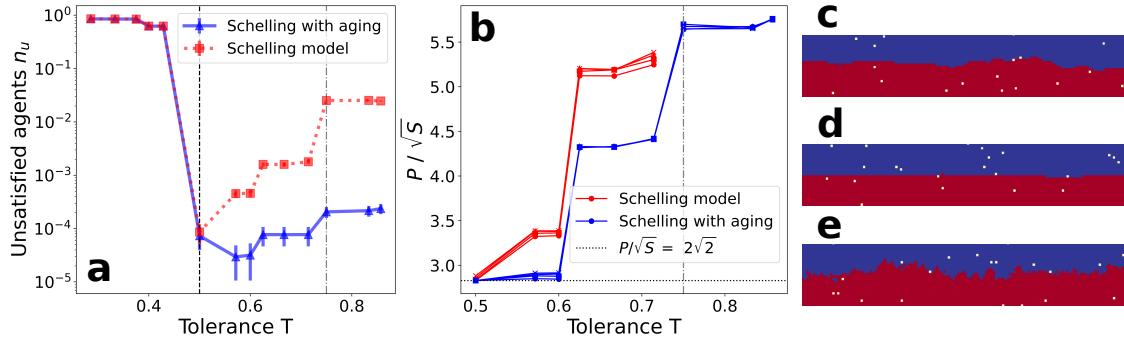


Figure 3.2: (a) Fraction of unsatisfied agents n_u at the stationary regime as a function of the tolerance parameter T . (b) Measure of the interface roughness between clusters of different kind of agents at the final stationary state P/\sqrt{S} as a function of the tolerance parameter T . Different markers indicate different system sizes: $L = 40$ (circles), 60 (squares), 80 (triangles) and 100 (crosses). Results are shown for both the Schelling model with and without aging. Numerical simulations are performed for $\rho_v = 0.5\%$ and averaged over $5 \cdot 10^4$ realizations. The frozen-segregated transition (dashed black line) and the segregated-mixed transition (gray dot-dashed line) are highlighted to differentiate the phases that the Schelling model exhibits. There are no values of P/\sqrt{S} for the Schelling model above $T = 3/4$ because the segregated-mixed transition occurs. (c) Final state interface zoom snapshot for $T = 0.57$ using the original model. (d) Final state interface zoom snapshot for $T = 0.57$ using the model with aging. (e) Same as c for $T = 0.86$.

roughness with the tolerance parameter T (see Fig. A.2b). This growth can be explained as an increase in tolerance means that agents are satisfied with fewer “same-kind” neighbors. Therefore, the interface is able to be rougher, keeping the agents in a satisfied state. In addition, notice that all values with different L collapse, so the dependence on the system size has been eliminated.

Comparing both models, one observes a lower interface roughness for the Schelling model with aging, regardless of the value of T . The closest value to the flat interface occurs for the first values of T after the frozen-segregated phase transition (shown in Fig. A.2d). In the original model, we observe higher values of P/\sqrt{S} due to the noise produced by the satisfied agents’ behavior (see Fig. A.2c). Moreover, aging allows us to obtain a segregated phase with even larger interface roughness than the maximum observed in the original model for large values of T (see Fig. A.2e). We remark that, when aging is introduced, agents try to join those of their own kind but are less and less prone to change location as time passes. Thus, in the Schelling model with aging, agents in the bulk of the clusters mainly do not move and those moving more often are located at the interface between agent kinds. At medium and large scales, this phenomenon leads to ergodicity breaking in the final state dynamics.

3.3.3 Segregated phase: coarsening dynamics

Diverse versions of the original Schelling Model exhibit different behaviors in terms of coarsening dynamics. Recent publications report a power-law like domain growth [0, 0]. We monitor here the evolution of the interface density $\langle \rho(t) \rangle$, which decreases as $\langle \rho(t) \rangle \sim t^{-\alpha}$ so the domains should grow in our model following a power-law with time.

The coarsening process of the Schelling model at the segregated phase ($0.5 \leq T < 0.75$) is displayed in Fig. A.3a and Fig. 3.4. We find that the average interface density follows a power-law decay with an exponent $\alpha \simeq 0.5$ for the limit of small vacancy density $\rho_v \rightarrow 0$, in agreement with the value reported for close variants of the Schelling model [0]. This exponent value is curious since the coarsening in the presence of a conserved quantity (but with local interactions) exhibits an exponent $\alpha = 1/3$ [0]. Nevertheless, the interactions in this model are not local, and the coarsening

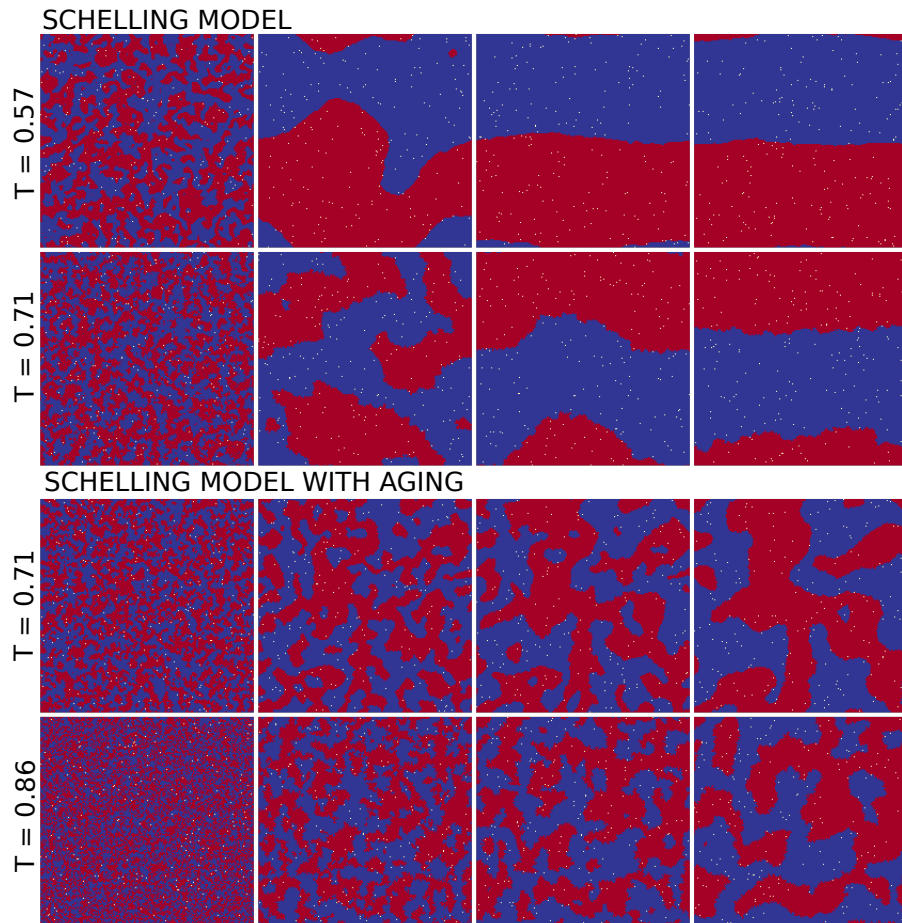


Figure 3.3: Average interface density $\langle \rho(t) \rangle$ as a function of time steps for different values of the tolerance parameter T using the Schelling model (a) and the version with aging (b). Average performed over $5 \cdot 10^3$ realizations. Fitted power-law in a black dashed line highlighting the estimated exponent value. We set system size $L = 200$ and $\rho_v = 0.005$.

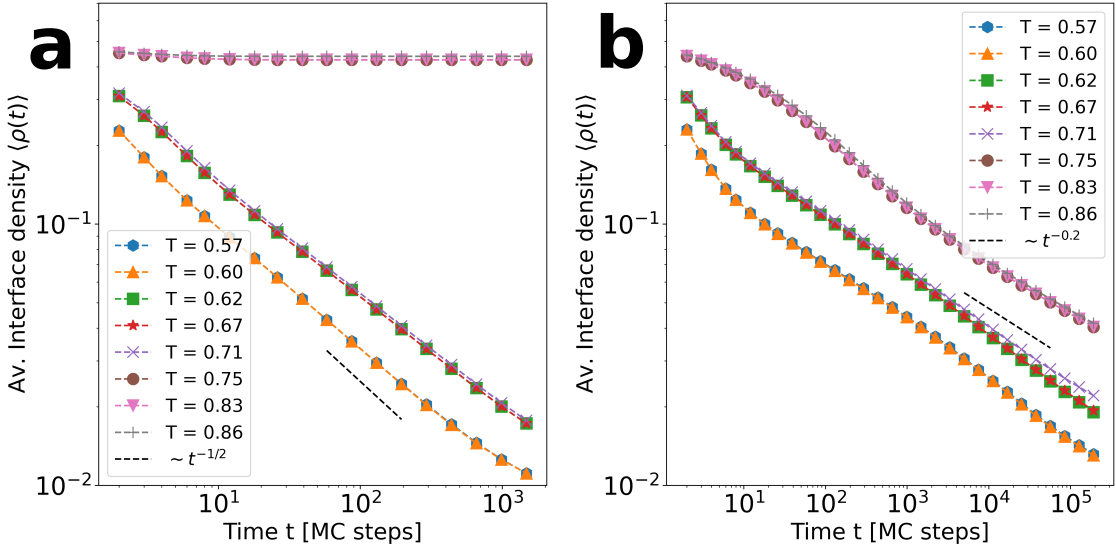


Figure 3.4: Coarsening towards the segregated state at two different values of T for both models. Snapshots are taken for 5, 500, 5000 and 50000 time steps ordered from left to right. We set system size $L = 200$ and $\rho_v = 0.005$.

exponent is more similar to the one in systems with a non-conserved order-parameter ($\alpha = 1/2$). Fig. A.3a shows as well how coarsening changes with the tolerance parameter. Even though the exponent α does not depend on T , we observe a certain delay when increasing T from 0.6 to 0.62. In the system evolution of Fig. 3.4, one can see how the behavior of the satisfied agents for higher tolerance values is translated into rougher interfaces, causing such delay. For $T > 0.75$, the system exhibits a transition towards a mixed state where the interface density fluctuates around $\rho = 0.5$, indicating that the state is constantly disordered.

The Schelling model with aging shows very different behavior (Fig. A.3b). As predicted by the phase diagram, the average interface density exhibits a power-law decay with time for all values of the tolerance T after the frozen-segregated transition. Still, the decay is slower than for the Schelling model, with $\langle \rho(t) \rangle \sim t^{-0.2}$. A mechanism that could be behind this behavior is that the model with aging counts more satisfied agents than the original model, and their probability to move becomes lower as time goes by. Moreover, satisfied agents inside a cluster will not move and the dynamics in the model take place at the interface. It is, therefore, more difficult for separated clusters to collide and merge, an effect that slows down the decay of the interface density. The persistence of small clusters becomes clear when the snapshots' evolution is compared for both models at the same tolerance value $T = 0.71$ (see Fig. 3.4). Moreover, while for the original model the initial clustering for $t = 500$ steps does not determine the final state, in the case of aging the bigger clusters present at the beginning of the evolution are the ones that keep growing, determining the shape of the system configuration after 50000 time steps. This is a dynamical effect, because the system in both cases tends to a final configuration with 2-clusters.

In the case of the Schelling model with aging, we observe an early cross-over in the dynamics (Fig. A.3b). For $T < 0.75$, the coarsening starts with an initial decay of $\langle \rho(t) \rangle$ faster than $t^{-0.2}$. This occurs because in this regime it is necessary sometimes for the aging effects to become relevant, and initially the system behaves as in the original model. Similarly, for $T \geq 0.75$, $\langle \rho(t) \rangle$ decays slowly for a moment before reaching the power-law behavior for large t values. Confirming this scenario, Fig. 3.4 shows that for $T = 0.86$, the system starts evolving similarly to a mixed state until some clusters are created. At this moment, aging prevents the clusters' desegregation, leading the system very slowly to coarsening dynamics and, eventually, to a fully segregated state.

Regarding the relaxation time to the final state, we see in Fig. 3.4 how for $T = 0.71$, the stationary state of the Schelling model is reached after approximately $t = 5000$ time steps. In contrast, the version with aging needs much more than 50000 steps to attain it. This highlights the important temporal difference between both models in terms of domain growth dynamics, which strongly increases the computational cost of the study of the stationary state of the model with aging. We have been thus able to study only medium and small system sizes in this final regime (see videos included as Supplementary Information S1 and S2).

The dynamics studied thus far are performed considering the limit $\rho_v \rightarrow 0$, but the analysis can be extended to higher vacancy densities. For the particular case of high ρ_v and low T , aging leads to the formation of a vacancy cluster at the interface between domains (see details in Supplementary information S3).

3.3.4 Aging breaks the asymptotic time-translational invariance

Here, we explore further time translational invariance (TTI) in the model dynamics. For this, we start by defining the two-time autocorrelation function $C(\tau, t_w)$ [0] as

$$C(\tau, t_w) = \left\langle \frac{1}{M} \sum_{i=1}^N \sigma_i(t_w + \tau) \sigma_i(t_w) \right\rangle, \quad (3.3)$$

where N is the system size, $\langle \cdot \rangle$ refers to averages over realizations, t_w is the waiting time to start the autocorrelation measurements, τ a time interval after t_w and M is a normalization factor defined as

$$M = \sum_{i=1}^N (\sigma_i(t_w + \tau) \sigma_i(t_w))^2. \quad (3.4)$$

which is computed at each realization.

The autocorrelation function is displayed for the Schelling model with $T = 0.75$ in Fig. 3.5a. We observe the curves decreasing with τ as expected, and that after a characteristic time period ($t_w^* \approx 5000$ for a system size of 80×80) they collapse into a single curve. This is the regime in which the dynamics becomes TTI, implying that the autocorrelation function does not depend any more on the waiting time, $C(\tau, t_w) = C(\tau)$ for $t_w > t_w^*$.

For the Schelling model with aging, the dynamics show some different features (Figs. 3.5b and 3.5c). First, the autocorrelation functions decay slower with τ in all the cases, which is connected to the long-lived small clusters mentioned previously. We do not find in the simulations any value of t_w^* for the systems to fall into a TTI regime. Not only that, but a scaling relation including both τ and t_w can be applied to collapse the autocorrelation curves (see insets Figs. 3.5b and 3.5c). This behavior is similar to glassy systems [0], therefore it is useful to use the mathematical description for those systems in our case. In this type of dynamics, a final stationary state is not attainable in the thermodynamic limit, and it is possible to decompose the autocorrelation function into an equilibrium part and an “aging” part (aging in the sense of non-equilibrium dynamics in glassy systems) [0, 0]:

$$C(\tau, t_w) \simeq C_{\text{eq}}(\tau) C_{\text{aging}} u(\tau, t_w) = C_{\text{eq}}(\tau) C_{\text{aging}} \left(\frac{h(\tau)}{h(t_w)} \right), \quad (3.5)$$

where C_{eq} describes the fast relaxation of the system components within each domain (TTI term), C_{aging} is a scaling function and $u(\tau, t_w)$ is a normalization factor which, in some cases, can be written as the quotient of an unknown function $h(t)$ at the two times τ and t_w . This function $h(t)$ is known to be related to the dynamical correlation length [0, 0]. In our case, we use $h(t) = t$ to scale the results in Fig. 3.5b (see inset). This scaling is valid for values of $T \in [0.5, 0.75]$. Nevertheless,

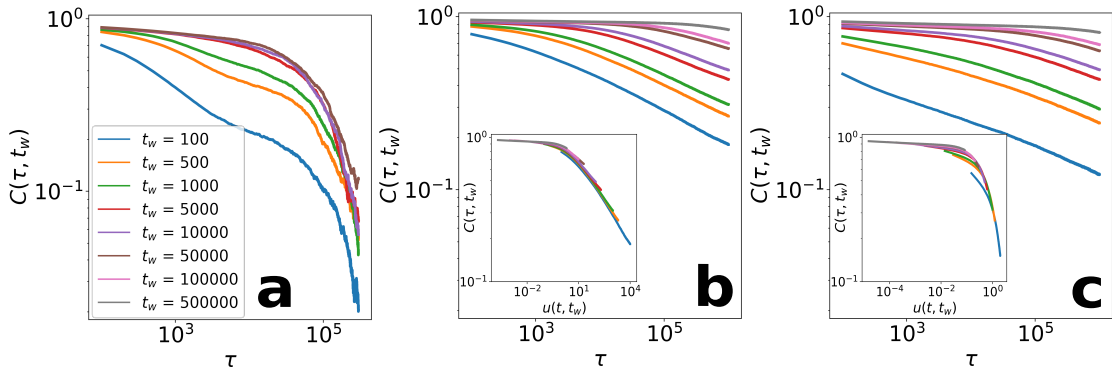


Figure 3.5: Two-times autocorrelation $C(\tau, t_w)$ as a function of the time period passed since the waiting time t_w . First, the autocorrelation is shown for the Schelling model at $T = 0.71$ in **a**, and for the version with aging at $T = 0.71$ in **b** and $T = 0.86$ in **c**. The insets are the result of the collapse using $u(\tau, t_w) = \tau/t_w$ (**b**) and $u(\tau, t_w) = \log(\tau + t_w)/\log(t_w) - 1$ (**c**). The curves correspond to different values of the waiting time t_w . Calculations performed on a 100×100 lattice averaged over $5 \cdot 10^4$ realizations.

higher values of T do not hold a linear scaling, and we need to turn to other functional forms as the normalization factor $u(\tau, t_w) = \log(\tau + t_w)/\log(t_w) - 1$ used in Fig. 3.5c. This indicates that for $T > 0.75$, the dynamical correlation length evolves in a different and slower way.

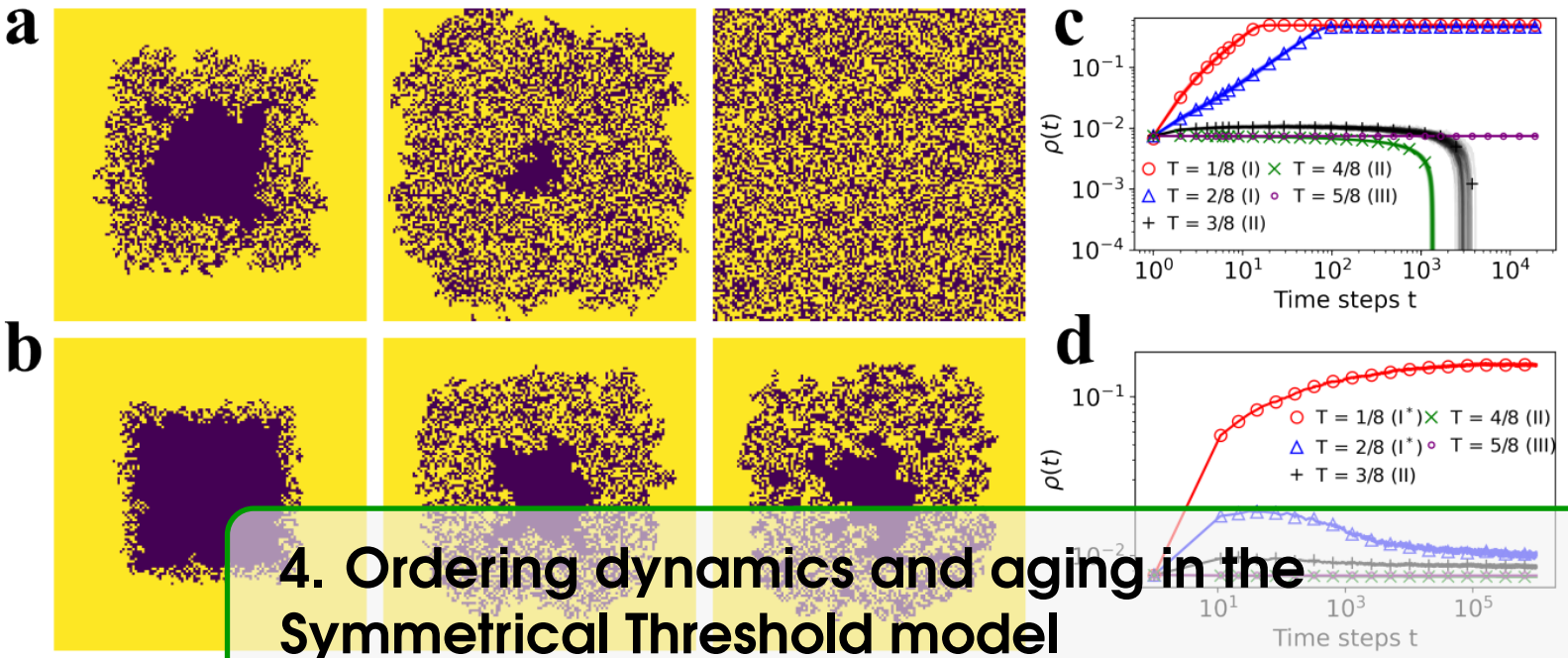
3.4 Summary and discussion

We have studied the effect of aging on a stochastic Threshold model, which combines long-range mobility with local short-range interactions. Specifically, taking as basis the noisy constrained Schelling model, we assign to the agents an internal clock counting the time spent in the same satisfying location. The probability of changing state decreases then inversely proportional to this time. Therefore, older satisfied agents are less prone to update resident locations. The original model displays a transition between a segregated phase and a mixed one as the tolerance control parameter T increases. This transition disappears when aging is introduced into the system, the mixed phase is replaced by a segregated phase even for high values of the tolerance parameter T . As a result, the model with aging presents a higher global satisfaction than without this effect for all values of the tolerance.

On the dynamical perspective, the relaxation towards the segregated phase features a coarsening phenomena characterized by a power-law decay of the average interface density with time $\langle \rho \rangle \sim t^{-\alpha}$. For the original model in the limit of low vacancy density, the exponent is around $\alpha = 1/2$. This exponent is also reported in other variants of the Schelling model [0, 0]. Aging gives rise to long-lived small clusters and a slower coarsening, reducing the exponent to $\alpha \simeq 0.2$. We investigated the autocorrelation functions in the segregated phase and found that aging breaks the asymptotic time-translational invariance of the dynamics. This result, along with a nontrivial scaling of the autocorrelation functions, establish close similarities with low-coarsening systems, such as glassy systems, and our Schelling model with aging for high values of the tolerance parameter. Moreover, this work studies the case for equal size populations ignores effects arising from the competition between different population sizes. Further work would be to study a joint effect of minority population and aging.

As for the implications of our results from a social perspective, we must note that the fact that aging favors segregation, inhibiting the segregation-mixed phase transition, is rather counter-intuitive, but gives support to the argument that segregation is a stochastically stable state and may prevail in an all-integrationist world [0]. Our model predicts the appearance of segregation even

for tolerance values close to one. Additionally, the model relaxation time multiplies manifold, which implies that if aging is present the natural state of this system seems to be generically out of equilibrium.



4. Ordering dynamics and aging in the Symmetrical Threshold model

4.1 Theorems

4.1.1 Several equations

This is a theorem consisting of several equations.

Theorem 4.1 — Name of the theorem. In $E = \mathbb{R}^n$ all norms are equivalent. It has the properties:

$$\| |\mathbf{x}| - |\mathbf{y}| \| \leq \| \mathbf{x} - \mathbf{y} \| \quad (4.1)$$

$$\left\| \sum_{i=1}^n \mathbf{x}_i \right\| \leq \sum_{i=1}^n \| \mathbf{x}_i \| \quad \text{where } n \text{ is a finite integer} \quad (4.2)$$

4.1.2 Single Line

This is a theorem consisting of just one line.

Theorem 4.2 A set $\mathcal{D}(G)$ is dense in $L^2(G)$, $|\cdot|_0$.

4.2 Definitions

A definition can be mathematical or it could define a concept.

Definition 4.1 — Definition name. Given a vector space E , a norm on E is an application, denoted $\| \cdot \|$, E in $\mathbb{R}^+ = [0, +\infty[$ such that:

$$\| \mathbf{x} \| = 0 \Rightarrow \mathbf{x} = \mathbf{0} \quad (4.3)$$

$$\| \lambda \mathbf{x} \| = |\lambda| \cdot \| \mathbf{x} \| \quad (4.4)$$

$$\| \mathbf{x} + \mathbf{y} \| \leq \| \mathbf{x} \| + \| \mathbf{y} \| \quad (4.5)$$

4.3 Notations

■ **Notation 4.1** Given an open subset G of \mathbb{R}^n , the set of functions φ are:

1. Bounded support G ;
2. Infinitely differentiable;

a vector space is denoted by $\mathcal{D}(G)$.

4.4 Remarks

This is an example of a remark.



The concepts presented here are now in conventional employment in mathematics. Vector spaces are taken over the field $\mathbb{K} = \mathbb{R}$, however, established properties are easily extended to $\mathbb{K} = \mathbb{C}$.

4.5 Corollaries

Corollary 4.1 — Corollary name. The concepts presented here are now in conventional employment in mathematics. Vector spaces are taken over the field $\mathbb{K} = \mathbb{R}$, however, established properties are easily extended to $\mathbb{K} = \mathbb{C}$.

4.6 Propositions

4.6.1 Several equations

Proposition 4.1 — Proposition name. It has the properties:

$$|||\mathbf{x}|| - ||\mathbf{y}||| \leq ||\mathbf{x} - \mathbf{y}|| \quad (4.6)$$

$$||\sum_{i=1}^n \mathbf{x}_i|| \leq \sum_{i=1}^n ||\mathbf{x}_i|| \quad \text{where } n \text{ is a finite integer} \quad (4.7)$$

4.6.2 Single Line

Proposition 4.2 Let $f, g \in L^2(G)$; if $\forall \varphi \in \mathcal{D}(G)$, $(f, \varphi)_0 = (g, \varphi)_0$ then $f = g$.

4.7 Examples

4.7.1 Equation Example

■ **Example 4.1** Let $G = \{x \in \mathbb{R}^2 : |x| < 3\}$ and denoted by: $x^0 = (1, 1)$; consider the function:

$$f(x) = \begin{cases} e^{|x|} & \text{si } |x - x^0| \leq 1/2 \\ 0 & \text{si } |x - x^0| > 1/2 \end{cases} \quad (4.8)$$

The function f has bounded support, we can take $A = \{x \in \mathbb{R}^2 : |x - x^0| \leq 1/2 + \varepsilon\}$ for all $\varepsilon \in]0; 5/2 - \sqrt{2}[$. ■

4.7.2 Text Example

■ **Example 4.2 — Example name.** Aliquam arcu turpis, ultrices sed luctus ac, vehicula id metus. Morbi eu feugiat velit, et tempus augue. Proin ac mattis tortor. Donec tincidunt, ante rhoncus luctus semper, arcu lorem lobortis justo, nec convallis ante quam quis lectus. Aenean tincidunt sodales massa, et hendrerit tellus mattis ac. Sed non pretium nibh. Donec cursus maximus luctus. Vivamus lobortis eros et massa porta porttitor. ■

4.8 Exercises

Exercise 4.1 This is a good place to ask a question to test learning progress or further cement ideas into students' minds. ■

4.9 Problems

Problem 4.1 What is the average airspeed velocity of an unladen swallow?

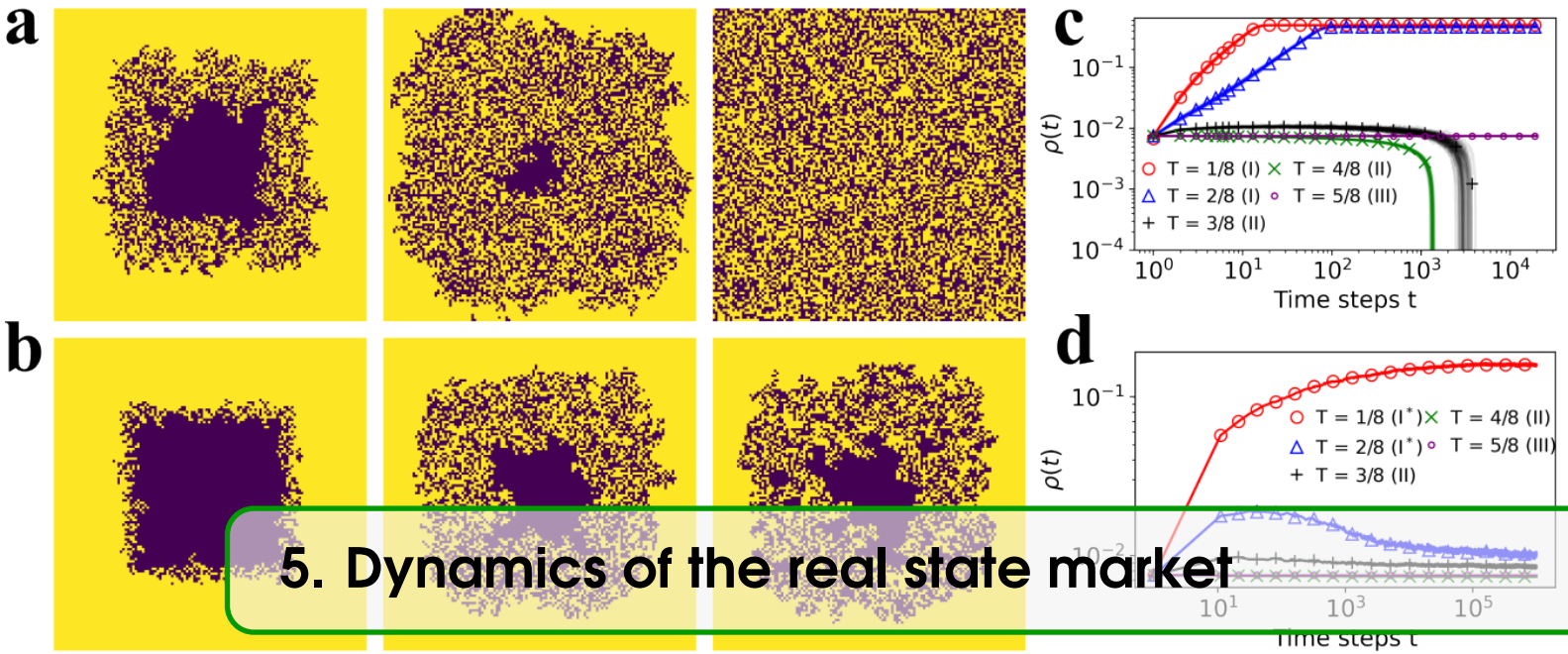
4.10 Vocabulary

Define a word to improve a students' vocabulary.

- **Vocabulary 4.1 — Word.** Definition of word.

Real estate agency dynamics

5	Dynamics of the real state market	53
5.1	Theorems	53
5.2	Definitions	53
5.3	Notations	53
5.4	Remarks	54
5.5	Corollaries	54
5.6	Propositions	54
5.7	Examples	54
5.8	Exercises	54
5.9	Problems	55
5.10	Vocabulary	55
6	Segmentation of the real state market	57
6.1	Table	57
6.2	Figure	57



5. Dynamics of the real state market

5.1 Theorems

5.1.1 Several equations

This is a theorem consisting of several equations.

Theorem 5.1 — Name of the theorem. In $E = \mathbb{R}^n$ all norms are equivalent. It has the properties:

$$\| |\mathbf{x}| - |\mathbf{y}| \| \leq \| \mathbf{x} - \mathbf{y} \| \quad (5.1)$$

$$\left\| \sum_{i=1}^n \mathbf{x}_i \right\| \leq \sum_{i=1}^n \| \mathbf{x}_i \| \quad \text{where } n \text{ is a finite integer} \quad (5.2)$$

5.1.2 Single Line

This is a theorem consisting of just one line.

Theorem 5.2 A set $\mathcal{D}(G)$ is dense in $L^2(G)$, $|\cdot|_0$.

5.2 Definitions

A definition can be mathematical or it could define a concept.

Definition 5.1 — Definition name. Given a vector space E , a norm on E is an application, denoted $\| \cdot \|$, E in $\mathbb{R}^+ = [0, +\infty[$ such that:

$$\| \mathbf{x} \| = 0 \Rightarrow \mathbf{x} = \mathbf{0} \quad (5.3)$$

$$\| \lambda \mathbf{x} \| = |\lambda| \cdot \| \mathbf{x} \| \quad (5.4)$$

$$\| \mathbf{x} + \mathbf{y} \| \leq \| \mathbf{x} \| + \| \mathbf{y} \| \quad (5.5)$$

5.3 Notations

■ **Notation 5.1** Given an open subset G of \mathbb{R}^n , the set of functions φ are:

1. Bounded support G ;
2. Infinitely differentiable;

a vector space is denoted by $\mathcal{D}(G)$.

5.4 Remarks

This is an example of a remark.



The concepts presented here are now in conventional employment in mathematics. Vector spaces are taken over the field $\mathbb{K} = \mathbb{R}$, however, established properties are easily extended to $\mathbb{K} = \mathbb{C}$.

5.5 Corollaries

Corollary 5.1 — Corollary name. The concepts presented here are now in conventional employment in mathematics. Vector spaces are taken over the field $\mathbb{K} = \mathbb{R}$, however, established properties are easily extended to $\mathbb{K} = \mathbb{C}$.

5.6 Propositions

5.6.1 Several equations

Proposition 5.1 — Proposition name. It has the properties:

$$|||\mathbf{x}|| - ||\mathbf{y}||| \leq ||\mathbf{x} - \mathbf{y}|| \quad (5.6)$$

$$||\sum_{i=1}^n \mathbf{x}_i|| \leq \sum_{i=1}^n ||\mathbf{x}_i|| \quad \text{where } n \text{ is a finite integer} \quad (5.7)$$

5.6.2 Single Line

Proposition 5.2 Let $f, g \in L^2(G)$; if $\forall \varphi \in \mathcal{D}(G)$, $(f, \varphi)_0 = (g, \varphi)_0$ then $f = g$.

5.7 Examples

5.7.1 Equation Example

■ **Example 5.1** Let $G = \{x \in \mathbb{R}^2 : |x| < 3\}$ and denoted by: $x^0 = (1, 1)$; consider the function:

$$f(x) = \begin{cases} e^{|x|} & \text{si } |x - x^0| \leq 1/2 \\ 0 & \text{si } |x - x^0| > 1/2 \end{cases} \quad (5.8)$$

The function f has bounded support, we can take $A = \{x \in \mathbb{R}^2 : |x - x^0| \leq 1/2 + \varepsilon\}$ for all $\varepsilon \in]0; 5/2 - \sqrt{2}[$. ■

5.7.2 Text Example

■ **Example 5.2 — Example name.** Aliquam arcu turpis, ultrices sed luctus ac, vehicula id metus. Morbi eu feugiat velit, et tempus augue. Proin ac mattis tortor. Donec tincidunt, ante rhoncus luctus semper, arcu lorem lobortis justo, nec convallis ante quam quis lectus. Aenean tincidunt sodales massa, et hendrerit tellus mattis ac. Sed non pretium nibh. Donec cursus maximus luctus. Vivamus lobortis eros et massa porta porttitor. ■

5.8 Exercises

Exercise 5.1 This is a good place to ask a question to test learning progress or further cement ideas into students' minds. ■

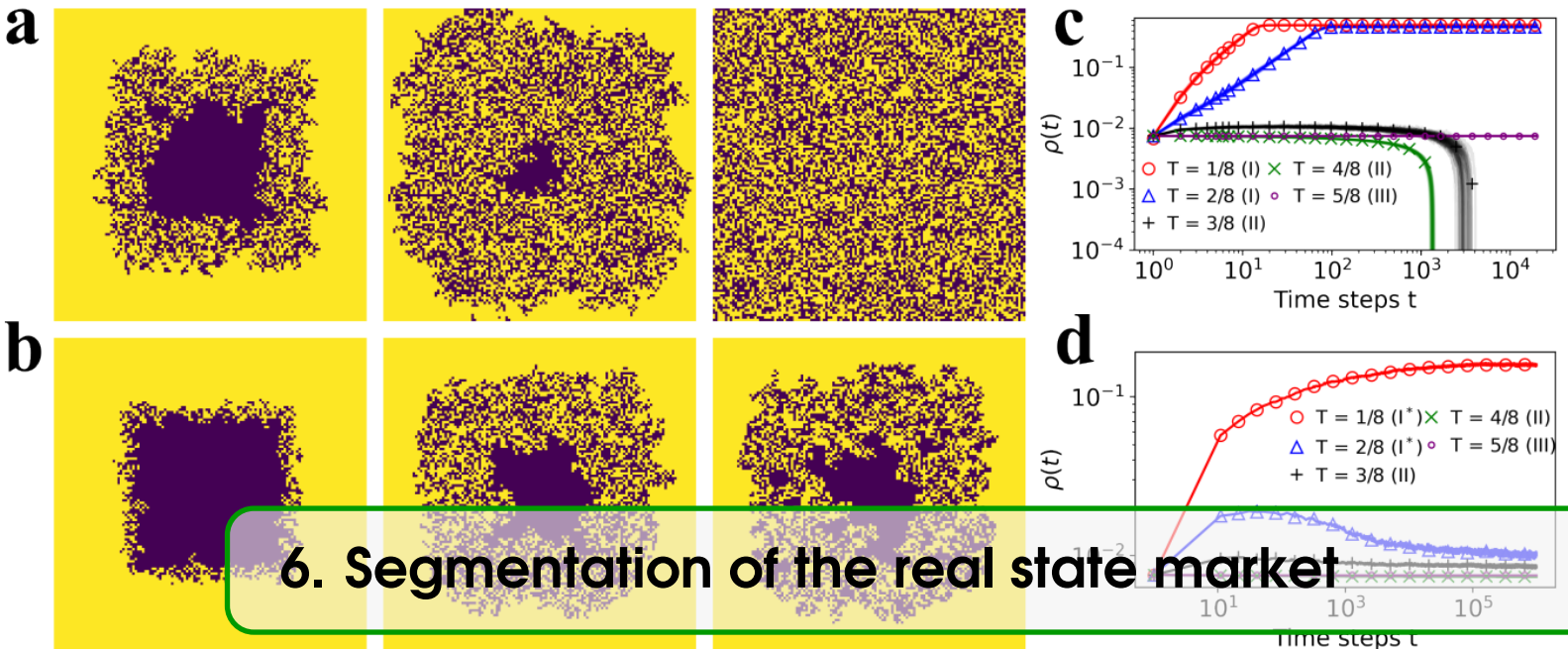
5.9 Problems

Problem 5.1 What is the average airspeed velocity of an unladen swallow?

5.10 Vocabulary

Define a word to improve a students' vocabulary.

- **Vocabulary 5.1 — Word.** Definition of word.



6. Segmentation of the real state market

6.1 Table

Lorem ipsum dolor sit amet, consectetur adipiscing elit. Praesent porttitor arcu luctus, imperdiet urna iaculis, mattis eros. Pellentesque iaculis odio vel nisl ullamcorper, nec faucibus ipsum molestie. Sed dictum nisl non aliquet porttitor. Etiam vulputate arcu dignissim, finibus sem et, viverra nisl. Aenean luctus congue massa, ut laoreet metus ornare in. Nunc fermentum nisi imperdiet lectus tincidunt vestibulum at ac elit. Nulla mattis nisl eu malesuada suscipit.

Treatments	Response 1	Response 2
Treatment 1	0.0003262	0.562
Treatment 2	0.0015681	0.910
Treatment 3	0.0009271	0.296

Table 6.1: Table caption.

Referencing Table 6.1 in-text using its label.

6.2 Figure

Lorem ipsum dolor sit amet, consectetur adipiscing elit. Praesent porttitor arcu luctus, imperdiet urna iaculis, mattis eros. Pellentesque iaculis odio vel nisl ullamcorper, nec faucibus ipsum molestie. Sed dictum nisl non aliquet porttitor. Etiam vulputate arcu dignissim, finibus sem et, viverra nisl. Aenean luctus congue massa, ut laoreet metus ornare in. Nunc fermentum nisi imperdiet lectus tincidunt vestibulum at ac elit. Nulla mattis nisl eu malesuada suscipit.



Figure 6.1: Figure caption.

Referencing Figure 6.1 in-text using its label.

Treatments	Response 1	Response 2
Treatment 1	0.0003262	0.562
Treatment 2	0.0015681	0.910
Treatment 3	0.0009271	0.296

Table 6.2: Floating table.



Figure 6.2: Floating figure.

Bibliography

Articles

- [0] Aishwarya Agarwal et al. “Swap Stability in Schelling Games on Graphs”. In: *Proceedings of the AAAI Conference on Artificial Intelligence* 34.02 (2020), pages 1758–1765. DOI: [10.1609/aaai.v34i02.5541](https://doi.org/10.1609/aaai.v34i02.5541) (cited on page 36).
- [0] Ezequiel Albano. “Interfacial roughening, segregation and dynamic behaviour in a generalized Schelling model”. In: *Journal of Statistical Mechanics-theory and Experiment - J STAT MECH-THEORY EXP* 2012 (Mar. 2012). DOI: [10.1088/1742-5468/2012/03/P03013](https://doi.org/10.1088/1742-5468/2012/03/P03013) (cited on pages 36, 40, 44).
- [0] R Amato et al. “Opinion competition dynamics on multiplex networks”. In: *New Journal of Physics* 19.12 (2017), page 123019. DOI: [10.1088/1367-2630/aa936a](https://doi.org/10.1088/1367-2630/aa936a) (cited on page 17).
- [0] Guilherme Ferraz de Arruda, Giovanni Petri, and Yamir Moreno. “Social contagion models on hypergraphs”. In: *Physical Review Research* 2.2 (2020). DOI: [10.1103/physrevresearch.2.023032](https://doi.org/10.1103/physrevresearch.2.023032) (cited on pages 17, 18).
- [0] Oriol Artíme, José J. Ramasco, and Maxi San Miguel. “Dynamics on networks: competition of temporal and topological correlations”. In: *Scientific Reports* 7.1 (2017). DOI: [10.1038/srep41627](https://doi.org/10.1038/srep41627) (cited on pages 18, 19).
- [0] Oriol Artíme et al. “Aging-induced continuous phase transition”. In: *Physical Review E* 98.3 (2018). DOI: [10.1103/physreve.98.032104](https://doi.org/10.1103/physreve.98.032104) (cited on pages 18–20, 36, 37).
- [0] A. L. Barabasi. “The origin of bursts and heavy tails in human dynamics”. In: *Nature* 435 (2005), page 207 (cited on pages 36, 37).
- [0] Albert-László Barabási. “Scale-free networks: a decade and beyond”. In: *Science* 325.5939 (2009), pages 412–413 (cited on page 19).
- [0] George Barmpalias, Richard Elwes, and Andrew Lewis-Pye. “Minority Population in the One-Dimensional Schelling Model of Segregation”. In: *Journal of Statistical Physics* 173.5 (2018), pages 1408–1458. DOI: [10.1007/s10955-018-2146-2](https://doi.org/10.1007/s10955-018-2146-2) (cited on page 36).
- [0] Frank M Bass. “A new product growth for model consumer durables”. In: *Management science* 15.5 (1969), pages 215–227 (cited on page 18).
- [0] L. Berthier and A. P. Young. “Aging dynamics of the Heisenberg spin glass”. In: *Physical Review B* 69.18 (May 2004). ISSN: 1550-235X. DOI: [10.1103/physrevb.69.184423](https://doi.org/10.1103/physrevb.69.184423). URL: <http://dx.doi.org/10.1103/PhysRevB.69.184423> (cited on page 43).
- [0] M. Blume, V.J. Emery, and Robert B. Griffiths. “Ising Model for the Lambda Transition and Phase Separation in He3-He4 Mixtures”. In: *Phys. Rev. A* 4 (1971), page 1071. DOI: <https://doi.org/10.1103/PhysRevA.4.1071> (cited on page 36).
- [0] Marian Boguñá et al. “Simulating non-Markovian stochastic processes”. In: *Physical Review E* 90.4 (2014). DOI: [10.1103/physreve.90.042108](https://doi.org/10.1103/physreve.90.042108) (cited on pages 18, 36).
- [0] Adrián Carro, Raúl Toral, and Maxi San Miguel. “The noisy Voter model on complex networks”. In: *Scientific Reports* 6.1 (2016). DOI: [10.1038/srep24775](https://doi.org/10.1038/srep24775) (cited on page 17).
- [0] Claudio Castellano, Miguel A. Muñoz, and Romualdo Pastor-Satorras. “Nonlinearq-Voter model”. In: *Physical Review E* 80.4 (2009). DOI: [10.1103/physreve.80.041129](https://doi.org/10.1103/physreve.80.041129) (cited on page 17).

- [0] Giulia Cencetti et al. “Temporal properties of higher-order interactions in social networks”. In: *Scientific Reports* 11.1 (2021). DOI: [10.1038/s41598-021-86469-8](https://doi.org/10.1038/s41598-021-86469-8) (cited on page 17).
- [0] Damon Centola, Víctor M. Eguíluz, and Michael W. Macy. “Cascade dynamics of complex propagation”. In: *Physica A: Statistical Mechanics and its Applications* 374.1 (2007), pages 449–456. DOI: [10.1016/j.physa.2006.06.018](https://doi.org/10.1016/j.physa.2006.06.018) (cited on pages 17, 18, 20, 30).
- [0] Hanshuang Chen et al. “Non-Markovian majority-vote model”. In: *Physical Review E* 102.6 (2020). DOI: [10.1103/physreve.102.062311](https://doi.org/10.1103/physreve.102.062311) (cited on pages 17–20).
- [0] Raj Chetty, Nathaniel Hendren, and Lawrence F. Katz. “The Effects of Exposure to Better Neighborhoods on Children: New Evidence from the Moving to Opportunity Experiment”. In: *American Economic Review* 106.4 (Apr. 2016), pages 855–902. DOI: [10.1257/aer.20150572](https://doi.org/10.1257/aer.20150572). URL: <http://dx.doi.org/10.1257/aer.20150572> (cited on page 36).
- [0] Terry Nichols Clark et al. “Amenities Drive Urban Growth”. In: *Journal of Urban Affairs* 24.5 (Dec. 2002), pages 493–515. DOI: [10.1111/1467-9906.00134](https://doi.org/10.1111/1467-9906.00134). URL: <http://dx.doi.org/10.1111/1467-9906.00134> (cited on page 36).
- [0] W. A. V. Clark and M. Fossett. “Understanding the social context of the Schelling segregation model”. In: *Proceedings of the National Academy of Sciences* 105.11 (2008), pages 4109–4114. DOI: [10.1073/pnas.0708155105](https://doi.org/10.1073/pnas.0708155105) (cited on page 35).
- [0] W.A.V. Clark. “Residential preferences and neighborhood racial segregation: A test of the schelling segregation model”. In: *Demography* 28.1 (1991), pages 1–19. DOI: [10.2307/2061333](https://doi.org/10.2307/2061333) (cited on page 35).
- [0] William A.V. Clark, Youqin Huang, and Suzanne Withers. “Does commuting distance matter?” In: *Regional Science and Urban Economics* 33.2 (Mar. 2003), pages 199–221. DOI: [10.1016/s0166-0462\(02\)00012-1](https://doi.org/10.1016/s0166-0462(02)00012-1). URL: [http://dx.doi.org/10.1016/s0166-0462\(02\)00012-1](http://dx.doi.org/10.1016/s0166-0462(02)00012-1) (cited on page 36).
- [0] Agnieszka Czaplicka, Raul Toral, and Maxi San Miguel. “Competition of simple and complex adoption on interdependent networks”. In: *Physical Review E* 94.6 (2016). DOI: [10.1103/physreve.94.062301](https://doi.org/10.1103/physreve.94.062301) (cited on page 18).
- [0] L Dall’Asta, C Castellano, and M Marsili. “Statistical physics of the Schelling model of segregation”. In: *Journal of Statistical Mechanics: Theory and Experiment* 2008.07 (July 2008), page L07002. ISSN: 1742-5468. DOI: [10.1088/1742-5468/2008/07/L07002](https://doi.org/10.1088/1742-5468/2008/07/L07002). URL: <http://dx.doi.org/10.1088/1742-5468/2008/07/L07002> (cited on pages 36, 38–40, 44).
- [0] Nancy A Denton. “The persistence of segregation: Links between residential segregation and school segregation”. In: *Minn. L. Rev.* 80 (1995), page 795 (cited on page 36).
- [0] Marina Diakonova, Maxi San Miguel, and Víctor M. Eguíluz. “Absorbing and shattered fragmentation transitions in multilayer coevolution”. In: *Physical Review E* 89.6 (2014). DOI: [10.1103/physreve.89.062818](https://doi.org/10.1103/physreve.89.062818) (cited on page 17).
- [0] Marina Diakonova et al. “Irreducibility of multilayer network dynamics: the case of the Voter model”. In: *New Journal of Physics* 18.2 (2016), page 023010. DOI: [10.1088/1367-2630/18/2/023010](https://doi.org/10.1088/1367-2630/18/2/023010) (cited on page 17).
- [0] Fernando Diaz-Diaz, Maxi San Miguel, and Sandro Meloni. “Echo chambers and information transmission biases in homophilic and heterophilic networks”. In: *Scientific Reports* 12.1 (2022). DOI: [10.1038/s41598-022-13343-6](https://doi.org/10.1038/s41598-022-13343-6) (cited on page 18).
- [0] Peter Sheridan Dodds, Kameron Decker Harris, and Christopher M. Danforth. “Limited Imitation Contagion on Random Networks: Chaos, Universality, and Unpredictability”. In: *Physical Review Letters* 110.15 (2013). DOI: [10.1103/physrevlett.110.158701](https://doi.org/10.1103/physrevlett.110.158701) (cited on page 18).

- [0] Peter Sheridan Dodds and Duncan J. Watts. “Universal Behavior in a Generalized Model of Contagion”. In: *Physical Review Letters* 92.21 (2004). DOI: [10.1103/physrevlett.92.218701](https://doi.org/10.1103/physrevlett.92.218701) (cited on page 18).
- [0] Nicolás Goles Domic, Eric Goles, and Sergio Rica. “Dynamics and complexity of the Schelling segregation model”. In: *Physical Review E* 83.5 (2011). DOI: [10.1103/physreve.83.056111](https://doi.org/10.1103/physreve.83.056111) (cited on page 36).
- [0] Paul Erdős, Alfréd Rényi, et al. “On the evolution of random graphs”. In: *Publ. Math. Inst. Hung. Acad. Sci* 5.1 (1960), pages 17–60 (cited on page 19).
- [0] J. Fernández-Gracia, V. M. Eguíluz, and M. San Miguel. “Update rules and interevent time distributions: Slow ordering versus no ordering in the voter model”. In: *Physical Review E* 84.1 (2011). DOI: [10.1103/physreve.84.015103](https://doi.org/10.1103/physreve.84.015103) (cited on pages 18–20, 36, 37).
- [0] Juan Fernández-Gracia, Víctor M. Eguíluz, and Maxi San Miguel. “Timing Interactions in Social Simulations: The Voter Model”. In: *Understanding Complex Systems* (2013), pages 331–352 (cited on pages 19, 20).
- [0] Juan Fernández-Gracia et al. “Is the Voter Model a Model for Voters?” In: *Physical Review Letters* 112.15 (2014). DOI: [10.1103/physrevlett.112.158701](https://doi.org/10.1103/physrevlett.112.158701) (cited on page 17).
- [0] Daniel S. Fisher and David A. Huse. “Ordered Phase of Short-Range Ising Spin-Glasses”. In: *Phys. Rev. Lett.* 56 (15 Apr. 1986), pages 1601–1604. DOI: [10.1103/PhysRevLett.56.1601](https://doi.org/10.1103/PhysRevLett.56.1601). URL: <https://link.aps.org/doi/10.1103/PhysRevLett.56.1601> (cited on page 43).
- [0] SERGE GALAM. “SOCIOPHYSICS: A REVIEW OF GALAM MODELS”. In: *International Journal of Modern Physics C* 19.03 (Mar. 2008), pages 409–440. DOI: [10.1142/s0129183108012297](https://doi.org/10.1142/s0129183108012297). URL: <http://dx.doi.org/10.1142/s0129183108012297> (cited on page 18).
- [0] L. Gauvin, J. Vannimenus, and J.-P. Nadal. “Phase diagram of a Schelling segregation model”. In: *The European Physical Journal B* 70.2 (July 2009), pages 293–304. ISSN: 1434-6036. DOI: [10.1140/epjb/e2009-00234-0](https://doi.org/10.1140/epjb/e2009-00234-0). URL: <http://dx.doi.org/10.1140/epjb/e2009-00234-0> (cited on pages 36–38).
- [0] Laetitia Gauvin, Jean-Pierre Nadal, and Jean Vannimenus. “Schelling segregation in an open city: A kinetically constrained Blume-Emery-Griffiths spin-1 system”. In: *Physical Review E* 81.6 (June 2010). ISSN: 1550-2376. DOI: [10.1103/physreve.81.066120](https://doi.org/10.1103/physreve.81.066120). URL: <http://dx.doi.org/10.1103/PhysRevE.81.066120> (cited on page 36).
- [0] James P. Gleeson. “Cascades on correlated and modular random networks”. In: *Physical Review E* 77.4 (2008). DOI: [10.1103/physreve.77.046117](https://doi.org/10.1103/physreve.77.046117) (cited on pages 18, 25, 27).
- [0] James P. Gleeson. “High-Accuracy Approximation of Binary-State Dynamics on Networks”. In: *Physical Review Letters* 107.6 (2011). DOI: [10.1103/physrevlett.107.068701](https://doi.org/10.1103/physrevlett.107.068701) (cited on pages 18, 25).
- [0] James P. Gleeson. “Binary-State Dynamics on Complex Networks: Pair Approximation and Beyond”. In: *Physical Review X* 3.2 (2013). DOI: [10.1103/physrevx.3.021004](https://doi.org/10.1103/physrevx.3.021004) (cited on pages 18, 25, 27, 73, 75).
- [0] James P. Gleeson and Diarmuid J. Cahalane. “Seed size strongly affects cascades on random networks”. In: *Physical Review E* 75.5 (2007). DOI: [10.1103/physreve.75.056103](https://doi.org/10.1103/physreve.75.056103) (cited on pages 18, 20, 25, 27).
- [0] James P. Gleeson et al. “Effects of Network Structure, Competition and Memory Time on Social Spreading Phenomena”. In: *Physical Review X* 6.2 (2016). DOI: [10.1103/physrevx.6.021019](https://doi.org/10.1103/physrevx.6.021019) (cited on page 18).

- [0] S. Gonçalves, M. F. Laguna, and J. R. Iglesias. “Why, when, and how fast innovations are adopted”. In: *The European Physical Journal B* 85.6 (June 2012). DOI: [10.1140/epjb/e2012-30082-6](https://doi.org/10.1140/epjb/e2012-30082-6). URL: <http://dx.doi.org/10.1140/epjb/e2012-30082-6> (cited on pages 18, 33).
- [0] C. Gracia-Lázaro et al. “Residential segregation and cultural dissemination: An Axelrod-Schelling model”. In: *Physical Review E* 80.4 (2009). DOI: [10.1103/physreve.80.046123](https://doi.org/10.1103/physreve.80.046123) (cited on page 36).
- [0] M. Granovetter. “Threshold models of collective behavior”. In: *American Journal of Sociology* 83 (1978), page 1420 (cited on page 35).
- [0] Mark Granovetter. “Threshold Models of Collective Behavior”. In: *American Journal of Sociology* 83.6 (1978), pages 1420–1443. DOI: [10.1086/226707](https://doi.org/10.1086/226707) (cited on pages 17, 18).
- [0] Mark Granovetter. “Economic Action and Social Structure: The Problem of Embeddedness”. In: *American Journal of Sociology* 91.3 (Nov. 1985), pages 481–510. DOI: [10.1086/228311](https://doi.org/10.1086/228311). URL: <http://dx.doi.org/10.1086/228311> (cited on page 36).
- [0] S. Grauwin et al. “Competition between collective and individual dynamics”. In: *Proceedings of the National Academy of Sciences* 106.49 (2009), pages 20622–20626. DOI: [10.1073/pnas.0906263106](https://doi.org/10.1073/pnas.0906263106) (cited on page 35).
- [0] Douglas Guilbeault and Damon Centola. “Topological measures for identifying and predicting the spread of complex contagions”. In: *Nature Communications* 12.1 (2021). DOI: [10.1038/s41467-021-24704-6](https://doi.org/10.1038/s41467-021-24704-6) (cited on page 18).
- [0] D. Gunton, M. San Miguel, and P.S. Sahni. “The dynamics of first order phase transitions”. In: *Phase transitions and critical phenomena* 8 (1983), pages 267–466 (cited on page 40).
- [0] Adam Hackett and James P. Gleeson. “Cascades on clique-based graphs”. In: *Physical Review E* 87.6 (2013). DOI: [10.1103/physreve.87.062801](https://doi.org/10.1103/physreve.87.062801) (cited on page 18).
- [0] Adam Hackett, Sergey Melnik, and James P. Gleeson. “Cascades on a class of clustered random networks”. In: *Physical Review E* 83.5 (2011). DOI: [10.1103/physreve.83.056107](https://doi.org/10.1103/physreve.83.056107) (cited on page 18).
- [0] Rainer Hegselmann. “Thomas C. Schelling and James M. Sakoda: The Intellectual, Technical, and Social History of a Model”. In: *Journal of Artificial Societies and Social Simulation* 20.3 (2017), page 15. DOI: [10.18564/jasss.3511](https://doi.org/10.18564/jasss.3511) (cited on page 35).
- [0] A. D. Henry, P. Pralat, and C.-Q. Zhang. “Emergence of segregation in evolving social networks”. In: *Proceedings of the National Academy of Sciences* 108.21 (2011), pages 8605–8610. DOI: [10.1073/pnas.1014486108](https://doi.org/10.1073/pnas.1014486108) (cited on page 36).
- [0] Nina Holden and Scott Sheffield. “Scaling limits of the Schelling model”. In: *Probability Theory and Related Fields* 176.1-2 (2019), pages 219–292. DOI: [10.1007/s00440-019-00918-0](https://doi.org/10.1007/s00440-019-00918-0) (cited on page 36).
- [0] J. Hoshen and R. Kopelman. “Percolation and cluster distribution. I. Cluster multiple labeling technique and critical concentration algorithm”. In: *Phys. Rev. B* 14 (8 Oct. 1976), pages 3438–3445. DOI: [10.1103/PhysRevB.14.3438](https://doi.org/10.1103/PhysRevB.14.3438). URL: <https://link.aps.org/doi/10.1103/PhysRevB.14.3438> (cited on page 38).
- [0] “How Behavior Spreads: The Science of Complex Contagions How Behavior Spreads: The Science of Complex Contagions Damon Centola Princeton University Press, 2018. 308 pp.” In: *Science* 361.6409 (2018), pages 1320–1320. DOI: [10.1126/science.aav1974](https://doi.org/10.1126/science.aav1974) (cited on page 17).
- [0] Iacopo Iacopini et al. “Simplicial models of social contagion”. In: *Nature Communications* 10.1 (2019). DOI: [10.1038/s41467-019-10431-6](https://doi.org/10.1038/s41467-019-10431-6) (cited on page 17).

- [0] J. L. Iribarren and E. Moro. “Impact of human activity patterns on the dynamics of information diffusion.” In: *Physical Review Letters* 103 (2009), page 038702 (cited on page 36).
- [0] José Luis Iribarren and Esteban Moro. “Impact of Human Activity Patterns on the Dynamics of Information Diffusion”. In: *Physical Review Letters* 103.3 (2009). DOI: [10.1103/physrevlett.103.038702](https://doi.org/10.1103/physrevlett.103.038702) (cited on page 18).
- [0] Pablo Jensen et al. “Giant Catalytic Effect of Altruists in Schelling’s Segregation Model”. In: *Physical Review Letters* 120.20 (2018). DOI: [10.1103/physrevlett.120.208301](https://doi.org/10.1103/physrevlett.120.208301) (cited on page 36).
- [0] Fariba Karimi and Petter Holme. “Threshold model of cascades in empirical temporal networks”. In: *Physica A: Statistical Mechanics and its Applications* 392.16 (2013), pages 3476–3483. DOI: [10.1016/j.physa.2013.03.050](https://doi.org/10.1016/j.physa.2013.03.050) (cited on page 18).
- [0] M. Karsai et al. “Small but slow world: How network topology and burstiness slow down spreading”. In: *Physical Review E* 83.2 (2011). DOI: [10.1103/physreve.83.025102](https://doi.org/10.1103/physreve.83.025102) (cited on page 18).
- [0] Márton Karsai et al. “Complex contagion process in spreading of online innovation”. In: *Journal of The Royal Society Interface* 11.101 (2014), page 20140694. DOI: [10.1098/rsif.2014.0694](https://doi.org/10.1098/rsif.2014.0694) (cited on page 18).
- [0] Márton Karsai et al. “Local cascades induced global contagion: How heterogeneous thresholds, exogenous effects, and unconcerned behaviour govern online adoption spreading”. In: *Scientific Reports* 6.1 (2016). DOI: [10.1038/srep27178](https://doi.org/10.1038/srep27178) (cited on page 18).
- [0] Leah A. Keating, James P. Gleeson, and David J. P. O’Sullivan. “Multitype branching process method for modeling complex contagion on clustered networks”. In: *Phys. Rev. E* 105 (3 Mar. 2022), page 034306. DOI: [10.1103/PhysRevE.105.034306](https://doi.org/10.1103/PhysRevE.105.034306). URL: <https://link.aps.org/doi/10.1103/PhysRevE.105.034306> (cited on page 29).
- [0] Pinaki Kumar et al. “On interevent time distributions of avalanche dynamics”. In: *Scientific Reports* 10.1 (2020). DOI: [10.1038/s41598-019-56764-6](https://doi.org/10.1038/s41598-019-56764-6) (cited on pages 18, 36).
- [0] Fabio Lamanna et al. “Immigrant community integration in world cities”. In: *PLOS ONE* 13.3 (2018), e0191612. DOI: [10.1371/journal.pone.0191612](https://doi.org/10.1371/journal.pone.0191612) (cited on page 35).
- [0] Maxime Lenormand et al. “Comparing and modelling land use organization in cities”. In: *Royal Society Open Science* 2.12 (2015), page 150449. DOI: [10.1098/rsos.150449](https://doi.org/10.1098/rsos.150449) (cited on pages 36, 37).
- [0] Quan-Hui Liu et al. “Impacts of opinion leaders on social contagions”. In: *Chaos: An Interdisciplinary Journal of Nonlinear Science* 28.5 (2018), page 053103. DOI: [10.1063/1.5017515](https://doi.org/10.1063/1.5017515) (cited on page 18).
- [0] Byungjoon Min and Maxi San Miguel. “Competing contagion processes: Complex contagion triggered by simple contagion”. In: *Scientific Reports* 8.1 (2018). DOI: [10.1038/s41598-018-28615-3](https://doi.org/10.1038/s41598-018-28615-3) (cited on page 18).
- [0] Michael Molloy and Bruce Reed. “A critical point for random graphs with a given degree sequence”. In: *Random Structures and Algorithms* 6.2-3 (1995), pages 161–180. DOI: [10.1002/rsa.3240060204](https://doi.org/10.1002/rsa.3240060204) (cited on pages 25, 73).
- [0] Bjarke Mønsted et al. “Evidence of complex contagion of information in social media: An experiment using Twitter bots”. In: *PLOS ONE* 12.9 (2017), e0184148. DOI: [10.1371/journal.pone.0184148](https://doi.org/10.1371/journal.pone.0184148) (cited on page 18).
- [0] M. E. J. Newman, S. H. Strogatz, and D. J. Watts. “Random graphs with arbitrary degree distributions and their applications”. In: *Physical Review E* 64.2 (2001). DOI: [10.1103/physreve.64.026118](https://doi.org/10.1103/physreve.64.026118) (cited on pages 25, 73).

- [0] Se-Wook Oh and Mason A. Porter. “Complex contagions with timers”. In: *Chaos: An Interdisciplinary Journal of Nonlinear Science* 28.3 (2018), page 033101. DOI: [10.1063/1.4990038](https://doi.org/10.1063/1.4990038) (cited on page 18).
- [0] Maxi San Miguel Oriol Artine Jose J. Ramasco. “Dynamics on networks: competition of temporal and topological correlations.” In: *Scientific Reports* 7 (2017), page 41627 (cited on page 36).
- [0] Diego Ortega, Javier Rodríguez-Laguna, and Elka Korutcheva. “A Schelling model with a variable threshold in a closed city segregation model. Analysis of the universality classes”. In: *Physica A: Statistical Mechanics and its Applications* 574 (2021), page 126010. DOI: [10.1016/j.physa.2021.126010](https://doi.org/10.1016/j.physa.2021.126010) (cited on page 36).
- [0] Diego Ortega, Javier Rodríguez-Laguna, and Elka Korutcheva. “Avalanches in an extended Schelling model: An explanation of urban gentrification”. In: *Physica A: Statistical Mechanics and its Applications* 573 (2021), page 125943. DOI: [10.1016/j.physa.2021.125943](https://doi.org/10.1016/j.physa.2021.125943) (cited on page 36).
- [0] Romualdo Pastor-Satorras et al. “Epidemic processes in complex networks”. In: *Reviews of Modern Physics* 87.3 (2015), pages 925–979. DOI: [10.1103/revmodphys.87.925](https://doi.org/10.1103/revmodphys.87.925) (cited on page 17).
- [0] A. F. Peralta and R. Toral. “Binary-state dynamics on complex networks: Stochastic pair approximation and beyond”. In: *Physical Review Research* 2.4 (2020). DOI: [10.1103/physrevresearch.2.043370](https://doi.org/10.1103/physrevresearch.2.043370) (cited on pages 25, 33).
- [0] A. F. Peralta et al. “Analytical and numerical study of the non-linear noisy Voter model on complex networks”. In: *Chaos: An Interdisciplinary Journal of Nonlinear Science* 28.7 (2018), page 075516. DOI: [10.1063/1.5030112](https://doi.org/10.1063/1.5030112) (cited on page 17).
- [0] Antonio F Peralta, Nagi Khalil, and Raúl Toral. “Reduction from non-Markovian to Markovian dynamics: the case of aging in the noisy-Voter model”. In: *Journal of Statistical Mechanics: Theory and Experiment* 2020.2 (2020), page 024004. DOI: [10.1088/1742-5468/ab6847](https://doi.org/10.1088/1742-5468/ab6847) (cited on pages 17–20, 25, 73).
- [0] Antonio F. Peralta, Nagi Khalil, and Raúl Toral. “Ordering dynamics in the Voter model with aging”. In: *Physica A: Statistical Mechanics and its Applications* 552 (2020), page 122475. DOI: [10.1016/j.physa.2019.122475](https://doi.org/10.1016/j.physa.2019.122475) (cited on pages 18–20, 25, 73).
- [0] Antonio F. Peralta, Nagi Khalil, and Raúl Toral. “Ordering dynamics in the voter model with aging”. In: *Physica A: Statistical Mechanics and its Applications* 552 (2020), page 122475. DOI: [10.1016/j.physa.2019.122475](https://doi.org/10.1016/j.physa.2019.122475) (cited on page 36).
- [0] Toni Pérez, Konstantin Klemm, and Víctor M. Eguíluz. “Competition in the presence of aging: dominance, coexistence, and alternation between states”. In: *Scientific Reports* 6.1 (2016). DOI: [10.1038/srep21128](https://doi.org/10.1038/srep21128) (cited on pages 18–20, 36).
- [0] Sidney Redner. “Reality-inspired Voter models: A mini-review”. In: *Comptes Rendus Physique* 20.4 (2019), pages 275–292. DOI: [10.1016/j.crhy.2019.05.004](https://doi.org/10.1016/j.crhy.2019.05.004) (cited on page 17).
- [0] Tim Rogers and Alan J McKane. “A unified framework for Schelling’s model of segregation”. In: *Journal of Statistical Mechanics: Theory and Experiment* 2011.07 (July 2011), P07006. ISSN: 1742-5468. DOI: [10.1088/1742-5468/2011/07/p07006](https://doi.org/10.1088/1742-5468/2011/07/p07006). URL: <http://dx.doi.org/10.1088/1742-5468/2011/07/P07006> (cited on page 36).
- [0] Sara Brin Rosenthal et al. “Revealing the hidden networks of interaction in mobile animal groups allows prediction of complex behavioral contagion”. In: *Proceedings of the National Academy of Sciences* 112.15 (2015), pages 4690–4695. DOI: [10.1073/pnas.1420068112](https://doi.org/10.1073/pnas.1420068112) (cited on page 18).

- [0] Diego Rybski et al. “Communication activity in a social network: relation between long-term correlations and inter-event clustering”. In: *Scientific Reports* 2.1 (2012). DOI: [10.1038/srep00560](https://doi.org/10.1038/srep00560) (cited on pages 18, 36).
- [0] S. Sassen. “The global city: introducing a concept”. In: *Brown Journal of World Affairs* 11 (2005), pages 27–43 (cited on page 35).
- [0] D. M. Saul, Michael Wortis, and D. Stauffer. “Tricritical behavior of the Blume-Capel model”. In: *Phys. Rev. B* 9 (11 June 1974), pages 4964–4980. DOI: [10.1103/PhysRevB.9.4964](https://doi.org/10.1103/PhysRevB.9.4964). URL: <https://link.aps.org/doi/10.1103/PhysRevB.9.4964> (cited on page 36).
- [0] Thomas Schelling. “Models of Segregation”. In: *American Economic Review* 59.2 (1969), page 488 (cited on page 35).
- [0] Thomas C Schelling. “Dynamic models of segregation”. In: *The Journal of Mathematical Sociology* 1.2 (1971), pages 143–186. DOI: [10.1080/0022250X.1971.9989794](https://doi.org/10.1080/0022250X.1971.9989794). URL: <https://doi.org/10.1080/0022250X.1971.9989794> (cited on page 35).
- [0] Egemen Sert, Yaneer Bar-Yam, and Alfredo J. Morales. “Segregation dynamics with reinforcement learning and agent based modeling”. In: *Scientific Reports* 10.1 (2020). DOI: [10.1038/s41598-020-68447-8](https://doi.org/10.1038/s41598-020-68447-8) (cited on page 36).
- [0] Munik Shrestha and Christopher Moore. “Message-passing approach for threshold models of behavior in networks”. In: *Physical Review E* 89.2 (2014). DOI: [10.1103/physreve.89.022805](https://doi.org/10.1103/physreve.89.022805) (cited on page 18).
- [0] Daniel Silver, Ultan Byrne, and Patrick Adler. “Venues and segregation: A revised Schelling model”. In: *PLOS ONE* 16.1 (Jan. 2021), e0242611. DOI: [10.1371/journal.pone.0242611](https://doi.org/10.1371/journal.pone.0242611). URL: <http://dx.doi.org/10.1371/journal.pone.0242611> (cited on pages 35, 36).
- [0] P. Singh et al. “Threshold-limited spreading in social networks with multiple initiators”. In: *Scientific Reports* 3.1 (2013). DOI: [10.1038/srep02330](https://doi.org/10.1038/srep02330) (cited on pages 18, 20).
- [0] V. Sood and S. Redner. “Voter Model on Heterogeneous Graphs”. In: *Physical Review Letters* 94.17 (2005). DOI: [10.1103/physrevlett.94.178701](https://doi.org/10.1103/physrevlett.94.178701) (cited on page 17).
- [0] Hans-Ulrich Stark, Claudio J. Tessone, and Frank Schweitzer. “Decelerating Microdynamics Can Accelerate Macrodynamics in the Voter Model”. In: *Physical Review Letters* 101.1 (2008). DOI: [10.1103/physrevlett.101.018701](https://doi.org/10.1103/physrevlett.101.018701) (cited on pages 18–20).
- [0] Hans-Ulrich Stark, Claudio J. Tessone, and Frank Schweitzer. “Decelerating Microdynamics Can Accelerate Macrodynamics in the Voter Model”. In: *Phys. Rev. Lett.* 101 (1 June 2008), page 018701. DOI: [10.1103/PhysRevLett.101.018701](https://doi.org/10.1103/PhysRevLett.101.018701). URL: <https://link.aps.org/doi/10.1103/PhysRevLett.101.018701> (cited on page 36).
- [0] Michele Starnini, James P. Gleeson, and Marián Boguñá. “Equivalence between Non-Markovian and Markovian Dynamics in Epidemic Spreading Processes”. In: *Physical Review Letters* 118.12 (2017). DOI: [10.1103/physrevlett.118.128301](https://doi.org/10.1103/physrevlett.118.128301) (cited on pages 17, 18).
- [0] D. Stauffer and S. Solomon. “Ising, Schelling and self-organising segregation”. In: *The European Physical Journal B* 57.4 (2007), pages 473–479. DOI: [10.1140/epjb/e2007-00181-8](https://doi.org/10.1140/epjb/e2007-00181-8) (cited on page 36).
- [0] Dietrich Stauffer. “A Biased Review of Sociophysics”. In: *Journal of Statistical Physics* 151.1-2 (2013), pages 9–20. DOI: [10.1007/s10955-012-0604-9](https://doi.org/10.1007/s10955-012-0604-9) (cited on page 36).
- [0] Samuel Unicomb, Gerardo Iñiguez, and Márton Karsai. “Threshold driven contagion on weighted networks”. In: *Scientific Reports* 8.1 (2018). DOI: [10.1038/s41598-018-21261-9](https://doi.org/10.1038/s41598-018-21261-9) (cited on page 18).

- [0] P. Van Mieghem and R. van de Bovenkamp. “Non-Markovian Infection Spread Dramatically Alters the Susceptible-Infected-Susceptible Epidemic Threshold in Networks”. In: *Physical Review Letters* 110.10 (2013). DOI: [10.1103/physrevlett.110.108701](https://doi.org/10.1103/physrevlett.110.108701) (cited on pages 17, 18).
- [0] Federico Vazquez, Víctor M. Eguíluz, and Maxi San Miguel. “Generic Absorbing Transition in Coevolution Dynamics”. In: *Physical Review Letters* 100.10 (2008). DOI: [10.1103/physrevlett.100.108702](https://doi.org/10.1103/physrevlett.100.108702) (cited on page 17).
- [0] André P Vieira, Eric Goles, and Hans J Herrmann. “Dynamics of extended Schelling models”. In: *Journal of Statistical Mechanics: Theory and Experiment* 2020.1 (2020), page 013212. DOI: [10.1088/1742-5468/ab5b8d](https://doi.org/10.1088/1742-5468/ab5b8d) (cited on page 36).
- [0] D. Vinkovic and A. Kirman. “A physical analogue of the Schelling model”. In: *Proceedings of the National Academy of Sciences* 103.51 (2006), pages 19261–19265. DOI: [10.1073/pnas.0609371103](https://doi.org/10.1073/pnas.0609371103) (cited on page 36).
- [0] Henry Wasserman and Gary Yohe. “Segregation and the Provision of Spatially Defined Local Public Goods”. In: *The American Economist* 45.2 (Oct. 2001), pages 13–24. DOI: [10.1177/056943450104500202](https://doi.org/10.1177/056943450104500202). URL: <http://dx.doi.org/10.1177/056943450104500202> (cited on page 36).
- [0] D. J. Watts. “A simple model of global cascades on random networks”. In: *Proceedings of the National Academy of Sciences* 99.9 (2002), pages 5766–5771. DOI: [10.1073/pnas.082090499](https://doi.org/10.1073/pnas.082090499) (cited on pages 17, 18, 20, 25).
- [0] Nicholas C Wormald et al. “Models of random regular graphs”. In: *London Mathematical Society Lecture Note Series* (1999), pages 239–298 (cited on page 19).
- [0] Yang Xu et al. “Quantifying segregation in an integrated urban physical-social space”. In: *Journal of the Royal Society Interface* 16.160 (2019), page 20190536. ISSN: 17425662. DOI: [10.1098/rsif.2019.0536](https://doi.org/10.1098/rsif.2019.0536). URL: <https://royalsocietypublishing.org/doi/abs/10.1098/rsif.2019.0536> (cited on page 37).
- [0] Junfu Zhang. “Residential segregation in an all-integrationist world”. In: *Journal of Economic Behavior and Organization* 54.4 (2004), pages 533–550. ISSN: 0167-2681. DOI: <https://doi.org/10.1016/j.jebo.2003.03.005>. URL: <https://www.sciencedirect.com/science/article/pii/S0167268103001768> (cited on page 44).
- [0] Matteo Zignani et al. “Walls-in-one: usage and temporal patterns in a social media aggregator”. In: *Applied Network Science* 1.1 (2016). DOI: [10.1007/s41109-016-0009-9](https://doi.org/10.1007/s41109-016-0009-9) (cited on pages 18, 36).

Books

- [0] Thomas M Liggett et al. *Stochastic interacting systems: contact, Voter and exclusion processes*. Volume 324. Springer Science & Business Media, 1999 (cited on page 17).
- [0] T Schelling. *Micromotives and Macrobbehavior*. Norton, New York, 1978 (cited on page 35).
- [0] Daniel Aaron Silver and Terry Nichols Clark. *Scenesapes: How qualities of place shape social life*. University of Chicago Press, 2016 (cited on page 36).
- [0] A P Young. *Spin glasses and random fields*. World Scientific, 1997. URL: libgen.li/file.php?md5=5941f917f91576aa2f77de1c40712f2c (cited on page 43).

Index

Corollaries, 48, 54

Definitions, 47, 53

Examples, 48, 54

 Equation, 48, 54

 Text, 48, 54

Exercises, 48, 54

Figure, 57

Notations, 47, 53

Problems, 49, 55

Propositions, 48, 54

 Several Equations, 48, 54

 Single Line, 48, 54

Remarks, 48, 54

Sectioning

 Paragraphs, 14

 Sections, 13

 Subsections, 13

 Subsubsections, 14

Table, 57

Theorems, 47, 53

 Several Equations, 47, 53

 Single Line, 47, 53

Vocabulary, 49, 55

A. Effect of a higher vacancy density ρ_v in the coarsening dynamics of the Schelling model

Since we restrain ourselves to the region $\rho_v < 0.5$, the increase/decrease of the number of vacancies does not change dramatically the behaviour. Above this value, we approach the segregated-dilute transition ($\rho_v \sim 0.62$). Nevertheless, it is worth to mention a few features we observe on the coarsening dynamics.

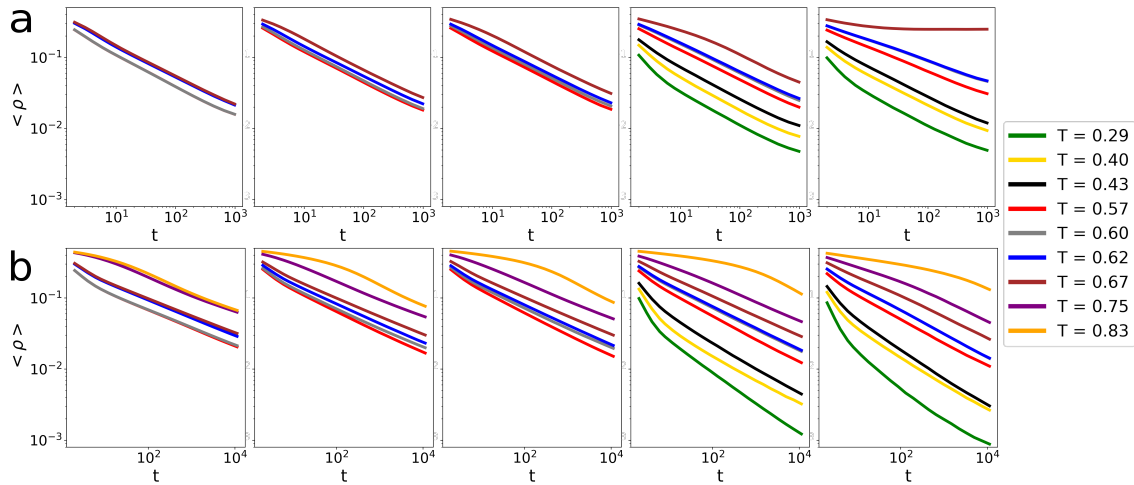


Figure A.1: Average interface density $\langle \rho(t) \rangle$ as a function of time steps for different values of the tolerance parameter T for the Schelling model (a) and the version with aging (b). The different plots show the evolution at a different value of the vacancy density, increasing from left to right $\rho_v = 0.005, 0.15, 0.2, 0.3$ and 0.45 . Average performed over 10^3 realisations with system size 100×100 .

Essentially, when we set a higher vacancy density, the number of agents which see vacancies at their surroundings increases. This results in a family of similar power-law decays towards the segregated state for every meaningful value of T (see Fig. A.1).

Moreover, a higher ρ_v allows us to study the coarsening phenomena for lower values of T according to the phase diagram for the original Schelling model. For those particular cases, when the aging is introduced, we observe a power law decay faster than without aging (Fig. A.1b). Therefore, the aging effect accelerates segregation in this region of the phase diagram, contrary as for lower values of ρ_v . This acceleration is not caused by reaching the 2-clusters state in less

Appendix A. Effect of a higher vacancy density ρ_v in the coarsening dynamics of the Schelling model

time. Since there is a large presence of vacancies, aging causes a formation of vacancy clusters at the interface. Fig. A.2 shows the final segregated state with and without aging. This spontaneous behaviour is result of the low tolerance combined with the persistence of clusters (once formed) due to aging effect and the large number of vacancies that allows the possibility of the formation of clusters at the interface.

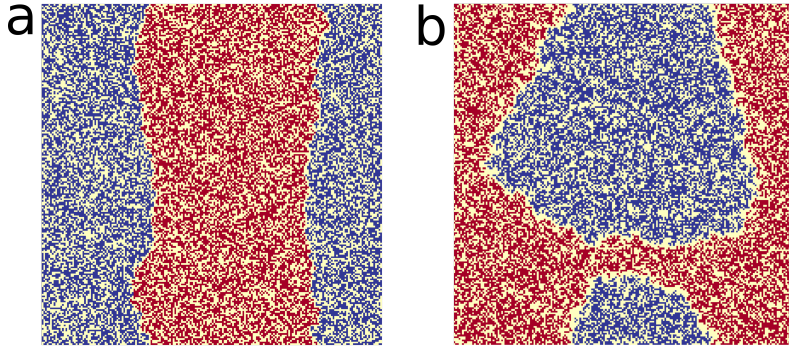


Figure A.2: Snapshots of the system at the final segregated state (after 10^6 MC steps) for the Schelling model (a) and the version with (b). System size 200×200 with $\rho_v = 0.45$ and $T = 0.29$.

In order to quantify this vacancy cluster formation, we define a measure inspired in the segregation coefficient:

$$s_v = \frac{1}{(L^2 \rho_v)^2} \sum_{\{c\}} n_c^2 \quad (\text{A.1})$$

where c is the size of a vacancy cluster and n_c is the number of clusters with size c . The sample average of s_v after reaching equilibrium is called the cluster coefficient of vacancies $\langle s_v \rangle$.

The results of this measure as a function of ρ_v for a few values of T are represented in Fig.A.3 for the Schelling model with and without aging. We observe an increasing dependence of $\langle s_v \rangle$ with ρ_v , for both models, but the effect reducing tolerance changes dramatically the behaviour for the case with aging, highlighting the vacancy cluster formation.

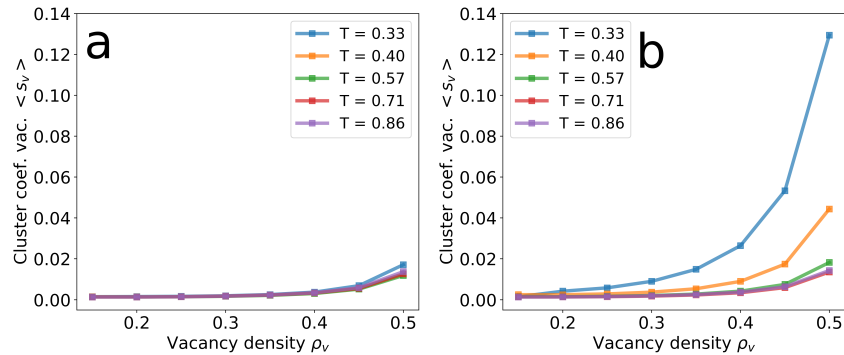
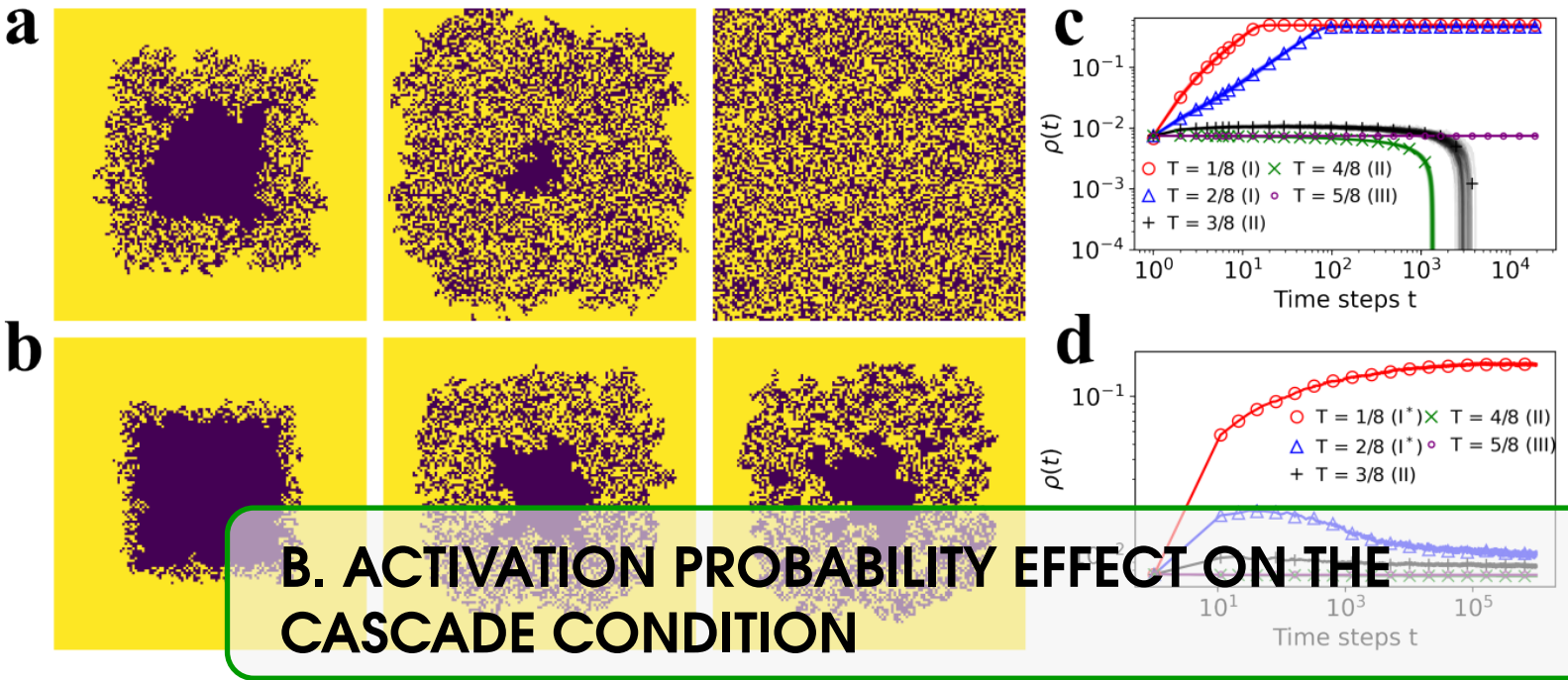


Figure A.3: Cluster coefficient of vacancies as a function of the vacancy density ρ_v for the Schelling model (a) and the version with (b) for different values of the tolerance T .



B. ACTIVATION PROBABILITY EFFECT ON THE CASCADE CONDITION

For our chosen activation probability $p_A = 1/(j+2)$ it has been shown that aging is not able to modify the cascade condition from the original Threshold model. It is natural to ask about the generality of this result. In fact, in Fig. B.1 we show that for an exponential activation probability ($p_A = \exp(-0.5(j+1))$), the cascade condition is modified and the system does not reach the absorbing state for any values of the average degree z and the threshold T considered before (compare with Fig. 2.1).

One may think that this different behavior is because not all nodes are able to activate and adopt the technology with the exponential activation function. To clarify this issue, we computed the probability that an agent never activates during the whole evolution. Since we are performing a Random Asynchronous update in a network of size N , the probability that an agent is not activated in an update attempt is the probability of not being chosen plus the probability of being chosen and not activating:

$$\Pr[\text{"agent is not activated in an attempt"}] = \left(1 - \frac{1}{N}\right) + \frac{1}{N}(1 - p_A(j)). \quad (\text{B.1})$$

As we are performing Monte-Carlo simulations, the probability of the agent being not activated after the N update attempts of the Monte-Carlo step is:

$$\Pr[\text{"agent is not activated in a MC step"}] = \left[\left(1 - \frac{1}{N}\right) + \frac{1}{N}(1 - p_A(j)) \right]^N. \quad (\text{B.2})$$

Therefore, the probability that an agent is never activated is the probability that the agent does not get activated during the evolution, in other words, after infinite Monte-Carlo steps (where after each Monte-Carlo, since it has not been activated, the internal time j increases by one):

$$\Pr[\text{"agent is never activated"}] = \prod_{j=0}^{\infty} \left[\left(1 - \frac{1}{N}\right) + \frac{1}{N}(1 - p_A(j)) \right]^N. \quad (\text{B.3})$$

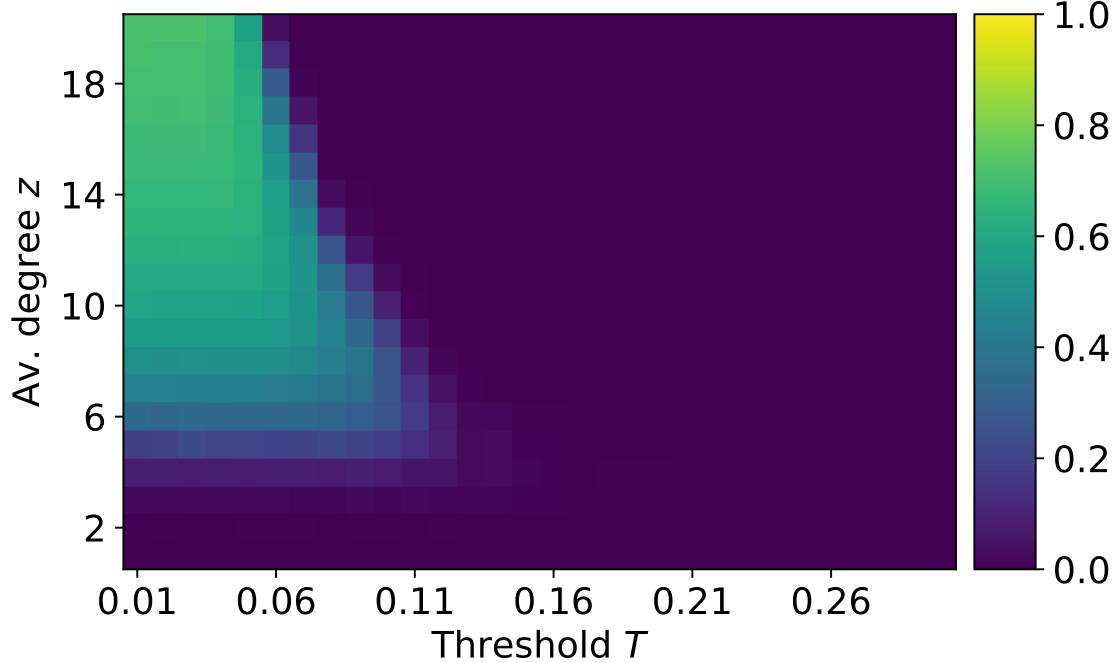
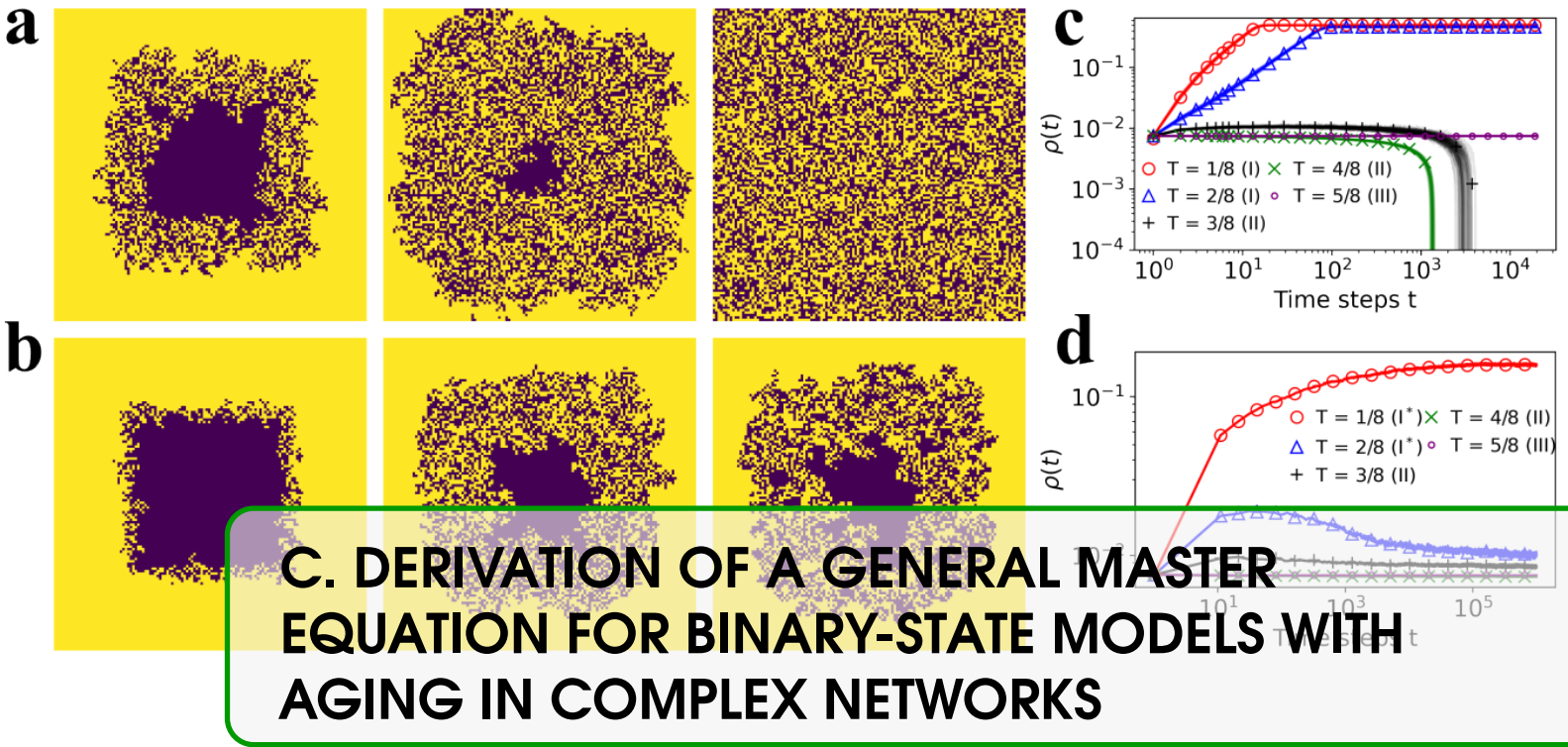


Figure B.1: Average density ρ of adopters for an Erdős-Rényi graph of mean degree z using the Symmetrical threshold model with endogenous aging with threshold T . The activation probability is exponential $p_A(j) = \exp(-0.5 * (j + 1))$. Color-coded values of ρ are from Monte Carlo simulations of the model without aging in a graph with $N = 10,000$ agents. Monte Carlo simulations are averaged over $M = 5 \times 10^4$ realizations.

For both activation probabilities, exponential ($p_A(j) = \exp(-0.5(j + 1))$) and power law ($p_A(j) = 1/(j + 2)$), following Eq. (B.3), the probability that an agent is never activated tends to 0 for the long time simulation limit $j_{\max} \rightarrow \infty$ for any system size N . Therefore, all agents in the system activate at least once during the simulation. Thus, the reason that an exponential activation probability is able to change the cascade condition and a power law function is not just an activation effect, it is due to a non-trivial balance between activation and the adoption process. Notice that this calculation is the same for both aging mechanisms (endogenous and exogenous) because the difference between those appear after the first activation.



C. DERIVATION OF A GENERAL MASTER EQUATION FOR BINARY-STATE MODELS WITH AGING IN COMPLEX NETWORKS

We consider binary-state dynamics on static, undirected, connected networks assuming a locally tree-like structure and in the limit of $N \rightarrow \infty$, following closely the approach used in Ref. [0] for binary-state dynamics in complex networks. The new ingredient is to consider the nodes with different age as different sets, what allows us to treat as Markovian the memory effects introduced by aging [0, 0]. We define $s_{k,m,j}(t)$ ($i_{k,m,j}(t)$) as the fraction of nodes that are susceptible (infected) and have degree k , m infected neighbors and age j at time t . The networks have degree distribution p_k and have been generated by the configuration model [0, 0]. The initial condition is set such that all agents have age $j = 0$ and there is a randomly chosen fraction ρ_0 of nodes infected:

$$\text{For } j > 0 \quad s_{k,m,j}(0) = 0 \quad i_{k,m,j}(0) = 0, \quad (C.1)$$

$$\text{For } j = 0 \quad s_{k,m,0}(0) = (1 - \rho_0) B_{k,m}[\rho_0] \\ i_{k,m,0}(0) = \rho_0 B_{k,m}[\rho_0],$$

where $B_{k,m}[\rho_0]$ is the binomial distribution with k attempts, m successes and ρ_0 is the initial fraction of infected agents that as the probability of success of the binomial. Now, we examine how $s_{k,m,j}$ changes in a time step. We consider separately the case $j = 0$ since its evolution is different from $j > 0$. See Fig. C.1 for a schematic representation of transitions involving $s_{k,m,j}$.

This is the way to reach the expressions of Eq. (C.2):

$$s_{k,m,j}(t + dt) = s_{k,m,j}(t) - F(k, m, j) s_{k,m,j} dt - F_R(k, m, j) s_{k,m,j} dt - F_A(k, m, j) s_{k,m,j} dt \\ + F_A(k, m, j-1) s_{k,m,j-1} dt - \omega(s_{k,m,j} \rightarrow s_{k,m+1,j+1}) s_{k,m,j} dt \\ - \omega(s_{k,m,j} \rightarrow s_{k,m-1,j+1}) s_{k,m,j} dt + \omega(s_{k,m+1,j-1} \rightarrow s_{k,m,j}) s_{k,m+1,j-1} dt \\ + \omega(s_{k,m-1,j-1} \rightarrow s_{k,m-1,j-1}) s_{k,m-1,j-1} dt, \quad (C.2)$$

$$s_{k,m,0}(t + dt) = s_{k,m,0}(t) - F(k, m, 0) s_{k,m,0} dt + \sum_{l=0}^{\infty} R(k, m, l) i_{k,m,l} dt + \sum_{l=1}^{\infty} F_R(k, m, l) s_{k,m,l} dt \\ - F_A(k, m, 0) s_{k,m,0} dt - \omega(s_{k,m,0} \rightarrow s_{k,m+1,1}) s_{k,m,0} dt - \omega(s_{k,m,0} \rightarrow s_{k,m-1,1}) s_{k,m,0} dt.$$

Similar equations can be found considering transitions for $i_{k,m,j}$. In these equations, the transition probabilities (described in detail in section 2.3.2) allow agents to change state (F and R), reset internal time ($j \rightarrow 0$) (F_R and R_R and age ($j \rightarrow j + 1$) (F_A and R_A). Notice that we have considered no transition increasing (or decreasing) the number of infected neighbors m , keeping constant the age j . This is because the age j is defined as the time spent in the current state (or since

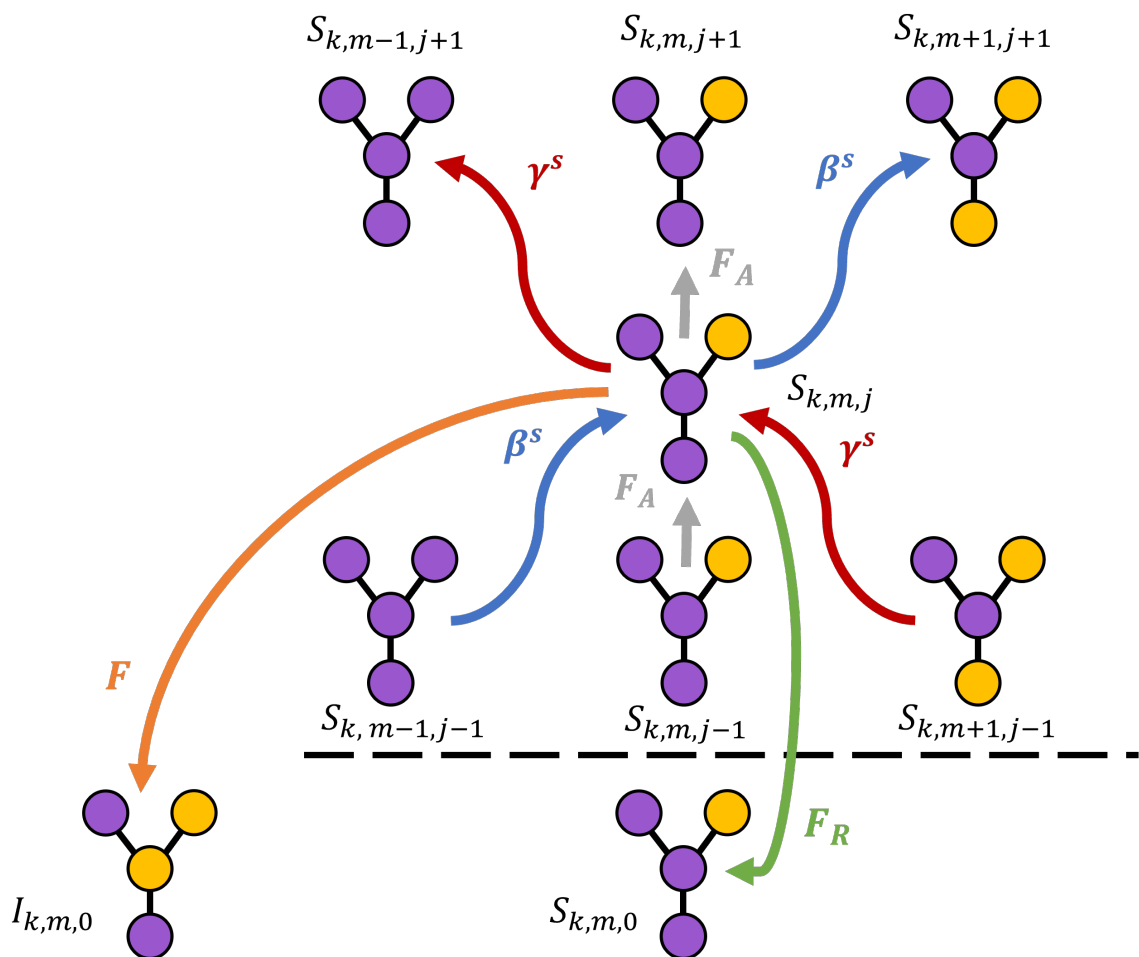


Figure C.1: Schematic representation of the transitions to or from the set $s_{k,m,j}$ ($j > 0$). We show the central node with some neighbors for different values m and j . Purple nodes are susceptible or non-adopters or spin-down, and yellow are infected or adopters or spin-up.

a reset). Therefore, if a node remains susceptible and the number of infected neighbors changes ($m \rightarrow m \pm 1$), the age of the node must increase ($j \rightarrow j + 1$). To determine the rate of these events, we use the same assumption as in Ref. [0]: we assume that the number of S-S edges change to S-I edges at a time-dependent rate β^s . Therefore, the transition rates are:

$$\begin{aligned}\omega(s_{k,m,j} \rightarrow s_{k,m+1,j+1}) &= (k - m) \beta^s, \\ \omega(s_{k,m-1,j-1} \rightarrow s_{k,m,j}) &= (k - m + 1) \beta^s.\end{aligned}\tag{C.3}$$

To determine the rate β^s , we count the change of S-S edges that change to S-I in a time step. This change is produced by a neighbor changing state from susceptible to infected. Thus, we can extract this information from the infection probability $F(k, m, j)$:

$$\beta^s = \frac{\sum_{j=0}^{\infty} \sum_{k=0}^{\infty} p_k \sum_{m=0}^k (k - m) F(k, m, j) s_{k,m,j}}{\sum_{j=0}^{\infty} \sum_{k=0}^{\infty} p_k \sum_{m=0}^k (k - m) s_{k,m,j}}.\tag{C.4}$$

A similar approximation is used to determine the transition rates at which S-I edges change to S-S edges. We write:

$$\begin{aligned}\omega(s_{k,m,j} \rightarrow s_{k,m-1,j+1}) &= m \gamma^s, \\ \omega(s_{k,m+1,j-1} \rightarrow s_{k,m,j}) &= (m + 1) \gamma^s,\end{aligned}\tag{C.5}$$

where the rate γ^s is computed using the recovery probability $R(k, m, j)$:

$$\gamma^s = \frac{\sum_{j=0}^{\infty} \sum_{k=0}^{\infty} p_k \sum_{m=0}^k (k - m) R(k, m, j) i_{k,m,j}}{\sum_{j=0}^{\infty} \sum_{k=0}^{\infty} p_k \sum_{m=0}^k (k - m) i_{k,m,j}}.\tag{C.6}$$

For standard models, one natural assumption is to consider the probability to age as the probability of neither changing state nor resetting:

$$\begin{aligned}F(k, m, j) + F_A(k, m, j) + F_R(k, m, j) &= 1, \\ R(k, m, j) + R_A(k, m, j) + R_R(k, m, j) &= 1.\end{aligned}\tag{C.7}$$

With this condition, taking the limit $dt \rightarrow 0$ of Eq. (C.2) we obtain the approximate master equation

Appendix C. DERIVATION OF A GENERAL MASTER EQUATION FOR BINARY-STATE MODELS WITH AGING IN COMPLEX NETWORKS

76

(AME) for the evolution of the different sets $s_{k,m,j}$, $s_{k,m,0}$ $i_{k,m,j}$ and $i_{k,m,0}$:

$$\begin{aligned}
 \frac{ds_{k,m,j}}{dt} &= -s_{k,m,j} - (k-m)\beta^s s_{k,m,j} - m\gamma^s s_{k,m,j} \\
 &\quad + (k-m+1)\beta^s s_{k,m-1,j-1} \\
 &\quad + (m+1)\gamma^s s_{k,m+1,j-1} \\
 &\quad + F_A(k, m, j-1) s_{k,m,j-1}, \\
 \frac{ds_{k,m,0}}{dt} &= -s_{k,m,0} - (k-m)\beta^s s_{k,m,0} - m\gamma^s s_{k,m,0} \\
 &\quad + \sum_{l=0}^{\infty} R(k, m, l) i_{k,m,l} + \sum_{l=0}^{\infty} F_R(k, m, l) s_{k,m,l}, \\
 \frac{di_{k,m,j}}{dt} &= -i_{k,m,j} - (k-m)\beta^i i_{k,m,j} - m\gamma^i i_{k,m,j} \\
 &\quad + (k-m+1)\beta^i i_{k,m-1,j-1} \\
 &\quad + (m+1)\gamma^i i_{k,m+1,j-1} \\
 &\quad + R_A(k, m, j-1) i_{k,m,j-1}, \\
 \frac{di_{k,m,0}}{dt} &= -i_{k,m,0} - (k-m)\beta^i i_{k,m,0} - m\gamma^i i_{k,m,0} \\
 &\quad + \sum_{l=0}^{\infty} F(k, m, l) s_{k,m,l} + \sum_{l=0}^{\infty} R_R(k, m, l) i_{k,m,l},
 \end{aligned} \tag{C.8}$$

where β^i and γ^i are similar rates as β^s (Eq. (C.4)) and γ^s (Eq. (C.6)), exchanging terms $s_{k,m,j}$ by $i_{k,m,j}$ and vice versa. These equations define a closed set of deterministic differential equations that can be solved numerically using standard computational methods for any complex network and any model aging via the infection/recovery, reset and aging probabilities (a general script in Julia is available in the author's GitHub repository [[link](#) [git](#)]).

The model is introduced via the transition probabilities (F, R, F_A, R_A, F_R, R_R), which may depend on the degree k , the number of infected neighbors m and the time spent in the actual state (or since a reset) j . For the Threshold model with aging, dynamics are monotonic and there are no age dynamics once the agent is infected $R(k, m, j) = R_A(k, m, j) = R_R(k, m, j) = 0$. Therefore, the equations for $s_{k,m,0}$ decouples from the equations for the variables $i_{k,m,j}$, reducing Eq.(C.8) to:

$$\begin{aligned}
 \frac{ds_{k,m,j}}{dt} &= -s_{k,m,j} - (k-m)\beta^s s_{k,m,j} \\
 &\quad + (k-m+1)\beta^s s_{k,m-1,j-1} \\
 &\quad + F_A(k, m, j-1) s_{k,m,j-1}, \\
 \frac{ds_{k,m,0}}{dt} &= -s_{k,m,0} - (k-m)\beta^s s_{k,m,0} \\
 &\quad + \sum_{l=0}^{\infty} F_R(k, m, l) s_{k,m,l}.
 \end{aligned} \tag{C.9}$$